Selectivities in Hydrocarbon Activation: Kinetic and Thermodynamic Investigations of Reversible 1,2-RH-Elimination from (silox)$_2$(^{t}Bu$_3$SiNH)TiR (silox = ^{t}Bu$_3$SiO)

Jordan L. Bennett and Peter T. Wolczanski*

Contribution from Baker Laboratory, Department of Chemistry, Cornell University, Ithaca, New York 14853

Received March 7, 1997[⊗]

Abstract: Addition of 2.0 equiv of Na(silox) to $TiCl_4(THF)_2$ afforded (silox)$_2TiCl_2$ (**1**), which yielded (silox)$_2$(^{t}Bu$_3$SiNH)TiCl (**2**-Cl) upon treatment with ^{t}Bu$_3$SiNLi. Grignard or alkyllithium additions to **2**-Cl or 1,2-RH-addition to transient (silox)$_2$Ti=NSi^{t}Bu$_3$ (**3**) produced (silox)$_2$(^{t}Bu$_3$SiNH)TiR (**2**-R; R = Me, Et, CH_2Ph = Bz, $CH{=}CH_2$ = Vy, ^{c}Bu, ^{n}Bu, Ph, H, ^{c}Pr, ^{c}Pe, CH_2-3,5-$Me_2C_6H_3$ = Mes, ^{neo}Hex, ^{c}Hex, η^3-H_2CHCH_2, η^3-$H_2CCHCHMe$). Insertions of C_2H_4, butadiene, HC_2H, and $HC_2{}^t$Bu into the titanium−hydride bond of **2**-H generated (silox)$_2$(^{t}Bu$_3$SiNH)TiR (**2**-R; R = Et, η^3-$H_2CCHCHMe$, Vy, *E*-CH=CH^{t}Bu). Trapping of **3** by donors L afforded (silox)$_2$LTi=NSi^{t}Bu$_3$ (**3**-L; L = OEt_2, THF (X-ray, two independent molecules: d(Ti=N) = 1.772(3), 1.783(3) Å), py, PMe_3, NMe_3, NEt_3) and metallacycles (silox)$_2$(^{t}Bu$_3$SiN)TiCR=CR′ (**3**-RC_2R'; RC_2R' = HC_2H, MeC_2Me, EtC_2Et, $HC_2{}^t$Bu) and (silox)$_2$(^{t}Bu$_3$SiN)TiCH_2CH_2 (**3**-C_2H_4). Kinetics of 1,2-RH-elimination from **2**-R revealed a first-order process (24.8 °C): R = Bz < Mes < H < Me ($1.54(10) \times 10^{-5}$ s^{-1}) < ^{neo}Hex < Et < ^{n}Bu < ^{c}Bu < ^{c}Pe < ^{c}Hex < ^{c}Pr < Vy < Ph. Kinetics data, large 1,2-RH/D-elimination KIE's (e.g., MeH/D, 13.7(9), 24.8 °C), and Eyring parameters (e.g., **2**-Me, $\Delta H^{\ddagger} = 20.2(12)$ kcal/mol, $\Delta S^{\ddagger} = -12(4)$ eu) portray a four-center, concerted transition state where the N···H···R linkage is nearly linear. Equilibrium measurements led to the following relative standard free energy scale: **2**-^{c}Hex > **2**-^{c}Pe > **2**-^{n}Pr ∼ **2**-^{n}Bu > **2**-^{neo}Hex > **2**-Et > **2**-^{c}Bu > **2**-CH_2SiMe_3 > **2**-Ph > **2**-Me > **2**-Bz > **2**-^{c}Pr ∼ **2**-Mes > **2**-Vy > **3**-C_2H_4 > **3**-NEt_3 > **2**-H > **3**-OEt_2 > **3**-EtC_2Et > **3**-MeC_2Me > **3**-THF > **3**-NMe_3 > **3**-PMe_3 > **3**-py. A correlation of $D(TiR)_{rel}$ to D(RH) revealed greater differences in titanium−carbon bond energies. THF loss from **3**-THF allowed a rough estimate of $\Delta G°$(**3**). Using thermochemical cycles, relative activation energies for 1,2-RH-addition were assessed: ^{c}HexH > ^{c}PeH > ^{n}BuH > ^{neo}HexH > EtH > BzH > ^{c}BuH > MesH > MeH > PhH > ^{c}PrH > VyH > **3**-C_2H_4 formation > H_2. On the basis of a parabolic model, C−H bond activation selectivities are influenced by the relative ground state energies of **2**-R and a parameter representing the reaction coordinate. A more compressed reaction coordinate for sp^2- vs sp^3-substrates eases their activation.

Introduction

Despite greater than 15 years of research on carbon−hydrogen bond activation,[1,2] explanations of selectivities in systems exhibiting concerted C−H bond-breaking events are still somewhat speculative, because the energetics of critical ground states are uncertain.[3] Understanding the factors that permit L_nM or a metal−ligand functionality to react with R^1H vs R^2H is very important, because the ultimate utilization of C−H bond reactivity depends crucially on whether the event can be made selective.

Systems based upon H atom abstractions manifest selectivities that essentially correlate inversely with the bond dissociation energies of the substrate C−H bonds,[4−6] but concerted systems contrast markedly, exhibiting almost the opposite trend. Oxidative additions of RH to coordinatively unsaturated d^8 and d^6 metal centers (i.e., $L_nM + RH \rightleftharpoons L_nHMR$)[1−3,7−9] and related late-metal, solvent-assisted heterolytic RH cleavages (i.e., $L_nM + RH \rightleftharpoons [L_nMR]^- + H^+$)[10−12] have dominated investigations in this area, and surprising parallels to these electrophilic attacks on RH have been discovered in d^0 early metal systems. σ-Bond metatheses of hydrocarbons with coordinatively unsaturated

[⊗] Abstract published in *Advance ACS Abstracts,* October 15, 1997.

(1) (a) Crabtree, R. H. In *The Chemistry of Alkanes and Cycloalkanes*; Patai, S., Rappoport, Z., Eds.; John Wiley & Sons: New York, 1992; p 653. (b) Arndtsen, B. A.; Bergman, R. G.; Mobley, T. A.; Peterson, T. H. *Acc. Chem. Res.* **1995**, *28*, 154−162. (c) Davies, J. A., Ed. *Selective Hydrocarbon Activation*; VCH: Weinheim, Germany, 1990. (d) Crabtree, R. H.; Hamilton, D. G. *Adv. Organomet. Chem.* **1988**, *28*, 299−338. (e) Graham, W. A. G. *J. Organomet. Chem.* **1986**, *300*, 81−91. (f) Green, M. L. H.; O'Hare, D. *Pure Appl. Chem.* **1985**, *57*, 1897−1910.

(2) Crabtree, R. H. *Chem. Rev.* **1995**, *95*, 987−1007.

(3) Leading references to d^8 oxidative additions and a set of ground state data crucial to understanding RH oxidative additions are included in: Jones, W. D.; Hessell, E. T. *J. Am. Chem. Soc.* **1993**, *115*, 554−562.

(4) (a) Wayland, B. B.; Ba, S.; Sherry, A. E. *J. Am. Chem. Soc.* **1991**, *113*, 5305−5311. (b) Zhang, X.-X.; Wayland, B. B. *J. Am. Chem. Soc.* **1994**, *116*, 7897−7898.

(5) Cook, G. K.; Mayer, J. M. *J. Am. Chem. Soc.* **1994**, *116*, 1855−1868.

(6) For related oxidation processes, see: Sheldon, R. A.; Kochi, J. K. *Metal Catalyzed Oxidations of Organic Compounds*; Academic Press: New York, 1981.

(7) For a classic study, see: (a) Jones, W. D.; Feher, F. J. *Acc. Chem. Res.* **1989**, *22*, 99−106. (b) Jones, W. D.; Feher, F. J. *J. Am. Chem. Soc.* **1984**, *106*, 1650−1664.

(8) For recent d^6 activations, see: (a) Burger, P.; Bergman, R. G. *J. Am. Chem. Soc.* **1993**, *115*, 10462−10463. (b) Arndtsen, B. A.; Bergman, R. G. *Science* **1995**, *270*, 1970−1973. (c) Luecke, H. F.; Arndtsen, B. A.; Burger, P.; Bergman, R. G. *J. Am. Chem. Soc.* **1996**, *118*, 2517−2518. (d) Holtcamp, M. W.; Labinger, J. A.; Bercaw, J. E. *J. Am. Chem. Soc.* **1997**, *119*, 848−849. Calculational support for the oxidative addition pathway is given in: (e) Strout, D. L.; Zaric, S.; Niu, S.; Hall, M. B. *J. Am. Chem. Soc.* **1996**, *118*, 6068−6069.

(9) For recent advances in catalytic dehydrogenation, see: (a) Maguire, J. A.; Petrillo, A.; Goldman, A. S. *J. Am. Chem. Soc.* **1992**, *114*, 9492−9498. (b) Gupta, M.; Hagen, C.; Kaska, W. C.; Cramer, R. E.; Jensen, C. M. *J. Am. Chem. Soc.* **1997**, *119*, 840−841.

S0002-7863(97)00741-5 CCC: $14.00

metal alkyl complexes (i.e., $L_nMR + R'H \rightleftharpoons L_nMR' + RH$) of the early metals,[13,14] lanthanides,[15,16] and actinides[17] show trends in reactivity that crudely mirror their late-metal counterparts.

Concerted 1,2-RH-additions across MX (X = O (R = OH, H,[18] R″NH),[19] NR′ (R = hydrocarbyl,[20−27] R″NH),[28,29] CR'_2)[30,31] multiple bonds comprise a relatively recent class of C−H bond cleavage reactions of which d^0 metal imido complexes[32] constitute the most prevalent subgroup. Hydrocarbon reactivity is typified by 1,2-additions of RH to imido functionalities of electrophilic transients $Cp_2Zr{=}N^tBu$ (R = arene,[26] sp^2-substrates),[27] $(^tBu_3SiNH)_2Zr{=}NSi^tBu_3$ (R = hydrocarbyl),[20,21] $(^tBu_3SiNH)_2Ti{=}NSi^tBu_3$ (R = benzene),[22] $(^tBu_3SiNH)Ta(=NSi^tBu_3)_2$ (R = methane, benzene),[23] $(^tBu_3SiNH)V(=NSi^tBu_3)_2$ (R = hydrocarbyl),[25] and $(silox)_2Ti{=}NSi^tBu_3$ (**3**, silox = $^tBu_3SiO$, R = hydrocarbyl).[24] During the course of seeking a stable 3-coordinate imido derivative, investigations of the last were initiated. While transient **3** remains elusive, the corresponding alkyl species, $(silox)_2(^tBu_3SiNH)TiR$ (**2**-R), undergo facile 1,2-RH-eliminations at 24.8 °C and are amenable to equilibrium studies that establish relative ground state energies.

Scheme 1

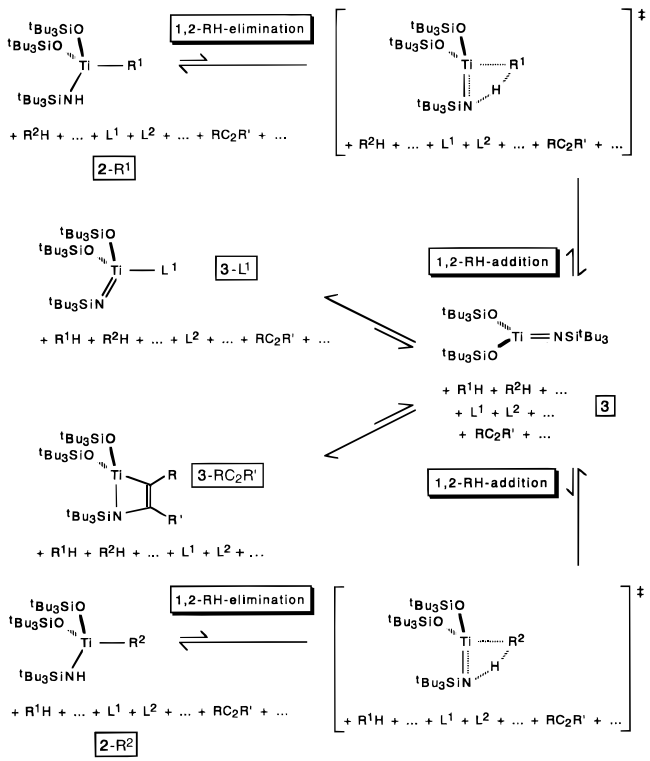

Scheme 1 illustrates the general scope of reactivity reported herein, showing 1,2-RH-elimination and -addition pathways and the trapping of $(silox)_2Ti{=}NSi^tBu_3$ (**3**) by Lewis bases and alkynes. Equilibrium studies are reported that link all **2**-R^n, **3**-L, and **3**-RC_2R', and kinetic investigations of 1,2-RH-elimination from **2**-R enable selectivities of 1,2-R^1H- vs 1,2-R^2H-addition to be determined as $\Delta\Delta G^{\ddagger}_{addn} = \Delta G^{\ddagger}_{addn}(R^1H) - \Delta G^{\ddagger}_{addn}(R^2H)$. The origin of these selectivities is presented in terms of a model that describes reactant (i.e., **2**-R) and product (i.e., **3**) free energy surfaces as intersecting parabolas, such that ground state and positional dependencies can be delineated. While certain trends are surprisingly similar to late-metal oxidative additions and other concerted activations, the greater selectivity exhibited by $(silox)_2Ti{=}NSi^tBu_3$ (**3**) may be rationalized on the basis of a different rate-determining event.

Results and Discussion

Syntheses and Spectral Characterizations. 1. $(silox)_2(^tBu_3SiNH)TiR$ (R = Cl (2-Cl), H (2-H), hydrocarbyl (2-R)). Treatment of $TiCl_4(THF)_2$ with 2 equiv of Na(silox) in diethyl ether for 4 h at 25 °C afforded colorless, crystalline $(silox)_2TiCl_2$ (**1**,[33] silox = $^tBu_3SiO$) in 90% yield upon recrystallization from hexanes (eq 1). The addition of $LiNHSi^tBu_3$ to **1** in ether at 25 °C for 30 min yielded colorless $(silox)_2(^tBu_3SiNH)TiCl$ (**2**-Cl) in 87% yield (eq 2), also after crystallization from hexanes.

(10) (a) Lin, M.; Sen, A. *Nature* **1994**, *368*, 613−614. (b) Kao, L.-C.; Hutson, A. C.; Sen, A. *J. Am. Chem. Soc.* **1991**, *113*, 700−701. (c) Sen, A.; Gretz, E.; Oliver, T. F.; Jiang, Z. *New J. Chem.* **1989**, *13*, 755−760. (d) Sen, A. *Acc. Chem. Res.* **1988**, *21*, 421−428.

(11) (a) Luinstra, G. A.; Labinger, J. A.; Bercaw, J. E. *J. Am. Chem. Soc.* **1993**, *115*, 3004−3005. (b) Labinger, J. A.; Herring, A. M.; Lyon, D. K.; Luinstra, G. A.; Bercaw, J. E.; Horváth, I. T.; Eller, K. *Organometallics* **1993**, *12*, 895−905.

(12) Periana, R. A.; Taube, D. J.; Evitt, E. R.; Loffler, D. G.; Wentrcek, P. R.; Voss, G.; Masuda, T. *Science* **1993**, *259*, 340−343.

(13) Guram, A. S.; Jordan, R. F.; Taylor, D. F. *J. Am. Chem. Soc.* **1991**, *113*, 1833−1835 and references therein

(14) (a) Quignard, F.; Lécuyer, C.; Choplin, A.; Olivier, D.; Bassett, J.-M. *J. Mol. Catal.* **1992**, *74*, 353−363. (b) Lécuyer, C.; Quignard, F.; Choplin, A.; Olivier, D.; Bassett, J.-M. *Angew. Chem., Int. Ed. Engl.* **1991**, *30*, 1660−1661. (c) Quignard, F.; Choplin, A.; Bassett, J.-M. *J. Chem. Soc., Chem. Commun.* **1991**, 1589−1590.

(15) Thompson, M. E.; Baxter, S. M.; Bulls, A. R.; Burger, B. J.; Nolan, M. C.; Santarsiero, B. D.; Schaefer, W. P.; Bercaw, J. E. *J. Am. Chem. Soc.* **1987**, *109*, 203−219.

(16) Watson, P. L.; Parshall, G. W. *Acc. Chem. Res.* **1985**, *18*, 51−56.

(17) Fendrick, C. M.; Marks, T. J. *J. Am. Chem. Soc.* **1986**, *108*, 425−437.

(18) Parkin, G.; Bercaw, J. E. *J. Am. Chem. Soc.* **1989**, *111*, 391−393.

(19) Howard, W. A.; Waters, M.; Parkin, G. *J. Am. Chem. Soc.* **1993**, *115*, 4917−4918.

(20) (a) Schaller, C. P.; Cummins, C. C.; Wolczanski, P. T. *J. Am. Chem. Soc.* **1996**, *118*, 591−611. (b) Cummins, C. C.; Baxter, S. M.; Wolczanski, P. T. *J. Am. Chem. Soc.* **1988**, *110*, 8731−8733.

(21) Schaller, C. P.; Bonanno, J. B.; Wolczanski, P. T. *J. Am. Chem. Soc.* **1994**, *116*, 4133−4134.

(22) Cummins, C. C.; Schaller, C. P.; Van Duyne, G. D.; Wolczanski, P. T.; Chan, E. A.-W.; Hoffmann, R. *J. Am. Chem. Soc.* **1991**, *113*, 2985−2994.

(23) Schaller, C. P.; Wolczanski, P. T. *Inorg. Chem.* **1993**, *32*, 131−144.

(24) Bennett, J. L.; Wolczanski, P. T. *J. Am. Chem. Soc.* **1994**, *116*, 2179−2180. Included herein is an estimate of the enthalpy for binding ethylene ($\Delta H_{\sigma-bind} \sim 11$ kcal/mol, $\Delta G_{\sigma-bind} \sim 9$ kcal/mol) to d^0 $(silox)_2Ti{=}NSi^tBu_3$ (**3**).

(25) de With, J.; Horton, A. D. *Angew. Chem., Int. Ed. Engl.* **1993**, *32*, 903−905. Upon reassessment of the data in this paper, $\Delta S^{\ddagger}_{elim} \sim 8(23)$ eu, a value lacking the precision necessary for interpretation: Bennett, J. L.; Wolczanski, P. T. Unpublished work.

(26) Walsh, P. J.; Hollander, F. J.; Bergman, R. G. *Organometallics* **1993**, *12*, 3705−3723.

(27) Lee, S. Y.; Bergman, R. G. *J. Am. Chem. Soc.* **1995**, *117*, 5877−5878.

(28) Zambrano, C. H.; Profilet, R. D.; Hill, J. E.; Fanwick, P. E.; Rothwell, I. P. *Polyhedron* **1993**, *12*, 689−708.

(29) Jolly, M.; Mitchell, J. P.; Gibson, V. C. *J. Chem. Soc., Dalton Trans.* **1992**, 1329−1330.

(30) (a) van der Heijden, H.; Hessen, B. *J. Chem. Soc., Chem. Commun.* **1995**, 145−146. (b) Coles, M. P.; Gibson, V. C.; Clegg, W.; Elsegood, M. R. J.; Porrelli, P. A. *J. Chem. Soc., Chem. Commun.* **1996**, 1963−1964. (c) Tran, E.; Legzdins, P. *J. Am. Chem. Soc.* **1997**, *119*, 5071−5072.

(31) (a) Lockwood, M. A.; Clark, J. R.; Parkin, B. C.; Rothwell, I. P. *J. Chem. Soc., Chem. Commun.* **1996**, 1973−1974. (b) Chamberlain, L. R.; Rothwell, I. P.; Huffmann, J. C. *J. Am. Chem. Soc.* **1986**, *108*, 1502−1509. (c) McDade, C.; Green, J. C.; Bercaw, J. E. *Organometallics* **1982**, *1*, 1629−1634. (d) Couturier, J.-L.; Paillet, C.; Leconte, M.; Basset, J. M.; Weiss, K. *Angew. Chem., Int. Ed. Engl.* **1992**, *31*, 628−631. (e) Polse, J. L.; Andersen, R. A.; Bergman, R. G. *J. Am. Chem. Soc.* **1996**, *118*, 8737−8738.

(32) (a) Wigley, D. E. *Prog. Inorg. Chem.* **1994**, *42*, 239−482. (b) Wigley, D. E.; Gray, S. D. In *Comprehensive Organometallic Chemistry II*; Abel, E. W., Stone, F. G. A., Wilkinson, G., Eds.; Pergamon Press: Oxford, U.K., 1995, Vol. 5, pp 57−153. (c) Nugent, W. A.; Mayer, J. M. *Metal-Ligand Multiple Bonds*; Wiley-Interscience: New York, 1988.

(33) Covert, K. J. Ph.D. Thesis, Cornell University, 1991.

$$TiCl_4(THF)_2 + 2Na(silox) \xrightarrow[25\ °C,\ 4\ h]{Et_2O} \underset{\mathbf{1}}{(silox)_2TiCl_2} + 2NaCl \quad (1)$$

$$\mathbf{1} + {}^tBu_3SiNHLi \xrightarrow[25\ °C,\ 30\ min]{Et_2O} \underset{\mathbf{2}\text{-Cl}}{(silox)_2({}^tBu_3SiNH)TiCl} + LiCl \quad (2)$$

Three distinct routes led to the preparation of (silox)$_2$(^{t}Bu$_3$SiNH)TiR (**2**-R, R = H, hydrocarbyl): metathesis of (silox)$_2$(^{t}Bu$_3$SiNH)TiCl (**2**-Cl) with appropriate alkyl anion equivalents, R-H bond activation by the thermally generated transient (silox)$_2$Ti=NSi^{t}Bu$_3$ (**3**), and olefin insertion into the Ti−H bond of (silox)$_2$(^{t}Bu$_3$SiNH)TiH (**2**-H). The extreme solubilities of certain hydrocarbyls hampered isolation and purification, and the yields of most derivatives were not optimized unless copious quantities of the complex were necessary for ensuing studies. ^{1}H NMR spectra of **2**-R revealed a 27 H singlet for the ^{t}Bu$_3$SiNH ligand that was typically slightly upfield of the 54 H silox resonance, a broader 1 H amide signal that varied with substituent, and the spectral signature of the hydrocarbyl; ^{13}C{^{1}H} NMR spectra possessed related features (Table 1). The NH chemical shifts (C_6D_6) of **2**-Cl and **2**-R essentially parallel those of (^{t}Bu$_3$SiNH)$_3$ZrX (X = Cl, hydrocarbyl),[20] roughly correlating with the electronegativity of the substituent.[22]

The reaction of (silox)$_2$(^{t}Bu$_3$SiNH)TiCl (**2**-Cl) with Grignard reagents generally proceeded smoothly, provided the subsequent elimination of RH from **2**-R was slow ($k_R < 1 \times 10^{-4}$ s^{-1}), permitting isolation of a reasonable amount of **2**-R. In some cases, alkyllithium reagents were required, although these reactions were often not as clean as the reactions of **2**-Cl with RMgX. Crude alkyl derivatives were typically >80% pure, and these often sufficed for kinetics studies.

Treatment of **2**-Cl in diethyl ether with excess (1.5 equiv) MeMgBr, EtMgCl, or PhCH$_2$MgCl for ∼1 h at 25 °C produced the corresponding alkyl amides, (silox)$_2$(^{t}Bu$_3$SiNH)TiR (**2**-R, R = Me, Et, Bz = PhCH$_2$) after swift workup from hexanes (eq 3). Alkyls **2**-Me and **2**-Et were colorless crystalline solids

$$\underset{\mathbf{2}\text{-Cl}}{(silox)_2({}^tBu_3SiNH)TiCl} + \begin{matrix}RMgX\\ X = Br,\ R = Me\\ X = Cl,\ R = Et,\ Bz\end{matrix} \xrightarrow[25\ °C,\ 1\ h]{Et_2O} \underset{\mathbf{2}\text{-R}}{(silox)_2({}^tBu_3SiNH)TiR} + MgXCl \quad (3)$$

R: Me, 76%; Et, 51%; Bz, 72%

while **2**-Bz was bright yellow. Initial attempts to synthesize **2**-Vy (Vy = CH=CH$_2$) from **2**-Cl and VyMgBr in Et$_2$O gave products derived from ethylene loss, prompting a switch to vinyllithium and lower temperatures. Freshly prepared, recrystallized vinyllithium was combined with **2**-Cl in diethyl ether, and the mixture was stirred at 0 °C for 15 min, providing (silox)$_2$(^{t}Bu$_3$SiNH)TiCH=CH$_2$ (**2**-Vy) as an off-white powder upon workup in hexanes (eq 4). **2**-Vy exhibited a classic ABX

$$\mathbf{2}\text{-Cl} + CH_2{=}CHLi \xrightarrow[0\ °C,\ 15\ min]{Et_2O} \underset{\mathbf{2}\text{-Vy, 30\%}}{(silox)_2({}^tBu_3SiNH)TiCH{=}CH_2} + LiCl \quad (4)$$

pattern with coupling constants consistent with a vinyl derivative: J_{cis} = 14.2 Hz, J_{trans} = 19.2 Hz, J_{gem} = 2.8 Hz. ^{13}C NMR (C_6D_{12}) spectroscopy corroborated the assignment, showing resonances at δ 189.01 (Ti−CH=) and δ 129.44 (=CH$_2$), while a ν(C=C) was observed in the IR spectrum at 1554 cm^{-1}.

Chloride **2**-Cl reacted within 5 min with cyclobutyllithium in diethyl ether at −30 °C, generating off-white (silox)$_2$(^{t}Bu$_3$SiNH)Ti^{c}Bu (**2**-^{c}Bu) upon crystallization from hexanes. Similarly, (silox)$_2$(^{t}Bu$_3$SiNH)Ti^{n}Bu (**2**-^{n}Bu) was synthesized by addition of ^{n}BuLi to **2**-Cl in diethyl ether at 0 °C (eq 5). The

$$\mathbf{2}\text{-Cl} + RLi \xrightarrow[-30\ °C \rightarrow 0\ °C,\ 5\ min]{Et_2O} \underset{\mathbf{2}\text{-R}}{(silox)_2({}^tBu_3SiNH)TiR} + LiCl \quad (5)$$

R: ^{c}Bu, 35% (90% purity); ^{n}Bu, 55% (90% purity)

alkyl **2**-^{n}Bu could not be induced to crystallize and was isolated as a precipitate upon filtration and removal of the volatiles. Metathesis was also used to obtain the deuterated amide phenyl complex (silox)$_2$(^{t}Bu$_3$SiND)TiPh (**2**-(ND)-Ph), which was conveniently isolated from hexanes in 39% yield after treatment of **2**-(ND)-Cl with phenyllithium in ether at 0 °C (eq 6). Neither

$$\underset{\mathbf{2}\text{-(ND)-Cl}}{(silox)_2({}^tBu_3SiND)TiCl} + C_6H_5Li \xrightarrow[0\ °C,\ 5\ min]{Et_2O} \underset{\mathbf{2}\text{-(ND)-Ph}}{(silox)_2({}^tBu_3SiND)TiC_6H_5} + LiCl \quad (6)$$

^{t}BuLi nor ^{t}BuCH$_2$Li successfully alkylated **2**-Cl, and while metathesis was observed with Me$_3$SiCH$_2$Li, byproducts seriously complicated subsequent isolation efforts.

Direct 1,2-RH-addition to transient (silox)$_2$Ti=NSi^{t}Bu$_3$ (**3**) was an attractive synthetic alternative for **2**-R species whose subsequent 1,2-RH-elimination was swift and in cases where a suitable RMgX or RLi was not readily available. The methyl complex (silox)$_2$(^{t}Bu$_3$SiNH)TiMe (**2**-Me) was typically used in the thermal generation of **3** because its synthesis was optimized (reproducibly >75%) and byproduct CH$_4$ could easily be removed as a competitive substrate via degassing. In a typical experiment, **2**-Me was dissolved in the neat hydrocarbon substrate or in a cyclohexane solution containing the desired hydrocarbon. The reaction solution was sealed in a glass bomb and heated at 55−80 °C for 3−24 h (eqs 7 and 8). At intervals,

$$\underset{\mathbf{2}\text{-Me}}{(silox)_2({}^tBu_3SiNH)TiMe} \xrightarrow[55-80\ °C,\ 3-24\ h]{RH/C_6H_{12}} \underset{\mathbf{3}}{[(silox)_2Ti{=}NSi{}^tBu_3]} + CH_4 \quad (7)$$

$$\mathbf{3} \rightarrow \underset{\mathbf{2}\text{-R}}{(silox)_2({}^tBu_3SiNH)TiR} \quad (8)$$

R: H, 67%; ^{c}Pr, 33%; ^{c}Pe, 43%; Mes, 42%; ^{neo}Hex, 20%; Ph, 69%

the reaction mixture was cooled and then frozen at 77 K and methane was removed by vacuum. Upon completion of the reaction, the volatiles were removed and the product was isolated by crystallization from hexanes. A synthesis of the hydride,[24,34,35] (silox)$_2$(^{t}Bu$_3$SiNH)TiH (**2**-H, δ(TiH) = 7.34, ν(TiH/D) = 1645/1180 cm^{-1}), was effected through this procedure, as were preparations of several hydrocarbyls, (silox)$_2$(^{t}Bu$_3$SiNH)TiR (**2**-R, R = ^{c}Pr, ^{c}Pe, ^{neo}Hex (^{neo}Hex = CH$_2$CH$_2$^{t}Bu), Mes (Mes = CH$_2$-3,5-Me$_2$C$_6$H$_3$), Ph). The hydrocarbyls were

Table 1. ^{1}H and ^{13}C{^{1}H} NMR Spectral Data for (^{t}Bu$_3$SiO)$_2$(^{t}Bu$_3$SiNH)TiR (**2**-R), (^{t}Bu$_3$SiO)$_2$LTi═NSi^{t}Bu$_3$ (**3**-L), (^{t}Bu$_3$SiO)$_2$TiC(R)═C(R)NSi^{t}Bu$_3$ (**3**-RCCR), and Related Complexes in C_6D_6 Unless Otherwise Noted[a,b]

	^{1}H NMR, δ(assgnt, mult, J (Hz))			^{13}C{1H} NMR, δ (assgnt, J (Hz))		
compound	((H$_3$C)$_3$C)$_3$[c]	NH	R/L	*C*(CH$_3$)$_3$[c]	*C*(CH$_3$)$_3$[c]	R/L
(silox)$_2$TiCl$_2$ (**1**)	1.22			29.86	24.14	
(silox)(^{t}Bu$_3$SiNH)TiCl (**2**-Cl)	1.30	9.01		30.81	23.99	
	1.28			31.12	23.65	
(silox)$_2$(^{t}Bu$_3$SiNH)TiH (**2**-H)	1.29	7.34	8.64 (TiH, s)	30.70	23.35	
	1.27				30.99	22.87
(silox)(^{t}Bu$_3$SiNH)TiMe (**2**-Me)	1.29	7.39	1.35 (CH$_3$, s)	30.78	23.75	47.30 (CH$_3$)
	1.27			31.12	23.41	
(silox)(^{t}Bu$_3$SiNH)TiEt (**2**-Et)	1.30	7.21	1.74 (CH$_3$, t, 7.4)	30.79	23.71	67.02 (CH$_2$)
	1.28		1.98 (CH$_2$, q, 7.4)	31.14	23.31	18.81 (CH$_3$)
(silox)$_2$(^{t}Bu$_3$SiNH)TiCH═CH$_2$ (**2**-Vy)[b]	1.36	7.96	6.10 (CH$_c$, dd, 19, 3)	31.11	24.20	129.44 (CH$_2$)
	1.34		6.18 (CH$_t$, dd, 14, 3)	31.43	23.84	189.01 (TiC)
			7.73 (CH, dd, 19, 14)			
(silox)$_2$(^{t}Bu$_3$SiNH)Ti-c-C$_3$H$_5$ (**2**-^{c}Pr)[d]	1.30	7.20	0.65−0.75 (CH$_\beta$, m)	30.82	23.73	13.39 (C$_\beta$)
	1.28		1.4−1.6 (TiCH, m)	31.15	23.38	57.87 (C$_\alpha$)
(silox)$_2$(^{t}Bu$_3$SiNH)TiC$_4$H$_9$ (**2**-^{n}Bu)[e]	1.31	7.24	0.8−1.0 (CH$_3$, m)	30.78	23.74	13.63 (CH$_3$)
	1.29		2.0−2.3 (CH$_2$, m)	31.14	23.34	27.94 (CH$_2$)
						36.10 (CH$_2$)
						74.46 (TiC)
(silox)$_2$(^{t}Bu$_3$SiNH)Ti-c-C$_4$H$_7$ (**2**-^{c}Bu)	1.31	7.10	1.97 (“quin”, 9.2)	30.80	23.64	22.20 (C$_\gamma$)
	1.28		2.19 (m)	31.14	23.23	36.42 (C$_\beta$)
			2.55 (m)			85.80 (C$_\alpha$)
			3.02 (“quin”, 8.9)			
			3.27 (“quin”, 9.2)			
(silox)$_2$(^{t}Bu$_3$SiNH)TiCH$_2$SiMe$_3$ (**2**-CH$_2$SiMe$_3$)	1.31	7.06	0.29 (CH$_3$, s)			
	1.29		2.04 (CH$_2$, s)			
(silox)$_2$(^{t}Bu$_3$SiNH)Ti-c-C$_5$H$_9$ (**2**-^{c}Pe)	1.32	7.10	0.75−1.05 (m, 2H)	30.87	23.70	27.46 (C$_\gamma$)
	1.30		1.55−2.60 (m, 7H)	31.22	23.31	36.78 (C$_\beta$)
						89.47 (C$_\alpha$)
(silox)$_2$(^{t}Bu$_3$SiNH)Ti(CH$_2$)$_2$^{t}Bu (**2**-^{neo}Hex)	1.32	7.24	0.91 (CH$_3$, s)	30.79	23.77	28.98 ((CH$_3$)$_3$)
	1.30		2.11 (Ti(CH$_2$)$_2$, m)	31.14	23.37	33.12 (CMe$_3$)
						47.74 (CH$_2$)
						70.64 (TiC)
(silox)$_2$(^{t}Bu$_3$SiNH)Ti-c-C$_6$H$_{11}$ (**2**-^{c}Hex)[a,f]	1.23	6.93	1.6−2.0 (CH, CH$_2$, m)			
	1.20		2.60 (CH$_2$, dm, 11)			
(silox)$_2$(^{t}Bu$_3$SiNH)TiCH═CH^{t}Bu (**2**-*E*-CH═CH^{t}Bu)[g]		7.63	1.01 (CH$_3$, s)			
			6.69 (CH, d, 17.8)			
			7.42 (TiCH, d, 17.8)			
(silox)$_2$(^{t}Bu$_3$SiNH)TiPh (**2**-Ph)[b]	1.30	8.27	7.0−7.2 (Ph$_{m,p}$, m)	31.11	24.22	126.84 (Ph)
	1.30		8.2 (Ph$_o$, “dt”, 7.8, 1.6)	31.45	23.82	134.74 (Ph)
						136.83 (Ph)
						187.74 (C$_{ipso}$)
[(silox)$_2$(^{t}Bu$_3$SiNH)Ti]$_2$(μ-η^1,η^1-1,4-C$_6$H$_4$) (**2**$_2$-C$_6$H$_4$)[b,h]				31.10	24.22	128.68 (Ar)
				31.40	23.82	191.70 (C$_{ipso}$)
(silox)(^{t}Bu$_3$SiNH)TiCH$_2$Ph (**2**-Bz)	1.26	7.75	3.30 (CH$_2$, s)	30.79	23.71	73.81 (CH$_2$)
	1.26		6.8−7.4 (Ph, m)	31.14	23.31	123.34 (Ph)
						127.92 (Ph)
						128.49 (Ph)
						148.76 (C$_{ipso}$)
(silox)$_2$(^{t}Bu$_3$SiNH)TiCH$_2$C$_6$H$_3$-3,5-Me$_2$ (**2**-Mes)	1.27	7.65	2.23 (CH$_3$, s)	30.76	23.73	21.43 (CH$_3$)
	1.27		3.31 (CH$_2$, s)	31.17	23.35	74.59 (TiC)
			6.55 (Ar H$_p$, s)			125.25 (C$_p$)
			6.96 (Ar H$_o$, s)			125.81 (C$_o$)
						137.48 (C$_m$)
						148.65 (C$_{ipso}$)
[silox)$_2$(^{t}Bu$_3$SiN)Ti]$_2$(μ_2:η^1,η^1-1,3-(CH$_2$)$_2$ C$_6$H$_3$-5-Me)			2.05 (CH$_3$, s)			
(**2**$_2$-C$_6$H$_3$(CH$_2$)$_2$Me)[a,i]			2.96 (CH$_2$, s)			
(silox)$_2$(^{t}Bu$_3$SiNH)Ti(η^3-H$_2$CCHCH$_2$)	1.22	7.53	1.57 (H$_{syn}$, dd, 6, 1.5)			115.93 (CH$_2$)
(**2**-η^3-H$_2$CCHCH$_2$)[a,b,j]	1.19		4.90 (CH, “tm”, 18)			133.43 (CH)
			7.25 (H$_{anti}$, dd, 18, 1.5)			
(silox)$_2$(^{t}Bu$_3$SiNH)Ti(η^3-H$_2$CCHCHMe)	1.23	7.36	2.60 (CH$_3$, d, 8)			
(**2**-η^3-H$_2$CCHCHMe)[a,b]	1.20		5.03 (CH, “sext”, 10)			
			5.77 (CH, br m)			
			6.05 (CH, “sext”, 10)			
[(silox)$_2$(^{t}Bu$_3$SiN)Ti]$_2$ (**3**$_2$)	1.19				31.26	24.01
	1.18				31.58	24.01
(silox)$_2$(THF)Ti═NSi^{t}Bu$_3$ (**3**-THF)	1.35		1.08 (α-CH$_2$, t, 6.6)	31.09	23.51	25.25 (β-CH$_2$)
	1.36		4.24 (β-CH$_2$, t, 6.6)	31.68	23.86	78.04 (α-CH$_2$)
(silox)$_2$(Et$_2$O)Ti═NSi^{t}Bu$_3$ (**3**-OEt$_2$)	1.35		0.88 (CH$_3$, t, 6.9)	31.12	23.52	12.85 (CH$_3$)
	1.33		4.16 (CH$_2$, q, 6.9)	31.65	23.89	70.93 (CH$_2$)
(silox)$_2$(Me$_3$N)Ti═NSi^{t}Bu$_3$ (**3**-NMe$_3$)[a,b]	1.22		2.96 (CH$_3$, s)	31.53	24.03	52.90 (CH$_3$)
	1.16			31.98	24.35	

Table 1 (Continued)

compound	^{1}H NMR, δ(assgnt, mult, J (Hz))			^{13}C{1H} NMR, δ (assgnt, J (Hz))		
	$((H_3C)_3C)_3$[c]	NH	R/L	$C(CH_3)_3$[c]	$C(CH_3)_3$[c]	R/L
(silox)$_2$(Et$_3$N)Ti=NSi^{t}Bu$_3$ (**3**-NEt$_3$)	1.32		0.95 (CH_3, t, 7.0)	31.35	23.74	13.64 (CH_3)
	1.29		4.14 (CH_2, q, 7.0)	31.85	24.11	49.97 (CH_2)
(silox)$_2$(py)Ti=NSi^{t}Bu$_3$ (**3**-py)	1.34		6.48 (py$_m$, m)	31.08	23.64	124.58 (py)
	1.38		6.70 (py$_p$, m)	31.70	24.08	140.49 (py)
			9.15 (py$_o$, m)			151.15 (py)
(silox)$_2$(Me$_3$P)Ti=NSi^{t}Bu$_3$ (**3**-PMe$_3$)	1.32		1.16 (CH_3, d, J_{PH} = 7.8)	31.39	23.85	14.76 (CH_3, J_{PC} = 19.8)
	1.35			31.99	24.22	
(silox)$_2$(^{t}Bu$_3$SiN)TiCH$_2$CH$_2$ (**3**-C$_2$H$_4$)[k]	1.26		3.08 (CH_2, br s)	30.99	24.02	50.04 (CH_2, J_{CH} = 146.5)
	1.23			31.88	24.58	
(silox)$_2$(^{t}Bu$_3$SiN)TiCH=CH (**3**-HC$_2$H)[b]	1.25		7.80 (TiCH, d, 11.1)	30.93	23.94	153.65 (NC)
	1.20		10.65 (NCH, d, 11.1)	31.49	24.13	198.31 (TiC)
(silox)$_2$(^{t}Bu$_3$SiN)TiCMe=CMe (**3**-MeC$_2$Me)[l]	1.24		2.24 (CH_3, s)	30.79	23.48	21.67 (CH_3)
	1.24		2.48 (CH_3, s)	31.65	24.5	22.30 (CH_3)
						162.05 (NC)
						216.99 (TiC)
(silox)$_2$(^{t}Bu$_3$SiN)TiCEt=CEt (**3**-EtC$_2$Et)[a,b,l,m]	1.23		2.33 (CH_2, q, 7.5)	31.09	23.92	166.53 (NC)
	1.26		2.89 (CH_2, q, 7.5)	32.0	25.3	223.69 (TiC)
(silox)$_2$(^{t}Bu$_3$SiN)TiC^{t}Bu=CH (**3**-^{t}BuC$_2$H)[b,m]	1.26		1.18 (CH_3, s)	31.03	23.78	152.27 (NC)
	1.26		10.72 (NCH, s)	31.59	24.21	225.50 (TiC)

[a] ^{1}H NMR in C_6D_{12} solvent. [b] ^{13}C{^{1}H} NMR in C_6D_{12} solvent. [c] First resonance due to (silox)$_2$; second due to ^{t}BuSiNH or ^{t}Bu$_3$SiN. [d] Other β-CH resonance obscured. [e] Other CH_2 resonances obscured. [f] Remaining H's obscured by ^{t}Bu resonances; low solubility and swift 1,2-^{c}HexH-elimination rate prevented observation by ^{13}C{^{1}H} NMR. [g] ^{t}Bu resonance obscured by those of **2**-H and **3**-^{t}BuC$_2$H. [h] Observed with **2**-Ph; solubility too low to enable confident ^{1}H NMR ^{t}Bu, etc. resonance assignments. [i] Observed with **2**-Mes; solubility too low to enable confident assignment of ^{t}Bu, etc. resonances, which are assumed to be obscured by **2**-Mes. [j] Remaining ^{13}C{^{1}H} resonances could not be differentiated from those of more soluble trace impurities. [k] Methylene resonance broad due to fluxionality; for description of −130 to 20 °C data in C_7D_{14}, see text. [l] Imide ^{t}Bu carbons very broad. [m] Other carbon assignments ambiguous with regard to trace impurities.

colorless, crystalline complexes, except for **2**-Mes and **2**-Ph, which were yellow.

In the case of the phenyl derivative, extended manipulation in cyclohexane led to the formation of a yellow insoluble material tentatively formulated as [(silox)$_2$(^{t}Bu$_3$SiNH)Ti]$_2$(μ-η^1,η^1-1,4-C$_6$H$_4$) (**2**$_2$-C$_6$H$_4$), the product of double C−H bond activation of benzene (eq 9). A dinuclear species was antici-

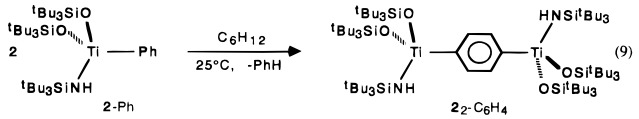

(9)

pated from precedents set in previous zirconium and tantalum (i.e., [(^{t}Bu$_3$SiNH)$_3$Zr]$_2$(μ-η^1,η^1-1,4-C$_6$H$_4$),[20] [(^{t}Bu$_3$SiNH)$_2$(^{t}Bu$_3$SiN)Ta]$_2$(μ-η^1,η^1-1,4-C$_6$H$_4$))[23] systems. As a testament to the more sterically accessible pocket of transient (silox)$_2$Ti=NSi^{t}Bu$_3$ (**3**), evidence of additional double activations was obtained. When **2**-Mes was allowed to stand in C_6D_{12}, ^{1}H NMR spectra gave evidence for [(silox)$_2$(^{t}Bu$_3$SiN)Ti]$_2$(μ-η^1,η^1-1,3-(CH$_2$)$_2$C$_6$H$_3$-5-Me) (**2**$_2$-C$_6$H$_3$(CH$_2$)$_2$Me) and free mesitylene (eq 10). In the synthesis of **2**-^{c}Bu (eq 5), part of the isolation and purification problems can be attributed to formation of a 1,3-cyclobutanediyl derivative. ^{1}H NMR spectra of crude product mixtures in attempted syntheses of **2**-CH$_2$SiMe$_3$ and **2**-^{c}Bu provided hints of the formation of sparingly soluble dinuclear

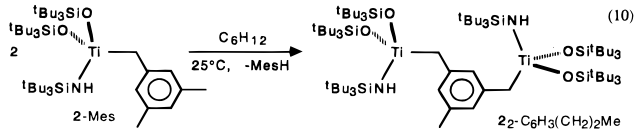

(10)

complexes. In these cases, steric hindrance to double activation is minimal, because the metals are either oppositely disposed about the substrate (e.g., 1,4-C$_6$H$_4$, 1,3-c-C$_4$H$_6$) or linked by a spacer of ≥3 atoms.

Considerable effort was expended toward the synthesis of the cyclohexyl complex, (silox)$_2$(^{t}Bu$_3$SiNH)TiC$_6$H$_{11}$ (**2**-^{c}Hex), considered the least thermodynamically stable yet observable alkyl. Thermolysis of (silox)$_2$(^{t}Bu$_3$SiNH)TiMe (**2**-Me) in neat cyclohexane for 7 d at 55 °C afforded a yellow, microcrystalline material that proved to be a mixture of (silox)$_2$(^{t}Bu$_3$SiNH)-TiC$_6$H$_{11}$ (**2**-^{c}Hex) and [(silox)$_2$Ti]$_2$(μ-NSi^{t}Bu$_3$)$_2$ (**3**$_2$), formulated as a dimer on steric grounds (eq 11). The composition was

$$\text{(silox)}_2(^t\text{Bu}_3\text{SiNH})\text{TiMe (}\mathbf{2}\text{-Me)} \xrightarrow[55\ ^\circ\text{C, 7 d}]{C_6H_{12}} \text{(silox)}_2(^t\text{Bu}_3\text{SiNH})\text{TiC}_6\text{H}_{11}\ (\mathbf{2}\text{-}^c\text{Hex}) + [(\text{silox})_2\text{Ti}]_2(\mu\text{-NSi}^t\text{Bu}_3)_2\ (\mathbf{3}_2) + \text{CH}_4 \quad (11)$$

difficult to assay because of the low solubilities of the species, especially **3**$_2$, but was estimated to be approximately 1:1 by NMR spectroscopy. The low solubility of the mixture limited its utility as a starting material, but solutions enriched in **2**-^{c}Hex were generated and used to determine the 1,2-^{c}HexH-elimination rate constant.

Derivatization of (silox)$_2$(^{t}Bu$_3$SiNH)TiH (**2**-H) was accomplished via insertion of ethylene into its titanium−hydride bond (eq 12), but this reaction was not amenable to a preparative scale because it required several hours, allowing 1,2-H$_2$-elimination to compete. For larger substrates, H$_2$ loss from **2**-H was observed, leading to allyl formation via C−H bond

(34) Discrete, terminal titanium hydrides are relatively uncommon. See: (a) Nöth, H.; Schmidt, M. *Organometallics* **1995**, *14*, 4601−4610. (b) You, Y.; Wilson, S. R.; Girolami, G. S. *Organometallics* **1994**, *13*, 4655−4657. (c) Cummins, C. C.; Schrock, R. R.; Davies, W. M. *Organometallics* **1992**, *11*, 1452−1545. (d) Frerichs, S. R.; Kelsey Stein, B.; Ellis, J. E. *J. Am. Chem. Soc.* **1987**, *109*, 5558−5560. (e) Pattiasina, J. W.; van Bolhuis, F.; Teuben, J. H. *Angew. Chem., Int. Ed. Engl.* **1987**, *26*, 330−331. (f) Aitken, C. T.; Harrod, J. F.; Samuel, E. *J. Am. Chem. Soc.* **1984**, *106*, 1859−1860. (g) Spaltenstein, E.; Palma, P.; Kreutzer, K. A.; Willoughby, C. A.; Davis, W. M.; Buchwald, S. L. *J. Am. Chem. Soc.* **1994**, *116*, 10308−10309.

(35) Bercaw, J. E.; Marvich, R. H.; Bell, L. G.; Brintzinger, H. H. *J. Am. Chem. Soc.* **1972**, *94*, 1219−1238.

$$\underset{\textbf{2}\text{-H}}{(\text{silox})_2(^t\text{Bu}_3\text{SiNH})\text{TiH}} + \text{CH}_2{=}\text{CH}_2 \xrightarrow[25\ ^\circ\text{C}]{C_6H_{12}} \underset{\textbf{2}\text{-Et}}{(\text{silox})_2(^t\text{Bu}_3\text{SiNH})\text{TiCH}_2\text{CH}_3} \quad (12)$$

activation by $(\text{silox})_2\text{Ti}{=}\text{NSi}^t\text{Bu}_3$ (**3**). The reactions of **2**-H with propene and either *cis*- or *trans*-2-butene afforded respective yellow η^3-allyl and red-orange η^3-1-methylallyl complexes according to eq 13. Despite being precipitated in nearly

$$\textbf{2}\text{-H} + \text{H}_3\text{CCH}{=}\text{CHR} \xrightarrow[25\ ^\circ\text{C}]{C_6H_{12}} (\text{silox})_2(^t\text{Bu}_3\text{SiNH})\text{Ti}(\eta^3\text{-H}_2\text{CCHCHR}) + \text{H}_2 \quad (13)$$

R = H (**2**-η^3-H_2CCHCH_2)
R = Me (**2**-η^3-$\text{H}_2\text{CCHCHMe}$)

quantitative yield, these derivatives were extremely difficult to characterize due to their limited solubility. In **2**-η^3-H_2CCHCH_2, separate *anti* (δ 7.25, J_{anti} =18, J_{gem} = 1.5 Hz) and *syn* (δ 1.57, J_{syn} = 6, J_{gem} = 1.5 Hz) resonances distinct from the central proton at δ 4.90 (m, J_{anti} = 18 Hz) are assigned on the basis of coupling magnitude, but must be considered tentative, since the chemical shifts are opposite that observed in typical static, d^n ($n \geq 0$) systems.[36] This oddity may be a consequence of the d^0 titanium center. Its $^{13}\text{C}\{^1\text{H}\}$ NMR spectrum revealed two resonances at δ 133.43 (CH) and δ 115.93 (CH_2), consistent with the expected C_s symmetry. The extremely low solubility of **2**-η^3-$\text{H}_2\text{CCHCHMe}$ prevented corroboration based on ^1H NMR assignments of the η^3-$\text{H}_2\text{CCHCHMe}$ ligand, and its stereochemistry could not be unambiguously determined. A related η^3-2-methylallyl species formed from **2**-H and isobutylene could not be spectrally (^1H and $^{13}\text{C}\{^1\text{H}\}$ NMR) discerned from trace impurites and was not pursued. Insertion of butadiene into the Ti−H bond of **2**-H provided an independent synthesis of **2**-η^3-$\text{H}_2\text{CCHCHMe}$ (eq 14). Formation

$$\textbf{2}\text{-H} + \text{H}_2\text{C}{=}\text{CHCH}{=}\text{CH}_2 \xrightarrow[25\ ^\circ\text{C}]{C_6H_{12}} \underset{\textbf{2}\text{-}\eta^3\text{-}\text{H}_2\text{CCHCHMe}}{(\text{silox})_2(^t\text{Bu}_3\text{SiNH})\text{Ti}(\eta^3\text{-H}_2\text{CCHCHMe})} \quad (14)$$

of the allyls occurred at a rate qualitatively similar to that for elimination of H_2 from **2**-H without olefin present, thereby rendering assistance of H_2 loss by olefin precomplexation unlikely.

In an NMR-tube reaction, acetylene inserted into the Ti−H bond of **2**-H to provide **2**-Vy, but this route was not viable because subsequent ethylene elimination proved to be swift, and azametallacyclobutene[26,37−42] $(\text{silox})_2(^t\text{Bu}_3\text{SiN})\text{TiCH}{=}\text{CH}$ (**3**-HC_2H) was produced. Likewise, ^{t}BuC≡CH was observed to insert into **2**-H to form $(\text{silox})_2(^t\text{Bu}_3\text{SiN})\text{Ti}(E\text{-CH}{=}\text{CH}^t\text{Bu})$ (**2**-*E*-$\text{CH}{=}\text{CH}^t\text{Bu}$) but subsequent elimination of $^t\text{BuCH}{=}\text{CH}_2$ followed by [2+2] addition of ^{t}BuC≡CH to the imide of **3** rendered this an unattractive synthetic pathway (eqs 15−17).

$$\underset{\textbf{2}\text{-H}}{(\text{silox})_2(^t\text{Bu}_3\text{SiNH})\text{TiH}} + \text{RC}{\equiv}\text{CH} \xrightarrow[25\ ^\circ\text{C}]{C_6D_{12}} (\text{silox})_2(^t\text{Bu}_3\text{SiNH})\text{TiCH}{=}\text{CHR} \quad (15)$$

R = H (**2**-Vy), ^{t}Bu (**2**-*E*-$\text{CH}{=}\text{CH}^t\text{Bu}$)

$$(\text{silox})_2(^t\text{Bu}_3\text{SiNH})\text{TiCH}{=}\text{CHR} \xrightarrow[25\ ^\circ\text{C}]{C_6D_{12}} [(\text{silox})_2\text{Ti}{=}\text{NSi}^t\text{Bu}_3] + \text{H}_2\text{C}{=}\text{CHR} \quad (16)$$

R = H (**2**-Vy), ^{t}Bu (**2**-*E*-$\text{CH}{=}\text{CH}^t\text{Bu}$)

3

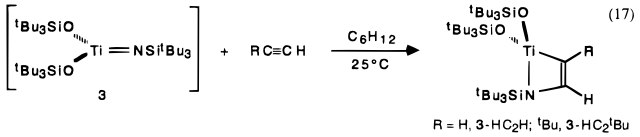

(17)

A crude estimate of the rate constant, $k_{\text{Vy-}^t\text{Bu}}$, for $\text{H}_2\text{C}{=}\text{CH}^t\text{Bu}$ loss from **2**-*E*-$\text{CH}{=}\text{CH}^t\text{Bu}$ is $7(4) \times 10^{-4}\ \text{s}^{-1}$, roughly 3 times faster than ethylene loss from **2**-Vy.

2. Adducts (silox)$_2$LTi=NSi^{t}Bu$_3$ (3-L). Adducts $(\text{silox})_2\text{LTi}{=}\text{NSi}^t\text{Bu}_3$ (**3**-L, L = OEt_2, THF, NMe_3, NEt_3, py, PMe_3) were synthesized by allowing any **2**-R species to stand in the appropriate donor solvent or solvent mixture for longer than 5 half-lives for RH elimination. In the case of ethereal adducts, stirring **2**-R, typically **2**-Me, in neat solvent afforded crude **3**-L (L = OEt_2 (**3**-OEt_2), THF (**3**-THF)), which could be purified by recrystallization from hexanes (eq 18). Adducts of pyridine,

$$\underset{\textbf{2}\text{-R}}{(\text{silox})_2(^t\text{Bu}_3\text{SiNH})\text{TiR}} \xrightarrow[25\ ^\circ\text{C}]{\text{L}} \underset{\textbf{3}\text{-L}}{(\text{silox})_2\text{LTi}{=}\text{NSi}^t\text{Bu}_3} + \text{RH} \quad (18)$$

L: OEt_2, 69%; THF, 40%

tertiary amines, and PMe_3 were synthesized in the same manner, except that a hexanes/L mixture was used as solvent (eq 19).

$$\underset{\textbf{2}\text{-R}}{(\text{silox})_2(^t\text{Bu}_3\text{SiNH})\text{TiR}} \xrightarrow[25\ ^\circ\text{C}]{\text{L, hexanes or } C_6D_{12}} \underset{\textbf{3}\text{-L}}{(\text{silox})_2\text{LTi}{=}\text{NSi}^t\text{Bu}_3} + \text{RH} \quad (19)$$

L: py, 66%; PMe_3, 48%; NMe_3; NEt_3

Donor adducts **3**-L were various shades of yellow and were extremely soluble in hydrocarbon solvents, which hampered their isolation. Trialkylamine adducts **3**-NR_3 (R = Me, Et) were only prepared (>90%) on an NMR (Table 1) tube scale in C_6D_{12}, and **3**-NEt_3 was markedly less soluble than the other **3**-L compounds, perhaps because the ethyls of NEt_3 interlock with the ^{t}Bu groups.

3. [2+2] Adducts (silox)$_2$(^{t}Bu$_3$SiN)TiCR=CR′ (3-RC$_2$R′). Azametallacyclobutenes[26,37−42] were formed by allowing **2**-R to eliminate RH in the presence of alkynes, similar to the synthesis of **3**-L. Typically, **2**-Me was allowed to stir in the presence of 1−3 equiv of alkyne (HC≡CH, MeC≡CMe,

(36) Collman, J. P.; Hegedus, L. S.; Norton, J. R.; Finke, R. G. *Principles and Applications of Organotransition Metal Chemistry*; University Science Books: Mill Valley, CA, 1987.
(37) Walsh, P. J.; Hollander F. J.; Bergman, R. G. *J. Am. Chem. Soc.* **1988**, *110*, 8729−8731.
(38) Walsh, P. J.; Carney, M. J.; Bergman, R. G. *J. Am. Chem. Soc.* **1991**, *113*, 6343−6345.
(39) (a) Walsh, P. J.; Baranger, A. M.; Bergman, R. G. *J. Am. Chem. Soc.* **1992**, *114*, 1708−1719. (b) Baranger, A. M.; Walsh, P. J.; Bergman, R. G. *Ibid.* **1993**, *115*, 2753−2763. (c) Meyer, K. E.; Walsh, P. J.; Bergman, R. G. *J. Am. Chem. Soc.* **1995**, *117*, 974−985.
(40) de With, J.; Horton, A. D.; Orpen, A. G. *Organometallics* **1993**, *12*, 1493−1496.
(41) (a) McGrane, P. L.; Jensen, M.; Livinghouse, T. *J. Am. Chem. Soc.* **1992**, *114*, 5459−5460. (b) Bryan, J. C.; Burrell, A. K.; Miller, M. M.; Smith, W. H.; Burns, C. J.; Sattelberger, A. P. *Polyhedron* **1993**, *12*, 1769−1777.
(42) Doxsee, K. M.; Farahi, J. B.; Hope, H. *J. Am. Chem. Soc.* **1991**, *113*, 8889−8898.

EtC≡CEt, ^{t}BuC≡CH) in hexanes (eq 20). Only the 2-butyne

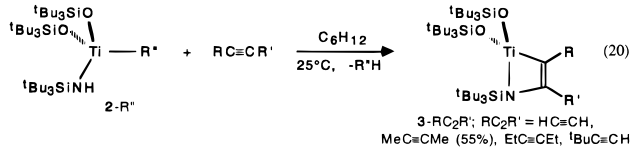

(20)

[2+2] adduct was isolated in 55% yield upon crystallization from hexanes, but all the adducts were generated numerous times on an NMR tube scale and characterized by ^{1}H and ^{13}C{^{1}H} NMR spectroscopy. These complexes appear to have more rigidity and/or steric congestion than the other species as evidenced by broad ^{t}Bu resonances in their ^{1}H and ^{13}C{^{1}H} NMR spectra; however, when **3**-MeC$_2$Me was heated to 100 °C in the NMR spectrometer probe, no tendency toward coalescence of the alkyne methyls was noted. The azametallacyclobutenes are dark burgundy in color and were previously noted as byproducts in the attempted insertion of alkynes into **2**-H (eqs 15−17). Unlike related oxametallacyclobutenes reported by Polse *et al.*,[43] which were observed in equilibrium with hydroxide acetylides, no evidence for the acetylide amide isomers of **3**-HC$_2$H and **3**-HC$_2$^{t}Bu (e.g., (silox)$_2$(^{t}Bu$_3$SiNH)-TiC≡CR, R = H, ^{t}Bu) was obtained, and they are considered to be ≥2.7 kcal/mol[44] endoergic with respect to the azametallacycles.

4. (silox)$_2$Ti═NSi^{t}Bu$_3$ (3) and C$_2$H$_4$. Trapping of thermally generated (silox)$_2$Ti═NSi^{t}Bu$_3$ (**3**, eq 8) by ∼2 equiv of ethylene (eqs 21 and 22) afforded the azametallacyclobutane (^{t}Bu$_3$SiO)$_2$-

$$[(\text{silox})_2\text{Ti}{=}\text{NSi}^t\text{Bu}_3] + \text{H}_2\text{C}{=}\text{CH}_2(\text{excess}) \xrightarrow[25\ ^\circ\text{C}]{C_6H_{12}}$$
$$\mathbf{3}$$
$$(\text{silox})_2(^t\text{Bu}_3\text{SiNH})\text{TiCH}{=}\text{CH}_2\ (\mathbf{2}\text{-Vy}) +$$
$$(^t\text{Bu}_3\text{SiO})_2(^t\text{Bu}_3\text{SiN})\text{TiCH}_2\text{CH}_2\ (\mathbf{3}\text{-C}_2\text{H}_4) \quad (21)$$

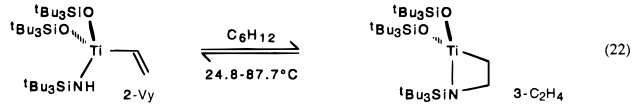

(22)

(^{t}Bu$_3$SiN)TiCH$_2$CH$_2$ (**3**-C$_2$H$_4$) and (silox)$_2$(^{t}Bu$_3$SiNH)TiCH═CH$_2$ (**2**-Vy), which was independently prepared via eq 4.[45] At early conversion of **2**-R to **3**, the product ratio for **3**-C$_2$H$_4$:**2**-Vy of 92:8 translated to a kinetic preference for [2+2] addition of ethylene to **3** versus C−H activation of $\Delta\Delta G^{\ddagger}_{addn} = -1.4$ kcal/mol. The ratio **3**-C$_2$H$_4$:**2**-Vy was redetermined at equilibrium to be 87:13 at 25 °C, corresponding to $\Delta G° = -1.2$ kcal/mol for eq 23. A van't Hoff analysis of the equilibrium constants determined over a 24.8−87.7 °C range for this reaction gave $\Delta H° = -5.72(11)$ kcal/mol and $\Delta S° = -15.2(3)$ eu.

NMR spectra of **3**-C$_2$H$_4$ exhibited the expected ^{t}Bu resonances and broad singlets at δ 3.08 (^{1}H) and δ 50.04 (^{13}C{^{1}H}, J_{CH} = 146.5 Hz) corresponding to the methylenes of the azametallacycle. In methylcyclohexane-d_{14}, the δ 3.09 resonance at 20 °C split into two multiplets at δ 2.57 and 3.60 when cooled to −130 °C, and line shape analysis of this fluxional process (−130 to +20 °C, $\Delta G^{\ddagger}$ (25 °C) = 8.9(10) kcal/mol) revealed a significant activation enthalpy of $\Delta H^{\ddagger} = 7.9(4)$ kcal/mol and small activation entropy of $\Delta S^{\ddagger} = -3(2)$ eu. The activation parameters were unchanged with 10 equiv of ethylene present, and no involvement of the free olefin was spectroscopically detected below 20 °C. The simplest dynamic process that renders the methylenes equivalent is ethylene rotation, and disruption of Ti═N(dπ/pπ)→C═C(pπ*) bonding, depicted in the azametallacycle as formal Ti−C and C−N bonds, is incurred regardless of pathway. Some TiO(dπ/pπ)→C═C(pπ*) backbonding could help mitigate olefin rotation, but the TiO π-bonding orbitals are so low in energy with respect to the π*-orbital of ethylene that significant stabilization is unlikely. Total loss of π-interaction leaves the ethylene bound solely by the corresponding C═C(π^b)→Ti(dσ) σ-bond to the d^0 metal center, and previous estimates place its binding enthalpy at ∼11 kcal/mol and free energy at ∼9 kcal/mol.[24]

Examples of azametallacyclobutanes such as **3**-C$_2$H$_4$ have surfaced in recent years. Horton *et al.* reported that treatment of (^{t}Bu$_3$SiNH)(Et$_2$O)V(═NSi^{t}Bu$_3$)$_2$ with ethylene resulted in displacement of ether and formation of (^{t}Bu$_3$SiNH)(^{t}Bu$_3$SiN)-VCH$_2$CH$_2$NSi^{t}Bu$_3$,[40] which exhibited ethylene fluxionality and slowly converted to the vinyl complex (^{t}Bu$_3$SiNH)$_2$(^{t}Bu$_3$SiN)-VCH═CH$_2$. Exposure of Cp$_2$Zr═N^{t}Bu(THF) to excess C$_2$H$_4$ and norbornene led to displacement of THF and formation of azazirconacyclobutanes, according to Bergman *et al.*[26] Rotation of the ethylene fragment of Cp$_2$^{t}BuNZrCH$_2$CH$_2$ was proposed to account for a fluxional process that equilibrated the methylenes (∼12−13 kcal/mol at 250 K) without exchange with free ethylene. An X-ray crystal structure of the norbornene adduct revealed a *d*(Zr−N) of 2.013(3) Å, slightly shorter than a typical zirconium−amide bond distance (e.g., Cp$_2$Zr(NH^{t}Bu)(3,5-Cl$_2$C$_6$H$_3$), *d*(Zr−N) = 2.060(3) Å),[27]and a normal *d*(Zr−C) of 2.241(3) Å[46] that corroborates the azametallacyclobutane depiction.

Olefin complexes of d^0 metals are expected to have low stability because of the lack of M(dπ)→C═C(π*) bonding, but some examples of olefins bound to formally d^0 metals have been reported. Kress and Osborn[47] found spectroscopic evidence for a W(VI) alkylidene−cycloheptene complex, alternatively described as a disrupted metallacyclobutane derivative, that displays fluxionality related to the azametallacycles above (e.g., $\Delta G^{\ddagger}_{rot}$(240 K) = 10.6(1) kcal/mol). More recently, Jordan *et al.*[48] and Casey and Hallenback[49] found structural and spectroscopic evidence, respectively, of pendant olefins binding purely via σ-interactions to d^0 metal centers (e.g., [Cp$_2$Zr(OCMe$_2$(CH$_2$)$_2$-CH═CH$_2$)][MeB(C$_6$F$_5$)$_3$],[48] Cp*$_2$Y(CH$_2$CH$_2$CMe$_2$CH═CH$_2$))[49] directly related to Ziegler−Natta systems.[50,51]

Molecular Structures. 1. (^{t}Bu$_3$SiO)$_2$(^{t}Bu$_3$SiNH)Ti-CH$_2$CH$_2$^{t}Bu (2-^{neo}Hex). After a struggle to obtain X-ray-quality crystals of **2**-Me, **2**-Bz, and several other alkyl derivatives, a single-crystal X-ray structural study (Table 2) of (^{t}Bu$_3$SiO)$_2$(^{t}Bu$_3$SiNH)TiCH$_2$CH$_2$^{t}Bu (**2**-^{neo}Hex) confirmed its constitution and geometry, as the molecular view in Figure 1

(43) Polse, J. L.; Andersen, R. A.; Bergman, R. G. *J. Am. Chem. Soc.* **1995**, *117*, 5393−5394.

(44) Assuming ≥1% of (silox)$_2$(^{t}Bu$_3$SiNH)TiC≡CR (**2**-C≡CR) could be observed by NMR spectroscopy relative to **3**-HC$_2$R, at 24.8 °C, $\Delta G° \geq RT \ln\{0.01/1-0.01\} \geq 2.7$ kcal/mol.

(45) Note the parallels to late-metal systems in: (a) Stoutland, P. O.; Bergman, R. G. *J. Am. Chem. Soc.* **1988**, *110*, 5732−5744. (b) Bell, T. W.; Brough, S. A.; Partridge, M. G.; Perutz, R. N.; Rooney, A. D. *Organometallics* **1993**, *12*, 2933−2941.

(46) Cardin, D. J.; Lappert, M. F.; Raston, C. L. *Chemistry of Organo-Zirconium and -Hafnium Compounds*; Ellis Horwood Limited: New York, 1986.

(47) Kress, J.; Osborn, J. A. *Angew. Chem., Int. Ed. Engl.* **1992**, *31*, 1585−1587.

(48) Wu, Z.; Jordan, R. F.; Petersen, J. L. *J. Am. Chem. Soc.* **1995**, *117*, 5867−5868.

(49) Casey, C. P.; Hallenbeck, S. L.; Pollock, D. W.; Landis, C. R. *J. Am. Chem. Soc.* **1995**, *117*, 9770−9771.

(50) Jordan, R. F. *Adv. Organomet. Chem.* **1991**, *32*, 325−387.

(51) Marks, T. J. *Acc. Chem. Res.* **1992**, *25*, 57−65.

Table 2. Crystallographic Data for Orthorhombic (^{t}Bu$_3$SiO)$_2$(^{t}Bu$_3$SiNH)TiCH$_2$CH$_2$^{t}Bu (**2**-^{neo}Hex) and (silox)$_2$Ti=NSi^{t}Bu$_3$(THF) (**3**-THF)

	2-^{neo}Hex	**3**-THF
formula	$C_{42}H_{94}NO_2Si_3Ti$	$C_{40}H_{89}NO_3Si_3Ti$
fw	777.35	764.29
space group:	*Pnma*	*Pbca*
λ, Å	0.7107	0.908
a, Å	18.445(10)	17.319(3)
b, Å	19.375(12)	25.447(5)
c, Å	14.200(14)	41.861(8)
V, Å^3	5075(7)	18449(6)
T, K	293(2)	165(5)
Z	4	16
ρ_{calc}, g/cm^3	1.017	1.101
μ, mm^{-1}	0.269	0.297
R [$I > 2\sigma(I)$]	0.1388	0.0637
R_w^2 [$I > 2\sigma(I)$]	0.2838	0.1749
GOF	1.397	0.972

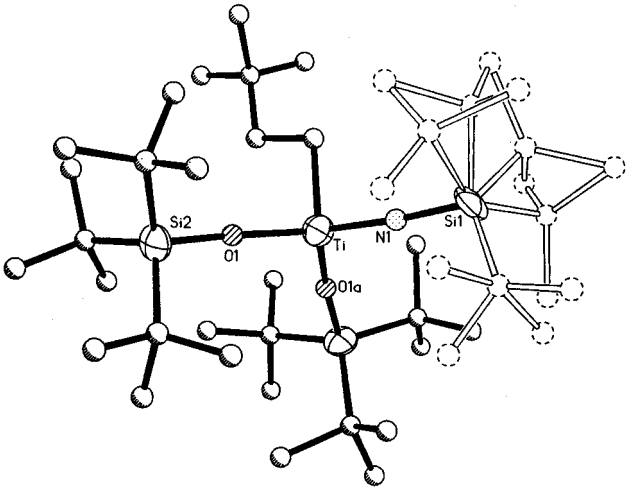

Figure 1. Molecular view of (silox)$_2$(^{t}Bu$_3$SiNH)TiCH$_2$CH$_2$^{t}Bu (**2**-CH$_2$CH$_2$^{t}Bu) showing a nonagostic neohexyl group (d(Ti−C) = 2.09(3) Å, ∠Ti−C−C = 111(2)°) and ^{t}Bu$_3$Si disorder. The silox and ^{t}Bu$_3$SiNH groups cannot be differentiated.

indicates. Although crystallographic C_s symmetry is enforced on the molecule, the structure solution exhibits severe disorder in the periphery of the ^{t}Bu$_3$SiX (X = O, NH) ligand on the mirror plane. Further unresolved disorder of the ^{t}Bu$_3$SiX ligands is likely, on the basis of the unusual discrepancy between the U_{iso} for O (U_{iso} = 69(5) Å^2) and N (U_{iso} = 10(6) Å^2); consequently, the amide and silox groups cannot be confidently distinguished. The pseudotetrahedral geometry possessed by **2**-^{neo}Hex (∠O−Ti−O/N = 115.7(24)° average, ∠C−Ti−O/N = 102.1(6)° average) reflects greater steric interactions among the ^{t}Bu$_3$Si-containing ligands. No evidence of an agostic interaction is evident, as judged by the normal Ti−C−C angle of 111(2)° and standard Ti−C bond length of 2.09(3) Å, which is comparable to the Ti−CH$_3$ bond distance in [(^{t}Bu$_3$CO)TiMe$_2$]-(μ-OMe)$_2$ of 2.063(10) Å.[52]

2. (^{t}Bu$_3$SiO)$_2$(THF)Ti=NSi^{t}Bu$_3$ (3-THF). A single-crystal X-ray structural determination of (^{t}Bu$_3$SiO)$_2$(THF)Ti=NSi^{t}Bu$_3$ (**3**-THF) revealed an asymmetric unit (Table 2, Figure 2) composed of two molecules that have essentially identical, slightly distorted tetrahedral geometries. To conclusively establish whether a silox/imide disorder, similar to the silox/amide disorder of **2**-^{neo}Hex, was problematic to **3**-THF, a high-quality data set was collected at 165(5) K using synchrotron radiation after conventional Mo Kα and Cu rotating-anode data sets failed to resolve the issue. Diffraction to better than 0.8 Å was observed, and data to 0.85 Å were used in a successful solution, resulting in a statistical distinction between d(Ti−N) and d(Ti−O).

One molecule (**A**) has a disordered THF and the other a disordered ^{t}Bu group (**B**), as the molecular views in Figure 2 illustrate, but common bond distances and angles are within error. Greater repulsion among the silox and imide ligands again accounts for the slightly distorted tetrahedral geometry of **3**-THF: ∠O$_{THF}$−Ti−(N/O) = 101.9(19)° average, ∠O−Ti−(N/O) = 115.9° average. The Ti−N−Si (173.0(27)° average) and Ti−O−Si (172.1(36)° average) angles are essentially identical, while the titanium−imide bond lengths (d(Ti−N) = 1.772(3), 1.783(3) Å) are significantly shorter than the silox Ti−O bonds of 1.824(4) Å (average), which are comparable to those of (silox)$_3$TiNH$_2$ (d(Ti−O) = 1.815 Å average).[53] Nearly linear M−O−Si linkages are normally observed,[54] and the similar imide linkage reflects the cylindrical symmetry imposed by pseudotetrahedral coordination of four potential π-donors, even though N(pπ) → Ti(dπ) donation is moderate since the d(Ti−N) is long relative to those of other complexes, which exhibit titanium−imide distances from 1.672 to 1.723 Å.[32]

The Lewis acidity possessed by (silox)$_2$Ti=NSi^{t}Bu$_3$ (**3**), localized in its vacant d_{z^2}/p_z (z-axis ⊥ to the ligand plane) hybrid orbital, plays the crucial role in capturing L or the pair of electrons in a C−H bond. Provided **3**-THF can be considered a rough model of the transient responsible for C−H bond activation, either **3** or the related hydrocarbon adduct (silox)$_2$-(RH)Ti=NSi^{t}Bu$_3$ (**3**-RH), its long Ti=N bond length may signify the availability of a nitrogen lone pair to function as an internal base in the 1,2-RH-addition process. In the related zirconium-based C−H bond activation system, a similar conclusion was applied to (^{t}Bu$_3$SiNH)$_2$(THF)Zr=NSi^{t}Bu$_3$,[20] whose d(Zr=N) of 1.978(8) Å was ∼0.1 Å longer than expected. The zirconium derivative also contains a d(Zr−O$_{THF}$) of 2.229(7) Å, which is slightly longer than the d(Ti−O$_{THF}$) of 2.037(1) Å corresponding to **3**-THF, once a 0.13 Å correction for differing covalent radii is applied. Although THF adducts of other titanium imides are not available for comparison, the bond lengths of the zirconium derivative and related congeners suggest that the O$_{THF}$(pπ)→Ti(dπ) interaction is minimal in **3**-THF, despite a favorable π-bonding orientation featuring a relatively flat THF (∠Ti−O−C = 124.8(24)° average) roughly aligned with the Ti=N vector.

Kinetics of 1,2-RH-Elimination. 1. Rate Expression. Monitoring by ^{1}H NMR spectroscopy revealed that thermolysis of (silox)$_2$(^{t}Bu$_3$SiNH)TiR (**2**-R) in benzene-d_6 produced RH and (silox)$_2$(^{t}Bu$_3$SiND)TiC$_6$D$_5$ (**2**-(ND)-C$_6$D$_5$), consistent with the following mechanism:

$$\underset{\textbf{2}\text{-R}}{(\text{silox})_2(^t\text{Bu}_3\text{SiNH})\text{TiR}} \xrightarrow[C_6D_6]{k_R(\text{elim})} \underset{\textbf{3}}{(\text{silox})_2\text{Ti}{=}\text{NSi}^t\text{Bu}_3} + \text{RH} \quad (23)$$

$$\textbf{3} \xrightarrow[C_6D_6]{k_{PhD}(\text{addn})} \underset{\textbf{2}\text{-(ND)-}C_6D_5}{(\text{silox})_2(^t\text{Bu}_3\text{SiND})\text{TiC}_6\text{D}_5} \quad (24)$$

$$\textbf{3} \xrightarrow[C_6D_6]{k_L(\text{trap})} \underset{\textbf{3}\text{-L}}{(\text{silox})_2\text{LTi}{=}\text{NSi}^t\text{Bu}_3} \quad (25)$$

Rate-determining loss of RH generated transient (silox)$_2$-Ti=NSi^{t}Bu$_3$ (**3**, eq 23), which was scavenged via C−D bond

(52) Lubben, T. V.; Wolczanski, P. T. *J. Am. Chem. Soc.* **1987**, *109*, 424−435.

(53) Mass, J. L.; Wolczanski, P. T. Unpublished results.

(54) Wolczanski, P. T. *Polyhedron* **1995**, *14*, 3335−3362 and references therein.

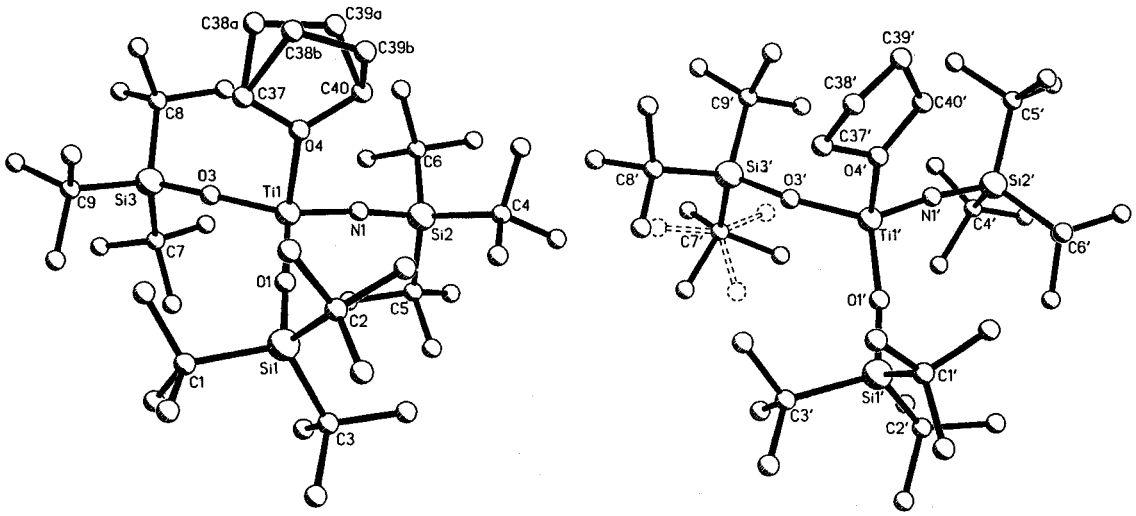

Figure 2. Molecular views of two independent molecules of (silox)$_2$(THF)Ti=NSi^{t}Bu$_3$ (**3**-THF), one exhibiting THF backbone disorder and the other (primed) revealing ^{t}Bu group disorder. Pertinent interatomic distances (Å) and angles (deg): Ti1−N1, 1.772(3); Ti1′−N1′, 1.783(3); Ti−OSi$_{av}$, 1.824(4); Ti−O(THF)$_{av}$, 2.037(3); N−Si$_{av}$, 1.684(3); O−Si$_{av}$, 1.644(3); N1−Ti1−O1, 114.38(12); N1′−Ti1′−O1′, 115.43(11); N1−Ti1−O3, 118.52(13); N1′−Ti1′−O3′, 116.26(11); N1−Ti1−O4, 103.17(10); N1′−Ti1′−O4′, 104.44(11); O1−Ti1−O3, 115.14(11); O1′−Ti1′−O3′, 115.54(11); O1−Ti1−O4, 103.17(10); O1′−Ti1′−O4′, 104.44(11); O3−Ti1−O4, 100.51(10); O3′−Ti1′−O4′, 99.17(10); Ti1−N1−Si2, 174.9(2); Ti1′−N1′−Si2′, 171.2(2); Ti1−O1−Si1, 175.6(2); Ti1′−O1′−Si1′, 172.9(2); Ti1−O3−Si3, 172.6(2); Ti1′−O3′−Si3′, 167.1(2); Ti1−O4−C37, 123.6(2); Ti1′−O4′−C37′, 121.5(3); Ti1−O4−C40, 126.2(2); Ti1′−O4′−C40′, 128.0(3).

activation to give **2**-(ND)-C$_6$D$_5$ (eq 24). Under these conditions, loss of RH proceeds to completion and follows first-order kinetics. The isotopically labeled product is inconsistent with a σ-bond metathesis pathway,[15] and precedent in related zirconium[20] and tantalum[23] systems suggested that the 1,2-RH-elimination/addition mechanism was operative.

Thermolysis of (silox)$_2$(^{t}Bu$_3$SiNH)TiMe (**2**-Me) at different concentrations of **2**-Me established that the reaction is first order in **2**-Me (k_{Me}(24.8 °C) ∼ 1.4 × 10^{-5} s^{-1}, Table 3). The reaction was zero order in [C$_6$D$_6$] according to experiments conducted in C$_6$D$_6$/C$_6$D$_{12}$ mixtures (24.8 °C, [C$_6$D$_6$] = 11.2 M (k_{Me} = 1.5(2) × 10^{-5} s^{-1}), 4.52 M (3(1) × 10^{-5} s^{-1}), 1.12 M (2.6(6) × 10^{-5} s^{-1}), but problems in integrating overlapping resonances rendered the rates imprecise. When the elimination was carried out in neat THF-d_8 or in C$_6$D$_6$ with 20 equiv of THF present, thereby producing (silox)$_2$(THF-d_8)Ti=NSi^{t}Bu$_3$ (**3**-THF-d_8, k_{Me} = 1.46(5) × 10^{-5}) or **3**-THF (k_{Me} = 1.54(7) × 10^{-5} s^{-1}, eqs 23 and 25), respectively, no variation in the rate constant was noted relative to neat benzene-d_6. The rate law for disappearance of **2**-Me, and by inference all remaining **2**-R conducted under the aforementioned conditions, is given in eq 26.

$$-\mathrm{d}[\mathbf{2}\text{-R}]/\mathrm{d}t = k_{obs}[\mathbf{2}\text{-R}]^1[\mathrm{trap}]^0 \qquad (26)$$

Furthermore, it is clear that solvent effects in this system are unremarkable, in corroboration of the proposed rate-determining 1,2-RH-elimination and constrained four-center transition state (Scheme 1).

2. Activation Parameters for 2-R (R = Me, ^{c}Pe, Bz). Eyring analyses were conducted for clean, first-order loss of RH from a primary alkyl (**2**-Me) and secondary alkyl (**2**-^{c}Pe) over a 24.8−71.3 °C range and for a benzylic alkyl (**2**-Bz) over a 24.8−90.2 °C range (Table 3). Similar analyses for **2**-Ph or other sp^2 (e.g., **2**-Vy) derivatives were precluded by the swiftness of their eliminations at elevated temperature. For all three species, a relatively large enthalpy of activation was observed, accompanied by a moderate, negative entropy of activation (**2**-Bz, $\Delta H^‡$ = 22.2(5) kcal/mol, $\Delta S^‡$ = −12(2) eu; **2**-Me, $\Delta H^‡$ = 20.2(12) kcal/mol, $\Delta S^‡$ = −12(4) eu; **2**-^{c}Pe, $\Delta H^‡$ = 19.6(6) kcal/mol, $\Delta S^‡$ = −12(2) eu). The activation parameters indicate significant bond-breaking occurring within a constrained, unimolecular transition state, thereby supporting the proposed 1,2-RH-elimination mechanism where amide reorganization to achieve R−Ti−N−H planarity is a critical feature.[55,56] Similar activation parameters have been observed for MeH loss from (^{t}Bu$_3$SiNH)$_3$ZrMe ($\Delta H^‡$ = 25.9(4) kcal/mol, $\Delta S^‡$ = −7(1) eu)[20] and ^{t}Bu$_3$SiNH$_2$ elimination from (^{t}Bu$_3$SiNH)$_3$TiCl ($\Delta H^‡$ = 23.3(8) kcal/mol, $\Delta S^‡$ = −11(2) eu),[22] which are processes considered 1,2-eliminations.

In order to interpret rates of 1,2-RH-elimination, it is assumed that enthalpies of activation are primarily responsible for the 3.5 kcal/mol range in observed $\Delta G^‡_{elim}$ values (22.2 (**2**-Ph) to 25.7 kcal/mol (**2**-Mes, **2**-Bz)). Disparate **2**-R (R = Me, ^{c}Pe, Bz) were chosen for the Eyring analyses in order to dispel the notion that variations in $\Delta S^‡$ could significantly affect trends in free energy of activation. It is noteworthy that three extremely different **2**-R derivatives gave essentially equal entropies of activation, yet the typical ±(2−4) eu error in $\Delta S^‡$ at 24.8 °C amounts to 0.6−1.2 kcal/mol, a lack of precision that again necessitates the assumption that activation entropies play an insignificant role in $\Delta G^‡_{elim}$ comparisons. In correlations below, it is argued that enthalpies of activation are critical to understanding the 1,2-RH-elimination rates of various **2**-R, a supposition buttressed by accompanying equilbrium studies.

3. 1,2-RH-Elimination Kinetic Isotope Effects. Loss of CH$_3$D from **2**-(ND)-Me proceeded with a large KIE at 24.8 °C (k_H/k_D = z_{Me} = 13.7(9)). A similar loss of toluene-d_1 from **2**-(ND)-Bz also exhibited a large primary KIE, which was measured at higher temperatures because of the sluggishness of the reaction. The values at 52.4 °C (z_{Bz} = 10.5(7)), 70.2 °C (z_{Bz} = 9.6(8)), and 90 °C (z_{Bz} = 5.6(2)) crudely extrapolate to a z_{Bz} near that of z_{Me} at 24.8 °C. The value obtained via loss of C$_6$H$_5$D from **2**-(ND)-Ph, z_{Ph} = 7.4(3) at 24.8 °C, is somewhat smaller in magnitude.

Large primary kinetic isotope effects are consistent with a four-center transition state in which the transfer of H from N to R is relatively linear and there are similar amounts of N−H bond-breaking and C−H bond-making character.[55,56] Support

(55) Carpenter, B. K. *Determination of Reaction Mechanisms*; Wiley-Interscience: New York, 1984.

(56) Lowry, T. H.; Richardson, K. S. *Mechanism and Theory in Organic Chemistry*, 3rd ed.; Harper and Row: New York, 1987.

for this transition state is evident from calculational studies of model systems such as $(H_2N)_3MMe$ (M = Ti, Zr, Hf)[57−60] and $(HO)_2(H_2N)TiMe$.[61] The smaller isotope effect observed for 2-Ph vs **2**-(ND)-Ph portends a less symmetric transition state for H transfer in 1,2-PhH/D-elimination (i.e., force constants that describe NH/D vs CH/D in the transition state are less similar in magnitude than those in the Me and Bz cases).

Equilibria Relating 2-R, 3-L, and 3-RCCR. ^{1}H NMR spectroscopy was used to monitor the approach to equilibrium of four types of reactions, indicated by the generic equations (27)−(30). In a typical experiment, an NMR tube was charged

$$\underset{\mathbf{2}\text{-R}}{(\text{silox})_2(^t\text{Bu}_3\text{SiNH})\text{TiR}} + \text{R}'\text{H} \rightleftharpoons \underset{\mathbf{2}\text{-R}'}{(^t\text{Bu}_3\text{SiO})_2(^t\text{Bu}_3\text{SiNH})\text{TiR}'} + \text{RH} \quad (27)$$

$$\underset{\mathbf{2}\text{-R}}{(\text{silox})_2(^t\text{Bu}_3\text{SiNH})\text{TiR}} + \text{L} \rightleftharpoons \underset{\mathbf{3}\text{-L}}{(^t\text{Bu}_3\text{SiO})_2\text{LTi}{=}\text{NSi}^t\text{Bu}_3} + \text{RH} \quad (28)$$

$$\underset{\mathbf{3}\text{-L}}{(^t\text{Bu}_3\text{SiO})_2\text{LTi}{=}\text{NSi}^t\text{Bu}_3} + \text{L}' \rightleftharpoons \underset{\mathbf{3}\text{-L}'}{(^t\text{Bu}_3\text{SiO})_2\text{L}'\text{Ti}{=}\text{NSi}^t\text{Bu}_3} + \text{L} \quad (29)$$

$$\underset{\mathbf{3}\text{-L}}{(^t\text{Bu}_3\text{SiO})_2\text{LTi}{=}\text{NSi}^t\text{Bu}_3} + \text{R}'\text{C}{\equiv}\text{CR}'' \rightleftharpoons \underset{\mathbf{3}\text{-R}'\text{C}_2\text{R}''}{(\text{silox})_2(^t\text{Bu}_3\text{SiN})\text{TiCR}'{=}\text{CR}''} + \text{L} \quad (30)$$

with **2**-R followed by addition of C_6D_{12} solvent and an excess of R′H, whose concentration was chosen to obtain a quantifiable range of K_{eq}. Convenient limits for observing equilibria were $-4 < \Delta G° < 4$ kcal/mol, although in some cases $\Delta G°$ values as high as 7.8 kcal/mol were determined.

In lieu of monitoring the approach to equilibrium from both sides of a reaction, which in some cases was unfeasible, verification of an established equilibrium was often attained via cross-checking through measurement of related, independent equilibria. As a direct consequence, each complex was linked to another via a ladder of relative standard free energies and arbitrarily set relative to **2**-^{c}Hex at 0.0 kcal/mol (Figure 3). In addition, the propagation of error was minimized by the cross-checks, which helped ensure that no single experiment having a large (but potentially unknown) systematic error could unduly skew all of the data. With all complexes in the ladder sharing a common free energy surface, each **2**-R position in the ladder marks the relative standard free energy of the complex and all other substrates (e.g., **2**-R^1 + R^2H + ... + L^1 + L^2 + ... + RC_2R' + ...). Likewise, each **3**-L position corresponds to the relative standard free energy of **3**-L^1 + R^1H + R^2H + ... + L^2 + ... + RC_2R' + ... Implicit in the energy scale is the assumption that various secondary effects, such as those derived from the medium of each individual experiment, are negligible. This assumption appears reasonable, given the covalent character of the complexes involved and the lack of evidence pertaining to significant solvent interactions, even in the aforementioned kinetic studies. The 19.1 kcal/mol ladder in Figure 3 is the result of a least-squares fit of the experimental data indicated by the arrows (see Supporting Information).

In relative terms, the least thermodynamically stable organotitanium species are the secondary alkyls **2**-^{c}Hex and **2**-^{c}Pe, followed by a host of sp^3-alkyls (^{n}Pr, ^{n}Bu, ^{neo}Hex, Et, ^{c}Bu, CH_2SiMe_3, Me) and finally the sp^2-alkyls (**2**-Ph, **2**-Vy, **2**-^{c}Pr). Two adducts of **3** (**3**-C_2H_4 and **3**-NEt_3) are less stable than the hydride **2**-H, which is in turn less stable than the remaining adducts and azametallacyclobutenes. The spread among the alkyl derivatives is only 5.5 kcal/mol, while the adducts range from azametallacyclobutane **3**-C_2H_4 at −6.7 kcal/mol to **3**-py at −19.1 kcal/mol, a range of 12.4 kcal/mol. Within the adducts, steric factors are important to relative stability. Triethylamine adduct **3**-NEt_3 is 9.0 kcal/mol less stable than the corresponding trimethyl derivative, **3**-NMe_3, and the azametallacycle derived from 2-butyne (**3**-MeC_2Me) is 4.0 kcal/mol more stable than the 3-hexyne adduct (**3**-EtC_2Et). Within the nitrogen bases, the least basic but planar and effectively smaller py ligand makes an adduct (**3**-py) that is 3.6 and 12.6 kcal/mol more stable than **3**-NMe_3 and **3**-NEt_3, respectively.

The temperature dependencies of selected equilibria were roughly determined in order to assess contributions from $\Delta S°$, which contains a factor based solely on the relative numbers of symmetry-equivalent hydrogens available for activation on the competing substrates. The statistical factor pertaining to **2**-R + R′H ⇌ **2**-R′ + RH (eq 28) may be trivially separated from the standard free energy change, yielding a corrected free energy according to eq 31. $\Delta G°_{corr}$ may be considered a "per H"

$$\Delta G°_{corr} = \Delta G° - RT\ln(W/W') \quad (31)$$

W (W') = number of equivalent H's on RH (R′H) that can be activated

standard free energy change for any given equilibrium. Van't Hoff analyses (24.8, 50.2, 70.2 °C) revealed standard entropy changes that are slightly larger in magnitude than the respective statistical contributions. For example, measurements of the **2**-Et + MeH ⇌ **2**-Me + EtH equilibrium yielded a $\Delta S°$ of −2.8(6) eu that includes −0.8 eu based on statistics. Similarly, **2**-CH_2SiMe_3 + MeH ⇌ **2**-Me + $SiMe_4$ was shown to have $\Delta S° = -6.8(24)$ eu, a value that incorporates −2.2 eu purely due to the statistics of available C−H bonds that can be activated. This equilibrium was chosen because the (trimethylsilyl)methyl group is extremely bulky and representative of **2**-R species whose entropic factors reflect this factor. The moderate $\Delta S°$ is still within 2σ of all the others, even though it is somewhat greater in magnitude. Other cases manifested even less deviation (e.g., **2**-Et + ^{c}PrH ⇌ **2**-^{c}Pr + EtH, $\Delta S° = -1.1(13)$). By inference from the selected temperature dependence studies, ground state entropic factors pertaining to each **2**-R state are also considered moderate and are deemed negligible in much of the remaining discussion. As a consequence, the standard enthalpy differences between states are considered to parallel the standard free energy differences exhibited in Figure 3.

Note that the equilibrium **3**-THF + C_2H_4 ⇌ **3**-C_2H_4 + THF is endoergic by 9.0 kcal/mol, whereas the related $Cp_2Zr{=}N^tBu(THF) + C_2H_4 \rightleftharpoons Cp_2{}^tBuNZrCH_2CH_2 + THF$ equilibrium was reported to be endoergic by only 1.6 kcal/mol at 25 °C.[26] Likewise, the displacement of ether by ethylene in $(^tBu_3SiNH)(Et_2O)V(=NSi^tBu_3)_2$ must also have a modest $\Delta G°$.[40] The dramatic difference exhibited by the titanium system is attributed to the greater electrophilicity of the group 4 bis(silox)-

(57) Cundari, T. R. *J. Am. Chem. Soc.* **1992**, *114*, 10557−10563.
(58) Cundari, T. R. *Organometallics* **1993**, *12*, 1998−2000.
(59) Cundari, T. R.; Gordon, M. S. *J. Am. Chem. Soc.* **1993**, *115*, 4210−4217.
(60) Cundari, T. R. *Organometallics* **1994**, *13*, 2987−2994.
(61) Cundari, T. R. *Organometallics* **1993**, *12*, 4971−4978.

Table 3. First-Order Rate Constants,[a] Free Energies of Activation, and Corresponding D(RH)[b] for 1,2-RH-Elimination of RH from (^{t}Bu$_3$SiO)$_2$(^{t}Bu$_3$SiNH)TiR (**2**-R) in C_6D_6, Producing (^{t}Bu$_3$SiO)$_2$(^{t}Bu$_3$SiND)TiC$_6$D$_5$ (**2**-(ND)-C$_6$D$_5$) (Exceptions Noted)

compound (solvent C_6D_6 or as noted)	$10^{-5}k$, s^{-1}	T (±0.3), °C	$\Delta G^{\ddagger}$, kcal/mol	[**2**-R], M	D(RH) kcal/mol
(silox)$_2$(^{t}Bu$_3$SiNH)TiCH$_2$C$_6$H$_3$Me$_2$ (**2**-Mes)	0.0872(7)	24.8	25.7	0.037	88.5(15)
(silox)$_2$(^{t}Bu$_3$SiNH)TiCH$_2$Ph (**2**-Bz)	0.086(6)[c]	24.8	25.7	0.038	88.5(15)
	2.26(5)[c,d]	52.4		0.038	
	17(1)[c,d]	70.2		0.037	
	92(2)[c,d]	90.2		0.032	
(silox)$_2$(^{t}Bu$_3$SiND)TiCH$_2$Ph (**2**-(ND)-Bz)	0.21(1)[d]	52.4		0.041	
	1.80(5)[d]	70.2		0.032	
	16.3(5)[d]	90.2		0.032	
(silox)$_2$(^{t}Bu$_3$SiNH)TiH (**2**-H)	0.58(5)[e]	24.8	24.6	0.045	104.2(1)
(silox)$_2$(^{t}Bu$_3$SiNH)TiCH$_3$ (**2**-Me)	1.54(10)[f]	24.8	24.0	0.041	104.9(1)
	1.42(7)	24.8		0.023	
	1.3(2)[g]	24.8		0.005	
	4.9(7)[f]	35.1		0.042	
	30(2)[f]	50.2		0.041	
	79(6)[f]	63.6		0.041	
	170(20)[f]	71.3		0.040	
2-Me in THF-d_8; product **3**-THF-d_8	1.46(5)[h]	24.8		0.05	
	1.5(2)[i]	24.8		0.05	
(**2**-Me in C_6D_{12}, [C_6D_6] = 4.52 M)	3(1)[i,j]	24.8		0.05	
(**2**-Me in C_6D_{12}, [C_6D_6] = 1.12 M)	2.6(6)[i,k]	24.8		0.05	
	1.54(7)[d,l]	24.8		0.049	
(silox)$_2$(^{t}Bu$_3$SiND)TiCH$_3$ (**2**-(ND)-Me)	0.112(6)[d,l]	24.8		0.045	
(silox)$_2$(^{t}Bu$_3$SiNH)TiCH$_2$CH$_2$^{t}Bu (**2**-^{neo}Hex)	1.71(8)	24.8	23.9	0.02	99.9(15)
(silox)$_2$(^{t}Bu$_3$SiNH)TiCH$_2$CH$_3$ (**2**-Et)	1.86(10)	24.8	23.9	0.042	101.1(4)
(silox)$_2$(^{t}Bu$_3$SiNH)TiCH$_2$(CH$_2$)$_2$CH$_3$ (**2**-^{n}Bu)	2.05(3)	24.8	23.8	0.04	99.9(19)
(silox)$_2$(^{t}Bu$_3$SiNH)Ti-c-C$_4$H$_7$ (**2**-^{c}Bu)	2.13(8)	24.8	23.8	0.04	96.5(10)
(silox)$_2$(^{t}Bu$_3$SiNH)Ti-c-C$_5$H$_9$ (**2**-^{c}Pe)	4.6(2)[m]	24.8	23.4	0.040	94.4(10)
	25(2)[m]	40.4		0.019	
	70(1)[m]	50.5		0.020	
	174(4)[m]	60.0		0.018	
	434(12)[m]	70.9		0.019	
(silox)$_2$(^{t}Bu$_3$SiNH)Ti-c-C$_6$H$_{11}$ (**2**-^{c}Hex)	8.8(6)	24(1)	23.0	0.04	95.6(10)
(silox)$_2$(^{t}Bu$_3$SiNH)Ti-c-C$_3$H$_5$ (**2**-^{c}Pr)	11.6(5)	24.8	22.8	0.042	106.3(3)
(silox)$_2$(^{t}Bu$_3$SiNH)TiCH=CH$_2$ (**2**-Vy)	23.9(4)	25(1)	22.4	0.043	111.2(8)
(silox)$_2$(^{t}Bu$_3$SiNH)TiC$_6$H$_5$ (**2**-Ph)	33.3(3)[n]	25.1	22.2	0.02	113.5(5)
(silox)$_2$(^{t}Bu$_3$SiND)TiC$_6$H$_5$ (**2**-(ND)-Ph)	6.7(8)[n]	24.8		0.02	

[a] Determined from nonlinear least-squares fitting of the differential form of the rate expression. For details regarding the individual experiments, consult the Experimental Section. [b] D(RH) values are from ref 62. [c] Values used in the Eyring plot (24.8−90.2 °C) obtained from triplicate runs. From a weighted nonlinear least-squares fit of the data: $\Delta H^{\ddagger}$ = 22.2(5) kcal/mol, $\Delta S^{\ddagger}$ = −12(2) eu. [d] Tandem measurements for obtaining the primary isotope effect: k_H/k_D(PhCH$_2$H/D loss) = 10.5(7) (52.4 °C), 9.6(8) (70.2 °C), 5.6(2) (90.2 °C); k_H/k_D(MeH/D loss) = 13.7(9). [e] Obtained from the instantaneous rate determined at early conversion. [f] Values used in the Eyring plot (24.8−71.3 °C) obtained from triplicate runs. From a weighted nonlinear least-squares fit of the data: $\Delta H^{\ddagger}$ = 20.2(12) kcal/mol, $\Delta S^{\ddagger}$ = −12(4) eu. [g] Obtained from dilution of a 0.017 M stock solution. [h] Compare to MeH loss from **2**-Me in C_6D_6; k(THF-d_8)/k(C_6D_6) = 0.95(7). [i] C_6D_6 and C_6D_6/C_6D_{12} runs conducted in parallel. [j] 90 equiv of C_6D_6. [k] 22 equiv of C_6D_6. [l] Conducted with 20 equiv of THF (product **3**-THF) for the purposes of obtaining k_H/k_D; note that k_{Me}(20 equiv THF)/k_{Me}(C_6D_6) = 1.00(8). [m] Values used in the Eyring plot (24.8−70.9 °C) obtained from triplicate runs. From a weighted nonlinear least-squares fit of the data: $\Delta H^{\ddagger}$ = 19.6(6) kcal/mol, $\Delta S^{\ddagger}$ = −13(2) eu. [n] Measurements used in determination of the primary isotope effect: k_H/k_D (PhH/D loss) = 7.4(3).

(amide)metal center in comparison to the later, less electropositive vanadium and metal centers ligated by better e$^-$-donors (e.g., Cp, imide). Steric factors also mitigate O(pπ)→Zr(dπ) bonding in Cp$_2$Zr=N^{t}Bu(THF).

Thermochemistry. 1. Relative *D*(TiR). The equilibria describing the interconversion of the **2**-R derivatives (eq 28) were used to determine relative Ti−R bond strengths. With some assumptions, the ΔH_{reacn} for eq 27 is dependent on the differences of the relative titanium−carbon and carbon−hydrogen bond strengths according to eq 32. The aforementioned statistical correction (eq 31) is included, but other entropic factors contributing to the free energies are assumed to be negligible or cancel, as implied by the temperature dependence studies. Likewise, enthalpic contributions such as heats of solvation of the various **2**-R and R′H are assumed to be negligible or cancel, as in previous cases.[20,23] With D(TiBz) arbitrarily chosen as a reference, the various relative titanium−carbon bond strengths corresponding to (silox)$_2$(^{t}Bu$_3$SiNH)TiR (**2**-R, eq 33) were compiled and plotted relative to the absolute D(RH) of the corresponding hydrocarbons, as shown in Figure 4.

$$\Delta H^{\circ}_{reacn} \approx [D(\mathrm{R'H}) - D(\mathrm{RH})] + [D(\mathrm{TiR}) - D(\mathrm{TiR'})] \quad (32)$$

$$D(\mathrm{TiR})_{rel} = [D(\mathrm{TiR}) - D(\mathrm{TiBz})] = \Delta H^{\circ}_{reacn} + [D(\mathrm{RH}) - D(\mathrm{BzH})] \quad (33)$$

Figure 4 displays a generally strong correlation of D(TiR)$_{rel}$ with D(RH)[62] (slope = 1.1, r = 0.95) that improves measurably when the R = Bz, Mes, H, and Ph points are removed (slope = 1.36, r = 0.995). Other researchers have noted a roughly linear correlation between D(RH) and D(L$_n$M−R) for disparate organometallic systems.[63−70] Its existence typically implies strong metal−carbon bonding and minimal involvement of

(62) (a) Berkowitz, J.; Ellison, G. B.; Gutman, D. *J. Phys. Chem.* **1994**, *98*, 2744−2765 and references therein. (b) Davico, G. E.; Bierbaum, V. M.; DePuy, C.H.; Ellison, G. B.; Squires, R. R. *J. Am. Chem. Soc.* **1995**, *117*, 2590−2599. (c) Martinho Simões, J. A.; Beauchamp, J. L. *Chem. Rev.* **1990**, *90*, 629−688. (d) D(H^{c}Pr): Baghal-Vayjooee, M. H.; Benson, S. W. *J. Am. Chem. Soc.* **1979**, *101*, 2838−2840. (e) D(H^{c}Bu): *CRC Handbook of Chemistry and Physics*, 75th ed.; CRC Press: Boca Raton, FL, 1994. (f) D(H^{neo}Hex) assumed to equal D(HBu). (g) D(HMes) assumed to equal D(HBz).

(63) Bryndza, H. E.; Fong, L. K.; Paciello, R. A.; Tam, W.; Bercaw, J. E. *J. Am. Chem. Soc.* **1987**, *109*, 1444−1456.

(64) Bryndza, H. E.; Domaille, P. J.; Tam, W.; Fong, L. K.; Paciello, R. A.; Bercaw, J. E. *Polyhedron* **1988**, *7*, 1441−1452.

(65) Bulls, A. R.; Bercaw, J. E.; Manriquez, J. M.; Thompson, M. E. *Polyhedron* **1988**, *7*, 1409−1428.

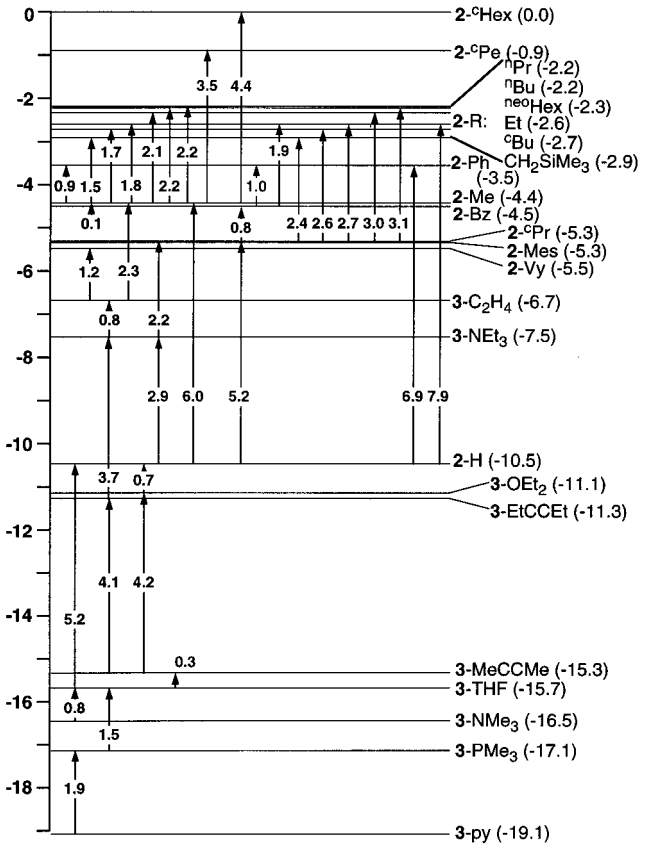

Figure 3. Ladder of standard free energies accorded hydrocarbyl (and hydride) states **2**-R, adduct states **3**-L, and metallacyclic states **3**-RC_2R' and **3**-C_2H_4, as defined in the text. (silox)$_2$(^{t}Bu$_3$SiNH)Ti^{c}Hex (**2**-^{c}Hex) was chosen as the reference state, hence each $\Delta G°$ in parentheses refers to the value for **2**-^{c}Hex + RH/L/RC_2R' + ... ⇌ **2**-R/**3**-RC_2R'/**3**-L + ^{c}HexH + ... These optimized values are derived from a least-squares fit of individual equilibria indicated by the arrows and listed in Supporting Information.

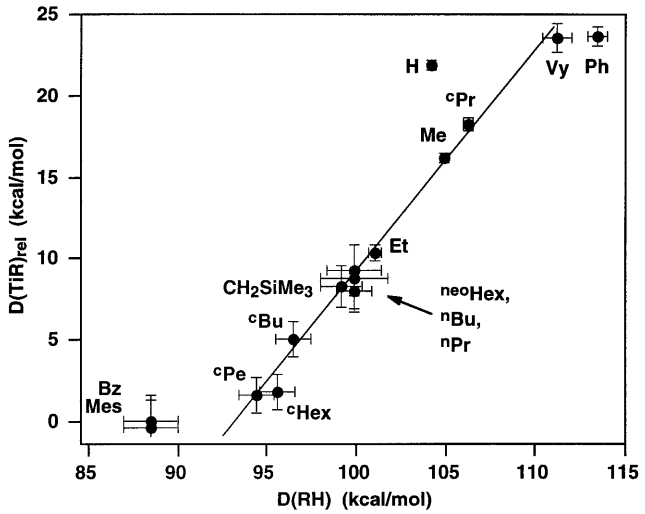

Figure 4. Relative Ti−C bond strengths (kcal/mol) in (silox)$_2$(^{t}Bu$_3$SiNH)TiR (**2**-R) versus the C−H bond strength of the corresponding hydrocarbon.[62] $D(\mathrm{TiR})_{rel} = D(\mathrm{TiR}) - D(\mathrm{TiBz})$ as in eq 33, with $\Delta H°_{reacn}$ estimated from $\Delta G°_{corr}$ (eq 31) as explained in the text. The line (slope = 1.36, $r = 0.9953$) is a least-squares fit to the points except Bz, Mes, H, and Ph. A least-squares line to all points had a slope of 1.1 (r = 0.95).

secondary effects; consequently, deviations from linearity may suggest that lesser effects (e.g., steric,[71] π-bonding, agostic,[72] etc.) may be operative. Note that the sp^3-centers, excluding benzylic bonds and adding the sp^2-like cyclopropyl and sp^2-vinyl, comprise a well-behaved group that reflects little deviation. Three of the larger substituents, cyclopentyl, neohexyl, and CH_2SiMe_3, show no deviation, while cyclohexyl is slightly (∼1−2 kcal/mol) destabilized relative to the line, but no more so than ^{n}Pr, and both are within reasonable error of the correlation and its assumptions. It is inferred that ground state steric effects are minimal, as corroborated by the X-ray crystallographic characterization of **2**-^{neo}Hex, and the assumption that entropic differences are minimal also gains credence.

The titanium−hydride bond is about 7 kcal/mol stronger than the line implies, but the magnitude of the difference is relatively small and typical of systems that manifest strong $D(L_nM-R(H))$,[63−70] where secondary influences are minimal. Presumably the unique s-orbital overlap of the hydride renders this ligand aberrant when grouped with hydrocarbyls. Unlike L_nM and the hydrocarbyls, hydride also has virtually no ability to accommodate charge[73] and is intrinsically less polarizable. The absence of any steric perturbation on the hydride ligand, here probably not a factor, and the lack of a significant ionic contribution to the correlated homonuclear H−H bond[70,74] have also been proposed to explain its unique character.

The remaining outlying hydrocarbyls may exhibit secondary ground state influences in addition to their intrinsic bond strengths, as defined by the correlation with D(RH). The benzyl and mesityl substituents have ∼6−7 kcal/mol of additional stabilization, whereas the metal−carbon bond of (silox)$_2$(^{t}Bu$_3$SiNH)TiPh (**2**-Ph) is weaker than expected by ∼4 kcal/mol. These substantial deviations in magnitude imply enthalpic rather than entropic origins. Agostic[72] or η^3-binding[75] of the benzyl and mesityl substituents could account for the apparent extra strength of their bonds. The J_{CH} of the benzyl methylene group remained at 124 Hz upon cooling from +25 to −70 °C, and the disposition of the aromatic signals in the ^{1}H NMR spectrum did not change substantially with temperature (−85 °C → 25 °C). Stretches in the infrared spectrum in the range 2350−2700 cm^{-1} are considered diagnostic for agostic C−H bonds,[72] but the IR spectrum of **2**-Bz was essentially featureless from 1600 to 2800 cm^{-1}. Coupled with the regular disposition of the neohexyl group in the X-ray crystal structure of (silox)$_2$(^{t}Bu$_3$SiNH)Ti$CH_2CH_2{}^t$Bu (**2**-^{neo}Hex), the absence of diagnostic spectral features in **2**-Bz suggests that an agostic interaction is not operative, but a minor, spectroscopically (NMR) undetectable stabilization (<7 kcal/mol) by an η^3-interaction is probable. In support, allyllic binding in (silox)$_2$(^{t}Bu$_3$SiNH)Ti(η^3-$H_2CCHCHR$) (R = H (**2**-η^3-H_2CCHCH_2), Me (**2**-η^3-H_2-CCHCHMe)) is strong, and X-ray crystal structures of related d^0 benzyl derivatives exhibit allylic stabilization.[75] Finally, while **2**-R are generally colorless, **2**-Bz is yellow, a color common to early-metal benzylic species that exhibit allylic

(66) Stoutland, P. O.; Bergman, R. G.; Nolan, S. P.; Hoff, C. D. *Polyhedron* **1988**, *7*, 1429−1440.
(67) Schock, L. E.; Marks, T. J. *J. Am. Chem. Soc.* **1988**, *110*, 7701−7715.
(68) Dias, A. R.; Martinho Simões, J. A. *Polyhedron* **1988**, *7*, 1531−1544.
(69) Diogo, H. P.; de Alencar Simoni, J.; Minas da Piedade, M. E.; Dias, A. R.; Martinho Simões, J. A. *J. Am. Chem. Soc.* **1993**, *115*, 2764−2774.
(70) Labinger, J. A.; Bercaw, J. E. *Organometallics* **1988**, *7*, 926−928.
(71) Halpern, J. *Inorg. Chem. Acta* **1985**, *100*, 41−48.
(72) Brookhart, M.; Green, M. L. H.; Wong, L. *Prog. Inorg. Chem.* **1988**, *36*, 1−124.
(73) Siegbahn, P. E. M. *J. Phys. Chem.* **1995**, *99*, 12723−12729.
(74) Pearson, R. G. *J. Chem. Soc., Chem. Commun.* **1968**, 65−67.
(75) (a) Davies, G. R.; Jarvis, J. A. J.; Kilbourn, B. T.; Pioli, A. J. P. *J. Chem. Soc., Chem. Commun.* **1971**, 677. (b) Davies, G. R.; Jarvis, J. A. J.; Kilbourn, B. T. *J. Chem. Soc., Chem. Commun.* **1971**, 1511−1512. (c) Bassi, I. W.; Allegra, G.; Scordamaglia, R.; Chioccola, G. *J. Am. Chem. Soc.* **1971**, *93*, 3787−3788.

bonding. Alternatively, the electron-withdrawing capability of a phenyl group may impart greater ionic character[73] to each metal−benzyl bond, thereby increasing D(MBz) relative to those of the remaining hydrocarbyls, or the benzyl point signifies the origin of nonlinearity in this correlation (*vide infra*).

The most difficult outlying substituent to rationalize is phenyl, whose modest ∼4 kcal/mol destabilization relative to the line is greater than a steric effect and counter to an expected increase in stability on the basis of the increased electron-withdrawing ability of an sp^2-center. (silox)$_2$(^{t}Bu$_3$SiNH)TiPh (**2**-Ph) contains three π-donors of electronegativity greater than that of the phenyl: two siloxides and the amide. The inclusion of even a very weak π-donor such as phenyl may provide unwanted competition for empty titanium d-orbitals used in X(pπ)→Ti(dπ) (X = N, O) bonding, resulting in a net destabilization relative to a substituent whose bonding is solely σ. Repeated attempts to gain structural information on **2**-Bz and **2**-Ph have failed.

The most important feature of the D(TiR)$_{rel}$ vs D(RH) correlation concerns the slope of the line, which is 1.36 with the outlying substituents removed, and still greater than one with those included. For comparison, Jones' D(RhR)$_{rel}$ vs D(RH) plot pertaining to Tp′(^{t}BuCH$_2$NC)Rh(H)R (Tp′ = HB(3,5-diethylpyrazoyl)$_3$) with the outlying R = CH$_2$Ph point removed has a slope of ∼1.5.[3] D(MR) typically do not approach D(RH) in magnitude; consequently, it is curious that differences in D(MR) are greater than differences in D(RH).

Covalent bonds are typically described by expressions that contain electronegativity differences, such as the Pauling equation[76] and Matcha's variant,[77] or components that describe electronic differences, such as the electrostatic, covalent, and transfer factors of the ECT approach developed by Drago.[78−80] Consider the simplest of these, the arithmetic mean formulation of the Pauling equation that describes D(MR) as a function of D(RH) and electronegativity parameters (eq 34; M = L$_n$M′; ξ

$$D(\mathrm{MR}) = D(\mathrm{RH}) + 0.5[D(\mathrm{MM}) - D(\mathrm{HH})] + \xi[(\chi_\mathrm{M} - \chi_\mathrm{R})^2 - (\chi_\mathrm{R} - \chi_\mathrm{H})^2] \quad (34)$$

is typically in kcal·mol^{-1}/EN unit^2). Its derivative shows that deviations from a slope of unity can be ascribed to how electronegativity differences vary with changes in D(RH) (eq 35). Because of the intrinsic interdependence of χ_R, χ_H, and

$$\partial D(\mathrm{MR})/\partial D(\mathrm{RH}) = 1 + \xi\partial[(\chi_\mathrm{M} - \chi_\mathrm{R})^2 - (\chi_\mathrm{R} - \chi_\mathrm{H})^2]/\partial D(\mathrm{RH}) \quad (35)$$

D(RH), it is difficult to predict the magnitude or sign of the deviation.

The lack of curvature and relatively small deviation from a slope of unity in the D(TiR)$_{rel}$ vs D(RH) correlation bear closer scrutiny. A few systems with related characteristics have been investigated thermochemically, and these exhibit strong, covalent metal−carbon bonds.[63−70] By fitting of the D(TiR)$_{rel}$ data to the Matcha variant of the Pauling equation and through related ECT-based procedures, crude estimates of the absolute bond strengths in (silox)$_2$(^{t}Bu$_3$SiNH)TiR (**2**-R) place D(TiMe) at ∼65 kcal/mol,[81] a value reasonable in view of thermochemical estimates on related cyclopentadienyl compounds.[68] In the Matcha analysis, best fits were determined with $\chi_\mathrm{Ti} \sim 2.7$,[81] a value near those of the hydrocarbyls ($\chi \sim 2.55-2.58$),[82,83] while the ECT treatment revealed a covalency for (silox)$_2$(^{t}Bu$_3$SiNH)-Ti approaching that of a methyl group. However, it is likely that determinations based on the Pauling equation and variants give erroneous χ(L$_n$M) values.[67,70,81]

While the methods above are subject to some interpretation, the Ti−R bonds of **2**-R are best described as covalent, with a lesser ionic component, yet such factors are responsible for the slope greater than 1. For example, if χ_M can be realistically assumed to be $< \chi_\mathrm{H} = 2.20$,[81] eq 35 predicts that ∂D(MX)/∂D(HX) will be >1; i.e., ionic contributions to M−R bonding are greater than in R−H bonding and cause the deviation from unity slope. Siegbahn has also concluded that ionic contributions are critical in related metal−carbon bonds.[73]

In (dppe)(Me)PtX and Cp*(Me$_3$P)$_2$RuX systems investigated by Bryndza *et al.*,[63,64] with hydrocarbyl and other substituents that span ΔD(HX) = 48 kcal/mol, the D(MX)$_{rel}$ vs D(HX) correlation was also basically linear with a slope of ∼1.0. Furthermore, deviations are apparently attenuated by changes in the ancillary ligand bond strengths, as evidenced by variations in D(RuP) as X was changed.[64] In essence, the data comply with Pauling's electroneutrality principle,[76] where the more polarizable L$_n$M fragment electronically adjusts in response to changes in X, thereby maintaining ∂D(MX)/∂D(HX) near unity while minimizing the total energy of L$_n$MX. In a similar vein, variation of both X(σ)→Ti(dσ) and X(pπ)→Ti(dπ) (X = O, N) components of silox and ^{t}Bu$_3$SiNH bonding may render the (silox)$_2$(^{t}Bu$_3$SiNH)Ti polarizable as R is varied in (silox)$_2$(^{t}Bu$_3$-SiNH)TiR (**2**-R), resulting in the generally linear D(MR)$_{rel}$ vs D(RH) correlation.

2. Thermodynamics of β-H-Elimination. Evidence of β-H-elimination from (silox)$_2$(^{t}Bu$_3$SiNH)TiR (**2**-R, R = ^{c}Hex, ^{c}Pe, ^{n}Pr, ^{n}Bu, ^{neo}Hex, Et, ^{c}Bu) has not been obtained. Construction of a thermodynamic cycle (eqs 36−38, 25 °C) allows assessment of the free energy of the reaction **2**-Et → **2**-H + C$_2$H$_4$ (eq 39),

$$\textbf{2}\text{-Et} + \mathrm{C_2H_4} \rightarrow \textbf{2}\text{-Vy} + \mathrm{C_2H_6} \qquad \Delta G^\circ = -2.9 \text{ kcal/mol} \quad (36)$$

$$\mathrm{C_2H_6(g)} \rightarrow \mathrm{H_2(g)} + \mathrm{C_2H_4(g)} \qquad \Delta G^\circ = +24.2 \text{ kcal/mol} \quad (37)$$

$$\textbf{2}\text{-Vy} + \mathrm{H_2} \rightarrow \textbf{2}\text{-H} + \mathrm{C_2H_4} \qquad \Delta G^\circ = -5.0 \text{ kcal/mol} \quad (38)$$

$$\textbf{2}\text{-Et} \rightarrow \textbf{2}\text{-H} + \mathrm{C_2H_4} \qquad \Delta G^\circ = +16.3 \text{ kcal/mol} \quad (39)$$

with the assumption that the ΔG° for ethane dehydrogenation is reasonable for cyclohexane solution as well as the gas phase (eq 37).[84] On the basis of these calculations, β-hydride elimination is expected to be endoergic by ∼16 kcal/mol.

The absence of vacant *cis*-coordination sites in pseudotetrahedral **2**-R, the nonlability of the ancillary ligands, and steric hindrance[85] are all kinetic factors that hamper β-hydride elimination. Additionally, Chisholm has pointed out that X(pπ)→M(dπ) interactions raise the energy of the empty orbitals

(76) Pauling, L. *The Nature of the Chemical Bond*, 3rd ed.; Cornell University Press: Ithaca, NY, 1960.
(77) Matcha, R. L. *J. Am. Chem. Soc.* **1983**, *105*, 4859−4862.
(78) Drago, R. S.; Wong, N. *Inorg. Chem.* **1995**, *34*, 4004−4007.
(79) Drago, R. S. *Applications of Electrostatic-Covalent Models in Chemistry*; Surfside Scientific Publishers: Gainesville, FL, 1994.
(80) Drago, R. S.; Wong, N. M.; Ferris, D. C. *J. Am. Chem. Soc.* **1992**, *114*, 91−98.
(81) Bennett, J. L.; Vaid, T. P.; Wolczanski, P. T. *Inorg. Chim. Acta*, in press. Although $\chi_\mathrm{Ti} \sim 2.7$ gave the best fit in the Matcha analysis, the χ_Ti value is misleading because the Pauling equation and variants are inherently limited (e.g., D(TiH) − D(TiR) is poorly assessed).
(82) Boyd, R. J.; Boyd, S. L. *J. Am. Chem. Soc.* **1992**, *114*, 1652−1655. Generally, sp^2-carbon centers are considered more electronegative that sp^3.
(83) Allen, L. C. *J. Am. Chem. Soc.* **1989**, *111*, 9003−9014.
(84) *CRC Handbook of Chemistry and Physics*; 75th ed.; CRC Press: Boca Raton, FL, 1994.
(85) Kruse, W. *J. Organomet. Chem.* **1972**, *42*, C39−C42.

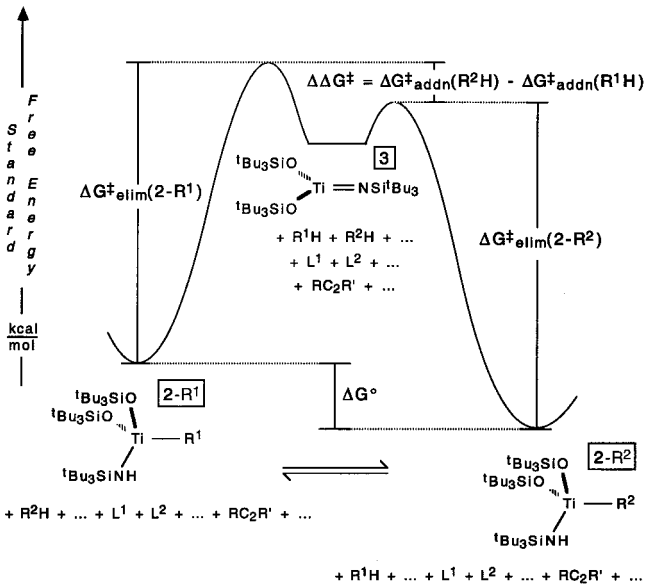

Figure 5. Standard free energy vs reaction coordinate diagram corresponding to the 1,2-RH-elimination/addition pathway of Scheme 1.

needed for a 5-coordinate d^0 olefin intermediate.[86] Assuming an ~18 kcal/mol barrier for the observed slow insertion of ethylene into **2**-H at 25 °C, the reverse β-H-elimination would have a $\Delta G^{\ddagger} \sim 36$ kcal/mol, with much of the activation having a thermodynamic origin. The stabilities of metal alkyls such as $Cp_2MX(^tBu)$,[87] $(Me_2N)_4Ta^tBu$,[86] and $(^tBu_3SiNH)(THF)^tBuTi{=}NSi^tBu_3$[22] and those of directly related systems[20,23] are probably best understood on the basis of thermodynamic considerations.[67]

Ground and Transition States Energies. 1. General Considerations. Figure 5 illustrates how the combination of kinetic and thermodynamic data in Table 3 and Figure 4, respectively, may be used to establish the transition state energy for each 1,2-RH-elimination and -addition event. From the standard free energy surface, differences in transition state energies (i.e., $\Delta G^{\ddagger}_{addn}(R^2H) - \Delta G^{\ddagger}_{addn}(R^1H)$), obtained from $\Delta G^{\ddagger}_{elim}$(**2**-$R^1$), $\Delta G^{\ddagger}_{elim}$(**2**-$R^2$), and ΔG° (or ΔG°_{corr}, eq 31) according to eq 40, permit evaluation of the most critical goal in this investigation—kinetic selectivities for the activation of an RH vs R′H bond.

$$\Delta\Delta G^{\ddagger}_{addn} = \Delta G^{\ddagger}_{addn}(R^2H) - \Delta G^{\ddagger}_{addn}(R^1H) = \Delta G^{\ddagger}_{elim}(\mathbf{2}\text{-}R^2) + \Delta G^{\circ} - \Delta G^{\ddagger}_{elim}(\mathbf{2}\text{-}R^1) \quad (40)$$

The compilation of ground and transition states for each $(silox)_2(^tBu_3SiNH)TiR$ (**2**-R) and ground states accorded each $(^tBu_3SiO)_2LTi{=}NSi^tBu_3$ (**3**-L) are not readily accommodated by a standard free energy vs reaction coordinate diagram; hence the data are presented in a stacked columnar graph in Figure 6. The ground and transition state energies are presented relative to the ground state of $(^tBu_3SiO)_2pyTi{=}NSi^tBu_3$ (**3**-py) at 0.0 kcal/mol. Ground states are graphed in order of decreasing energy and are represented by shaded columns, the $\Delta G^{\ddagger}_{elim}$(**2**-R)'s from Table 3 are indicated with unshaded columns, and the sum of the two for a specific **2**-R provides the requisite transition state energy for 1,2-RH-elimination/addition relative to **3**-py. Each relative standard free energy refers to a state

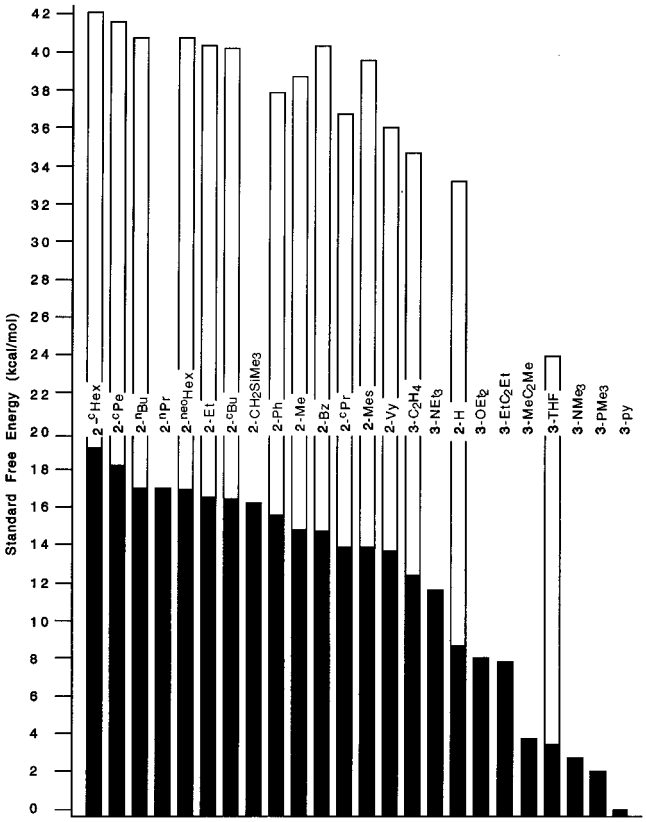

Figure 6. Ground and transition state free energies (kcal/mol, 1 M standard states) of **2**-R^n (i.e., **2**-R^1 + R^2H + ... + L^1 + L^2 + ... + RC_2R' + ...), **3**-L^n (i.e., **3**-L^1 + R^1H + R^2H + ... + L^2 + ... + RC_2R' + ...) and **3**-RC_2R' (i.e., **3**-RC_2R' + R^1H + R^2H + ... + L^1 + L^2 + ... + $R''C_2R'''$ + ...) relative to the reference ground state of $(^tBu_3SiO)_2pyTi{=}NSi^tBu_3$ (**3**-py) at 0.0 kcal/mol. Ground states are represented by shaded columns, $\Delta G^{\ddagger}_{elim}$(RH)'s with unshaded columns, and transition state energies for 1,2-RH-elimination/addition by the sum of the two. Cyclohexane and benzene solvent effects are assumed to be negligble or equivalent.

composed of the organometallic species plus all of the other hydrocarbons, dative ligands, and alkynes in a 1 M standard state, with one caveat; cyclohexane and benzene, the solvents used for the respective equilibria and rate studies, are considered to be equivalent in terms of influence on the relative state energies. For simplicity, these energies are referred to as the energy of the organometallic species, i.e., **2**-R or **3**-L.

2. Relative Energy of $(silox)_2Ti{=}NSi^tBu_3$ (3). The isolation of $(silox)_2Ti{=}NSi^tBu_3$ (**3**) was a paramount goal of this project, since absolute second-order rate constants for the activation of RH by **3** could then be measured. Although this has not been achieved, estimates of the free energy pertaining to **3** + R^1H + R^2H + ... + L^1 + L^2 + ... + $RC{\equiv}CR'$ + ... (referred to as the ground state of **3**) can be made. Because addition of RH to **3** should be exoergic for all RH, the relative energy of **3** will be higher than the energy of **2**-^{c}Hex, 19.1 kcal/mol relative to **3**-py.

An experiment that yields an upper bound on the energy of **3** is loss of THF-d_8 from **3**-THF-d_8 (3.7 kcal/mol relative to **3**-py), which was measured in C_6D_6 with 15 or 43 equiv of THF present ([THF] = 0.81 M, $k = 5.2 \times 10^{-3}$ s^{-1}, $\Delta G^{\ddagger}$ = 20.5 kcal/mol; [THF] = 1.96 M, $k = 4.0 \times 10^{-3}$ s^{-1}) and in neat THF ([THF] = 12.3 M, $k = 3.4 \times 10^{-3}$ s^{-1}) as shown in eq 41.[88] The data support a dissociative or dissociative

(86) Chisholm, M. H.; Tan, L.-S.; Huffman, J. C. *J. Am. Chem. Soc.* **1982**, *104*, 4879−4884.

(87) (a) Buchwald, S. L.; Kreutzer, K. A.; Fisher, R. A. *J. Am. Chem. Soc.* **1990**, *112*, 4600−4601. (b) Buchwald, S. L.; Lum, R. T.; Fisher, R. A.; Davis, W. M. *J. Am. Chem. Soc.* **1989**, *111*, 9113−9114.

(88) Loss of L from **3**-L is not always straightforward. Exchange of py-d_5 with $(silox)_2(^tBu_3SiN{=})Tipy$ (**3**-py) is faster than that of **3**-THF, an observation suggestive of an associative substitution. Further studies are underway by L. M. Slaughter and P. T. Wolczanski.

$$(\text{silox})_2(\text{THF-}d_8)\text{Ti}{=}\text{NSi}^t\text{Bu}_3 \xrightarrow[24.8\ ^\circ\text{C}]{C_6D_6/\text{THF}} \underset{\textbf{3}\text{-THF-}d_8}{} (\text{silox})_2(\text{THF})\text{Ti}{=}\text{NSi}^t\text{Bu}_3 + \text{THF-}d_8 \quad (41)$$
$$\textbf{3}\text{-THF}$$

interchange process whose transition state must have an energy equal to or greater than that of **3**, whose maximum can therefore considered to be 24.2 kcal/mol. The bracketed energy region where **3** resides (i.e., 19.1 kcal/mol < $\Delta G^\circ(\mathbf{3}) \leq$ 24.2 kcal/mol) can be narrowed further since ΔG° for **2**-^{c}Hex $\rightleftharpoons$ **3** + ^{c}HexH is likely to be >3 kcal/mol (i.e., **3** is not observed in solutions containing **2**-^{c}Hex and $\mathbf{3}_2$). Capture of $(\text{silox})_2\text{Ti}{=}\text{NSi}^t\text{Bu}_3$ (**3**) by THF was considered to be almost barrierless (i.e., dissociative interchange), leading to $\Delta G^\circ(\mathbf{3}) = 24(1)$ kcal/mol for the purposes of further discussion.

With this estimate of the free energy of $(\text{silox})_2\text{Ti}{=}\text{NSi}^t\text{Bu}_3$ (**3**), $\Delta G^\ddagger_{\text{addn}}$(RH) for **3** + RH → **2**-R can be roughly assessed according to eq 42. The $\Delta G^\ddagger_{\text{addn}}$(RH) values calculated range

$$\Delta G^\ddagger_{\text{addn}} \sim \Delta G^\circ(\textbf{2}\text{-R, relative to } \textbf{3}\text{-py}) + \Delta G^\ddagger_{\text{elim}}(\textbf{2}\text{-R}) - 24(1)\ \text{kcal/mol} \quad (42)$$

from $\Delta G^\ddagger_{\text{addn}}(H_2) \sim 9(1)$ kcal/mol to $\Delta G^\ddagger_{\text{addn}}(^c\text{HexH}) \sim 18(1)$ kcal/mol and represent rare, experimentally supported, quantitative estimates of the barrier for activation of a C−H (or H−H) bond, in this case a 1,2-RH-addition to transient $(\text{silox})_2\text{Ti}{=}\text{NSi}^t\text{Bu}_3$ (**3**). Calculations by Cundari result in a barrier of $\Delta H^\ddagger_{\text{addn}} \sim 14.5$ kcal/mol for CH_4 addition to $(H_2N)_2\text{Ti}{=}\text{NH}$, a value consistent with the experimental $\Delta G^\ddagger_{\text{addn}} \sim 15$ kcal/mol.[60] The value of ΔG°(**3**) also allows for a crude estimate of its imide π-bond strength as 34−40 kcal/mol.[89]

3. Intramolecular Competitions. While the majority of the selectivity data obtained was determined from the relative ground state and $\Delta G^\ddagger$'s for 1,2-RH-elimination according to Figures 5 and 6, some intramolecular competitions were used to check the data. Transient $(\text{silox})_2\text{Ti}{=}\text{NSi}^t\text{Bu}_3$ (**3**) was generated by thermolysis (25 °C) of $(\text{silox})_2(^t\text{Bu}_3\text{SiNH})\text{Ti}^c\text{Pr}$ (**2**-^{c}Pr) in the presence of 20 equiv of toluene in C_6D_{12} solution (eqs 43 and 44). Resonances attributable to **2**-Bz and **2**-Ar,

$$(\text{silox})_2(^t\text{Bu}_3\text{SiNH})\text{Ti}^c\text{Pr} \xrightarrow[25\ ^\circ\text{C}]{C_6D_{12}} \underset{\textbf{2}\text{-}^c\text{Pr}}{} [(\text{silox})_2\text{Ti}{=}\text{NSi}^t\text{Bu}_3] + {}^c\text{PrH} \quad (43)$$
$$\textbf{3}$$

$$\textbf{3} + \underset{(20\ \text{equiv})}{C_7H_8} \rightarrow \underset{\textbf{2}\text{-Bz}}{(\text{silox})_2(^t\text{Bu}_3\text{SiNH})\text{TiBz}} + (\text{silox})_2(^t\text{Bu}_3\text{SiNH})\text{TiC}_6\text{H}_4\text{Me} \quad (44)$$
$$\textbf{2}\text{-Ar}$$

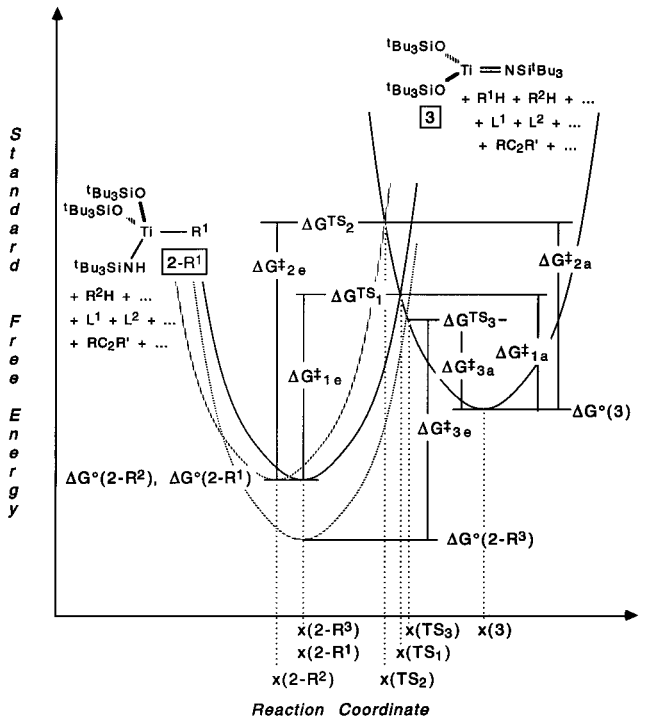

Figure 7. 1,2-RH-Elimination/addition reactant and product standard free energy surfaces (kcal/mol, 1 M standard states) of **2**-R^n (i.e., **2**-R^1 + R^{2}H + ... + L^1 + L^2 + ... + RC$_2$R′ + ...) and **3** (i.e., **3** + R^{1}H + R^{2}H + ... + L^1 + L^2 + ... + RC$_2$R′ + ...) represented by parabolas defined by the respective standard free energies (ΔG°(**2**-R^n), ΔG°(**3**)) and corresponding positional coordinates, x(**2**-R^n) and x(**3**). Transition states (ΔG^{TS_n}) are located at $x(\text{TS}_n)$ such that the extent of 1,2-RH-elimination can be assessed as $\{x(\text{TS}_n) - x(\textbf{2}\text{-R}^n)\}/\{x(\textbf{3}) - x(\textbf{2}\text{-R}^n)\}$, and the extent of 1,2-RH-addition, as $\{x(\textbf{3}) - x(\text{TS}_n)\}/\{x(\textbf{3}) - x(\textbf{2}\text{-R}^n)\}$ (see Appendix).

considered as *para*- and *meta*-activation products due to the presence to two diagnostic methyl signals,[20] were observed by ^{1}H NMR spectroscopy. At 34% conversion of **2**-^{c}Pr, a kinetic ratio of **2**-Bz:**2**-Ar of 1:24 was observed. Since detection of **2**-Bz was not accomplished under true early conversion conditions (usually <10%), activation of an aryl C−H bond over a benzylic one is preferred by <−1.9 kcal/mol. By assuming $\Delta G^\ddagger_{\text{elim}}(\textbf{2}\text{-Ph}) \sim \Delta G^\ddagger_{\text{elim}}(\textbf{2}\text{-Ar})$, eq 40 predicts an aryl vs benzyl activation preference of −2.5 kcal/mol, a value in decent agreement. In a related competition for **3** by ethylene, formation of the metallacycle $(^t\text{Bu}_3\text{SiO})_2(^t\text{Bu}_3\text{SiN})\text{TiCH}_2\text{CH}_2$ (**3**-C_2H_4) was favored over $(\text{silox})_2(^t\text{Bu}_3\text{SiNH})\text{TiCH}{=}\text{CH}_2$ (**2**-Vy) by −1.4 kcal/mol, while $\Delta G^\circ = -1.2$ kcal/mol. In an initial rate study, loss of ethylene from **3**-C_2H_4 occurred with $\Delta G^\ddagger_{\text{diss}} = 22.1(2)$ kcal/mol, in excellent agreement with $-\Delta G^\circ + \Delta G^\ddagger_{\text{elim}}$(**2**-Vy) + $\Delta\Delta G^\ddagger_{\text{addn}} = \Delta G^\ddagger_{\text{diss}}(C_2H_4) = 22.2$ kcal/mol (eq 40).[24]

Parabolic Model of the Reaction Coordinate. 1. General Considerations.[20] The standard free energy vs reaction coordinate diagram of Figure 5 is depicted as overlapping parabolas[56,93,94] corresponding to the ground state **2**-R^1 + R^{2}H + ... + L^1 + L^2 + ... + RC$_2$R′ + ... (solid line, state **2**-R^1) and the intermediate state **3** + R^{1}H + R^{2}H + ... + L^1 + L^2 + ... + RC$_2$R′ + ... (state **3**) in Figure 7. The diagram assumes similar parabolic surfaces for **2**-R^1, **2**-R^2, etc., a single surface for **3**,

(89) Consider Figure 6 and the addition of MeH to $(\text{silox})_2\text{Ti}{=}\text{NSi}^t\text{Bu}_3$ (**3**): **3** + MeH ⇌ **2**-Me. From the assessment of ΔG°(**3**), $\Delta G^\circ_{\text{reacn}} \sim -9$ kcal/mol, and assuming D(TiMe) ∼ 65−71 kcal/mol[68,81] and $\Delta S^\circ_{\text{reacn}} \sim -30$ eu ($T\Delta S^\circ \sim -9$ eu), $\Delta H^\circ_{\text{reacn}}$ can be estimated as −18 kcal/mol and applied to the following (D(HMe) = 105 kcal/mol, D(NH) = 92 kcal/mol):[60,62] $\Delta H^\circ_{\text{reacn}} \sim D(\text{Ti}{=}\text{N}) + D(\text{HMe}) - [D(\text{TiMe}) + \text{D(NH)} + D(\text{TiN})]$; $\Delta H^\circ_{\text{reacn}} \sim -18 \sim \text{D}(\pi(\text{TiN})) + 13 - D(\text{TiMe})$. The difference between the titanium−nitrogen interaction in **3** vs **2**-Me (i.e., D(Ti=N) − D(Ti−N))[60] is taken to be the imide π-bond enthalpy, D(π(TiN)) ∼ 34−40 kcal/mol. It is greater than gas phase estimates of $D(\text{Ti}{=}\text{NH}^+) \sim 25$ kcal/mol,[90] consistent with $\Delta G^\ddagger_{\text{rot}} \sim D(\pi(\text{Ta}{=}\text{C})) \geq 20$ kcal/mol for $(\text{MeC}_5\text{H}_4)\text{-CpMeTa}{=}\text{CH}_2$,[91] and somewhat less than Gable's estimate of ∼50 kcal/mol for $D(\pi(\text{Re}{=}\text{O}))$ in Cp*ReO_3.[92]

(90) (a) Clemmer, D. E.; Sunderlin, L. S.; Armentrout, P. B. *J. Phys. Chem.* **1990**, *94*, 3008−3015. (b) Clemmer, D. E.; Sunderlin, L. S.; Armentrout, P. B. *J. Phys. Chem.* **1990**, *94*, 208−217.

(91) (a) Schrock, R. R.; Sharp, P. R. *J. Am. Chem. Soc.* **1978**, *100*, 2389−2399. (b) Schrock, R. R.; Messerle, L. W.; Wood, C. D.; Guggenberger, L. J. *J. Am. Chem. Soc.* **1978**, *100*, 3793−3800.

(92) Gable, K. P.; Phan T. N. *J. Am. Chem. Soc.* **1993**, *115*, 3036−3037.

(93) Hammond, G. S. *J. Am. Chem. Soc.* **1955**, *77*, 334−338.

(94) Thornton, E. R. *J. Am. Chem. Soc.* **1967**, *89*, 2915−2927.

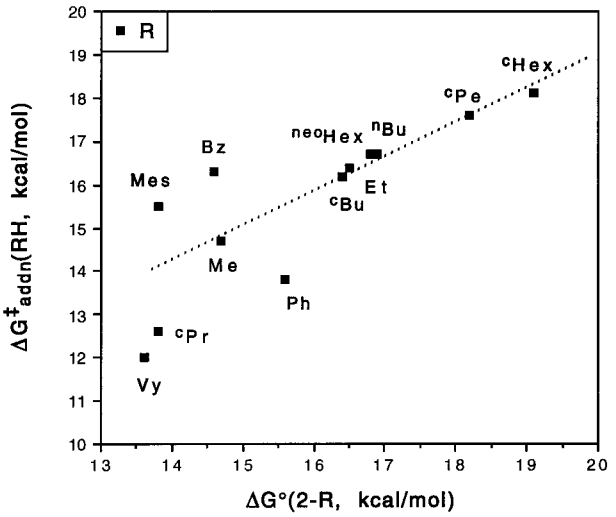

Figure 8. Linear free energy relationship as defined by $\Delta\Delta G^{\ddagger}_{addn} = \Delta G^{\ddagger}_{addn}(R^2H) - \Delta G^{\ddagger}_{addn}(R^1H) \sim \beta\{\Delta G°(\mathbf{2}\text{-}R^2) - \Delta G°(\mathbf{2}\text{-}R^1)\}$ (eq 45, referenced to $\Delta G°(\mathbf{3}) = 24$ kcal/mol, $\beta(sp^3) = 0.77$, $R^2 = 0.98$).

and two variables to interconnect them: (1) the relative standard free energies accorded the ground states of **2**-R^n and **3**, as determined via the measured equilibria and above estimates of $\Delta G°(\mathbf{3})$; (2) the reaction coordinate defined by the disposition of **2**-R^n (x(**2**-R^n)) relative to **3** (x(**3**)). The use of surfaces with like curvature for all **2**-R^n is necessary to employ this simple model, and there exists reasonable justification for this assumption. Since the reaction coordinate for each **2**-R^n contains elements of Ti−C and N−H bond-breaking accompanied by TiN(π) and C−H bond-making, the corresponding parabolic surfaces are expected to be quite alike. This is especially the case in the relatively low energy region relevant to these reactions, where $\Delta G^{\ddagger}_{elim}$(**2**-R^n) ~ 20 kcal/mol << D(TiR^n) ~ 65 kcal/mol[68,81] or D(NH) ~ 92 kcal/mol[60,62] and $\Delta G^{\ddagger}_{addn}$(R^{n}H) << D(R^{n}H) etc. Under these circumstances the relevant bond stretches, bends, etc. are well described as harmonic oscillators, leading to a surface that is parabolic as a sum of such components. Furthermore, if the curvatures were different, the surface would be expected to be the steepest for **2**-Ph and **2**-Vy, which have the strongest D(Ti−R); a greater steepness would lead to greater transition state energies and higher respective $\Delta G^{\ddagger}_{addn}$ and $\Delta G^{\ddagger}_{elim}$, *yet the opposite is observed for these hydrocarbyls*. The model also assumes that transfer between the surfaces is adiabatic and that coupling between the reactant (**2**-R) and product (**3**) surfaces occurs to the same degree for each **2**-R^n and can be neglected. While the reaction coordinate is not measured directly, by assuming similar surfaces for **2**-R^1, **2**-R^2, etc. relative to a common intermediate surface (**3**), one can calculate x(**2**-R^n) relative to x(**3**), because knowledge of $\Delta G^{\ddagger}_{elim}$(R^{n}H) affords a unique disposition of each **2**-R^n parabola relative to that of **3** (see Appendix).

In Figure 7, the left surfaces are centered at x(**2**-R^n) and correspond to each **2**-R^n state at lower energy than the upper right surface that describes state **3**, whose position is denoted as x(**3**). The respective transition states for 1,2-RH-elimination are positioned at x(TS$_n$), and the extent of reaction[95] at that point can be assessed as $\{x(TS_n) - x(\mathbf{2}\text{-}R^n)\}/\{x(\mathbf{3}) - x(\mathbf{2}\text{-}R^n)\}$, providing a numerical estimate of the "early" or "late" character of the 1,2-RH-elimination. Likewise, the extent of 1,2-RH-addition can be assessed as $\{x(\mathbf{3}) - x(TS_n)\}/\{x(\mathbf{3}) - x(\mathbf{2}\text{-}R^n)\}$.

(95) For views of related reaction coordinates, see: (a) Crabtree, R. H.; Holt, E. M.; Lavin, M. E.; Morehouse, S. M. *Inorg. Chem.* **1985**, *24*, 1986−1992. (b) Crabtree, R. H. *Angew. Chem., Int. Ed. Engl.* **1993**, *32*, 789−805. (c) Bürgi, H. B.; Dunitz, J. *Acc. Chem. Res.* **1983**, *16*, 153−161.

2. 1,2-RH-Addition to (silox)$_2$Ti=NSi^{t}Bu$_3$. Figure 6 highlights the general correspondence between ground state and transition state energies for 1,2-RH-elimination/addition. The ease of RH addition to (silox)$_2$Ti=NSi^{t}Bu$_3$ (**3**) generally parallels the respective ground state energies of **2**-R, indicating the predominant factor in R−H bond activation selectivity is the strength of the titanium−carbon bond that will eventually be formed. Therefore, the slope of the D(TiR)$_{rel}$ vs D(RH) line (Figure 4) is the *critical indicator of selectivity*. If all versions of eq 27 were effectively thermoneutral (i.e., $\partial D(TiR)_{rel}/\partial D(RH) \sim 1$), there would be no thermodynamic impetus behind the kinetic selectivity in hydrocarbon activation. Lacking any pronounced secondary effects (i.e., steric etc.), such a system would exhibit stochastic selectivity.

Figure 8 graphs $\Delta G^{\ddagger}_{addn}$(RH, calculated with $\Delta G°(\mathbf{3}) = 24$ kcal/mol) as a function of $\Delta G°$(**2**-R) and reveals the effect of the free energy on $\Delta\Delta G^{\ddagger}_{addn}$. Generally, the greater the stability of **2**-R, the easier the activation of the corresponding hydrocarbon. The relationship is fairly linear (eq 45) for the sp^3-

$$\Delta\Delta G^{\ddagger}_{addn} = \Delta G^{\ddagger}_{addn}(R^2H) - \Delta G^{\ddagger}_{addn}(R^1H) \sim \beta\{\Delta G°(\mathbf{2}\text{-}R^2) - \Delta G°(\mathbf{2}\text{-}R^1)\} \quad (45)$$

substituents, and the line of slope $\beta = 0.77$ ($R^2 = 0.98$) provides a numerical indication of the thermodynamic influence on transition state energies. In the parabolic model of Figure 7, a substantial slope occurs where differences in 1,2-RH-addition activation energies (e.g., $\Delta G^{\ddagger}_{1a} - \Delta G^{\ddagger}_{3a}$) approach the differences in the ground states of the products (e.g., $\Delta G°(\mathbf{2}\text{-}R^1) - \Delta G°(\mathbf{2}\text{-}R^3)$), provided the ground states of **2**-R^1 and **2**-R^3 are positionally similar (i.e., x(**2**-R^1) ~ x(**2**-R^3)), and the dispositions of the respective transition states are distinct from **3** (i.e., x(TS$_1$) and x(TS$_3$) are not near x(3), and $\partial\Delta G°(\mathbf{3})/\partial x(\mathbf{3}) << 0$). When RH addition to **3** is not very "early" along the reaction coordinate, $\partial\Delta G^{\ddagger}_{addn}/\partial\Delta G°$ will be relatively linear and approach unity, as in this situation.

1,2-R(sp^3)H-addition to transient (silox)$_2$Ti=NSi^{t}Bu$_3$ occurs with a transition state of balanced character, consistent with the relatively low energy estimate of **3** and correspondingly high estimates of $\Delta G^{\ddagger}_{addn}$(R(sp^3)H) ~ 14.7−18.1 kcal/mol. Kinetic isotope effect data that portray the transition state as symmetric—carbon−hydrogen bond-breaking and metal−carbon bond-making are both important—corroborate this depiction. No significant deviations occur within the sp^3-group, suggesting that steric factors are similar in both ground and transition states, entropic influences are relatively constant, and variations in x(**2**-R^n) must correlate with $\Delta G°(\mathbf{2}\text{-}R^n)$.

Two other groups of hydrocarbyls are evident from the plot in Figure 8: sp^2-hybridized derivatives, including **2**-^{c}Pr, and benzyl and mesityl. It is more difficult than expected (~1−2 kcal/mol) for **3** to activate the benzylic bonds of toluene and mesitylene relative to sp^3 C−H bonds, yet clearly much of the aforementioned 6−7 kcal/mol of ground state stabilization accorded **2**-Bz, and by inference **2**-Mes, translates to their respective transition states. Noting that the ground states of **2**-Me and **2**-Bz are similar in energy, consider the surfaces of **2**-R^1 (R^1 = Me) and **2**-R^2 (R^2 = Bz) in Figure 9 to be representative. $\Delta G^{\ddagger}_{addn}$(MeH) is lower than $\Delta G^{\ddagger}_{addn}$(BzH), i.e., $\Delta G^{\ddagger}_{1a} < \Delta G^{\ddagger}_{2a}$, because a higher transition state for the benzyl, $\Delta G(TS_2)$, results from a lesser disposition along the reaction coordinate, i.e., x(**2**-R^2) < x(**2**-R^1). As another example, transition states for 1,2-RH-addition of mesitylene and ethane to **3** are approximately equal (i.e., $\Delta G^{TS_{Mes}} \sim \Delta G^{TS_{Et}}$), despite ground state differences that clearly favor mesityl activation (i.e., $\Delta G°(\mathbf{2}\text{-Mes}) < \Delta G°(\mathbf{2}\text{-Et})$). Given the constraints of the model,

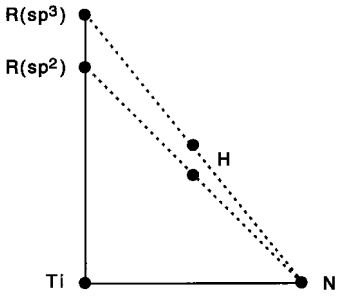

Figure 9. Depiction of transition states for 1,2-R(sp^3)H- and 1,2-(R(sp^2)H-addition/elimination that reveal a more compressed reaction coordinate (and correspondingly less reorganizational energy) for H-transfer to an sp^2-hydrocarbyl.

the similar $\Delta G^{\ddagger}_{addn}$ values necessarily derive from x(**2**-Mes) < x(**2**-Et), the relative dispositions of the hydrocarbyl ground states.

The origin of the displacement in reaction coordinate cannot be discerned from the model, but the probable weak η^3-coordination of the benzyl and mesityl substituents could dramatically change x(**2**-Bz) and x(**2**-Mes) from an sp^3-hydrocarbyl position. η^3-Coordination may result in an α-carbon that is significantly further from the amide hydrogen, one that requires greater bond length and angular changes than those of a simple hydrocarbyl in achieving the transition state geometry. In essence, the additional olefinic interaction of the η^3-coordination mode provides a greater thermodynamic impetus for benzylic activation that is partially offset by a greater reaction coordinate. It is also conceivable that inductive influences of the phenyl and 3,5-dimethyphenyl substituents on **2**-CH_2R' may provide differing stabilizations to the ground and transition states of the repective benzyl and mesityl species, thereby changing the nature of reactant and product surface coupling, but such effects are beyond the predictability of the parabolic model and are exceedingly difficult to experimentally address.[96]

(silox)$_2$(^{t}Bu$_3$SiNH)TiPh (**2**-Ph) could be interpreted as having either a ground state destabilization or transition state stabilization of ∼1.5 kcal/mol, factors that would also have to be applied to **2**-^{c}Pr and **2**-Vy. While comprising a small data set, the two sp^2-substituents and cyclopropyl appear to parallel the line in Figure 8, indicating that ground state influences on the transition states of the sp^2- and sp^3-substituents are the same (i.e., β(sp^3's) ∼ β(sp^2's)), albeit with different intercepts. Transition state stabilization via p-orbital participation is often invoked to explain speedier rates of sp^2-substituents in various reactions. Greater coupling between reactant and product free energy surfaces would accommodate this rationale, but a simpler explanation—one that is less subject to interpretation—is provided by the reaction coordinate. The sp^2-hybridized substituents (C(sp^2) r_{cov} ∼ 0.67 Å) possess inherently shorter bond lengths than corresponding sp^3-derivatives (C(sp^3) r_{cov} ∼ 0.77 Å),[76] and a correspondingly compressed reaction coordinate for 1,2-RH-elimination/addition will translate into swifter additions (i.e., $\{x(\mathbf{3}) - x(\mathrm{TS(sp^2)})\}/\{x(\mathbf{3}) - x(\mathbf{2}\text{-R(sp}^2))\} < \{x(\mathbf{3}) - x(\mathrm{TS(sp^3)})\}/\{x(\mathbf{3}) - x(\mathbf{2}\text{-R(sp}^3))\}$. Figure 9 illustrates this principle by depicting symmetric transition states for R(sp^3)H and R(sp^2)H 1,2-RH-addition/elimination that indicate H-transfer occurs over a shorter distance for the latter, provided the R···H···N distance is greater than d(Ti−N). As a consequence of the more compressed reaction coordinate, less reorganizational energy is needed for a 1,2-R(sp^2)H-addition or -elimination event, which translates into generally swifter rates.

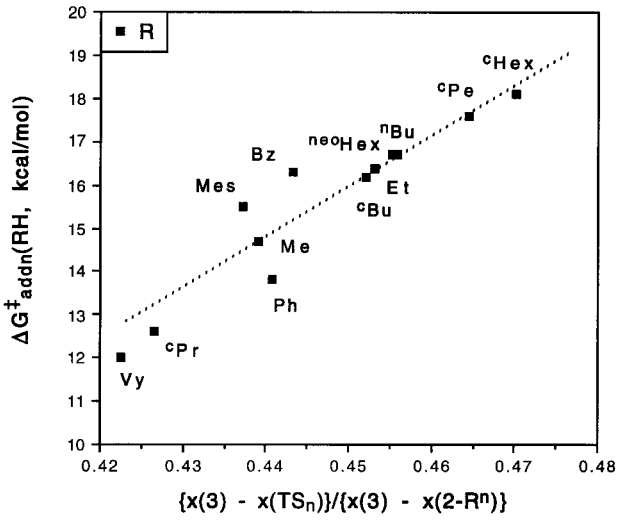

Figure 10. $\Delta G^{\ddagger}_{addn}$(RH) vs $\{x(\mathbf{3}) - x(\mathrm{TS}_n)\}/\{x(\mathbf{3}) - x(\mathbf{2}\text{-R}^n)\}$, a measure of the reaction coordinate derived from the parabolic model (see Appendix). The line is a least-squares fit to the sp^3 data (m = 110, R^2 = 0.99).

To emphasize the interdependence of 1,2-RH-addition selectivities on ground state energies and the reaction coordinate, Figure 10 plots $\Delta G^{\ddagger}_{addn}$(RH, calculated with $\Delta G°(\mathbf{3})$ = 24 kcal/mol) vs extent of reaction, $\{x(\mathbf{3}) - x(\mathrm{TS}_n)\}/\{x(\mathbf{3}) - x(\mathbf{2}\text{-R}^n)\}$ (see Appendix). The latter is <0.5 for all cases,[97] implicating somewhat early transition states, and an earlier ΔG^{TS_n} generally corresponds to a swifter addition of RH. The data again break roughly into the same three groups: sp^3-substituents (0.44−0.47), benzylic substituents (∼0.44), and sp^2-substituents, including **2**-^{c}Pr (0.42−0.44). The denominators of the positional parameters differentiate the groups, but the slope within each should be similar in this particular regime (i.e., $x(\mathrm{TS}_n)$ are not near $x(\mathbf{3})$, and $\partial\Delta G(\mathbf{3})/\partial x(\mathbf{3}) << 0$). Assuming a relatively constant $\{x(\mathbf{3}) - x(\mathbf{2}\text{-R}^n)\}$ within each group, it may be inferred that $\{x(\mathbf{3}) - x(\mathrm{TS}_n)\}$ changes are primarily due to ground state energy differences of **2**-R. Within the sp^3-substituents, the dependence of $\Delta\Delta G^{\ddagger}_{addn}$ on $\Delta\{x(\mathbf{3}) - x(\mathrm{TS}_n)\}/\{x(\mathbf{3}) - x(\mathbf{2}\text{-R}^n)\}$ is quite striking, with R^2 = 0.99. While the sample sizes are small, it may be inferred from the graph that similar dependencies affect the sp^2-groups and benzylic groups; differing ground states influence the sp^3, sp^2, and benzylic sets of $\{x(\mathbf{3}) - x(\mathrm{TS}_n)\}/\{x(\mathbf{3}) - x(\mathbf{2}\text{-R}^n)\}$ to the same degree.

In summary, the 1,2-RH-addition/elimination (R = hydrocarbyl) preferences may be rationalized solely on the basis of the relative free energies of **2**-R^n and an understanding that the putative four-center transition state has geometric parameters influenced by the ground state structure of **2**-R (e.g., d(Ti−R)). Additional or alternative effects, such as those affecting coupling of reactant and product free energy surfaces (i.e., p-orbital participation of the sp^2-substituents), may be present but are unnecessary for interpretation of the data; computational support of such influences has not been discovered.[57−61]

Dihydrogen addition has been excluded in part on the basis that H-binding via an s-orbital is intrinsically different from that of sp^n-hybridized substituents. Normally, the nondirectionality of the s-orbital is held responsible for faster rates in

(96) Many aryl substituents (X) change the electron-donating or -withdrawing capacity of CH_2Ph or Ph, but appropriate D(H−C_6H_4X) and D(H−$CH_2C_6H_4$X) are unknown and assumed to be equivalent to D(H−Ph) and D(H−CH_2Ph) from Benson additivity relationships (Benson, S. D. *Thermochemical Kinetics*; John Wiley & Sons: New York, 1968). The origin and interpretation of such substituent effects are thereby rendered moot.

(97) Since the parabolic surfaces of **2**-R and **3** are equivalent (see Appendix), the transition state of a thermoneutral reaction is at $x(\mathrm{TS}_n)$ = 0.5, and the transition states of endothermic and exothermic reactions are necessarily positioned at <0.5 and >0.5, respectively.

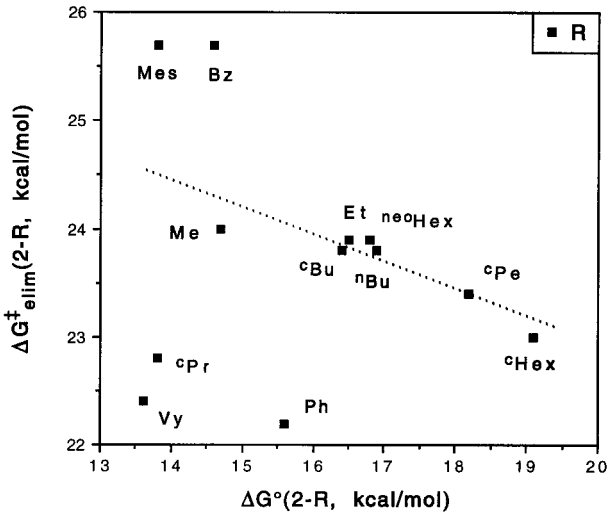

Figure 11. Linear free energy relationship as defined by $\Delta\Delta G^{\ddagger}_{elim} = \Delta G^{\ddagger}_{elim}(\mathbf{2}\text{-}R^2) - \Delta G^{\ddagger}_{elim}(\mathbf{2}\text{-}R^1) \sim \beta'\{\Delta G^{\circ}(\mathbf{2}\text{-}R^2) - \Delta G^{\circ}(\mathbf{2}\text{-}R^1)\}$ (eq 46, referenced to $\Delta G^{\circ}(\mathbf{3}) = 24$ kcal/mol, $\beta(sp^3) = -0.23$, $R^2 = 0.83$).

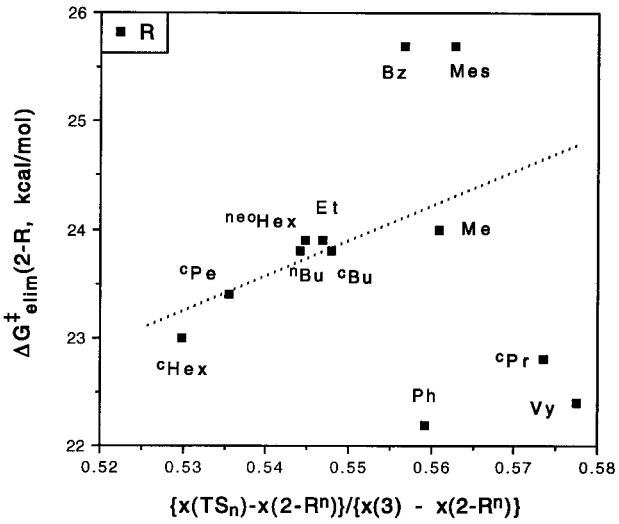

Figure 12. $\Delta G^{\ddagger}_{elim}(\mathbf{2}\text{-R})$ vs $\{x(TS_n) - x(\mathbf{2}\text{-}R^n)\}/\{x(\mathbf{3}) - x(\mathbf{2}\text{-}R^n)\}$, a measure of the reaction coordinate derived from the parabolic model (see Appendix). The line is a least-squares fit to the sp^3 data ($m = 32$, $R^2 = 0.78$).

various insertions (e.g., $L_nM(olefin)H \rightarrow L_nMR$), and the parabolic model could assimilate this logic through greater coupling of the **2**-R and **3** surfaces. The $\mathbf{3} + H_2 \rightleftharpoons \mathbf{2}\text{-H}$ reaction coordinate is expected to be greatly compressed relative to the hydrocarbyls, again supporting swifter H_2 addition. In contrast, the difficulty in polarizing the H−H bond, a critical factor in the assessment of ground state energetics, may slow dihydrogen addition/elimination. In conclusion, parabolas used to model **2**-R (R = hydrocarbyl) may poorly describe **2**-H.

3. 1,2-RH-Elimination from 2-R. By the principle of microscopic reversibility, the preceding model provides complementary trends in 1,2-RH-elimination from **2**-R. The relationship between $\Delta G^{\ddagger}_{elim}(\mathbf{2}\text{-}R^2)$ and $\Delta G^{\circ}(\mathbf{2}\text{-R})$ in Figure 11 can be interpreted within the same three groups: sp^3- and sp^2-substituents and **2**-CH_2Ar. A moderate correlation within the sp^3-group (eq 46, $R^2 = 0.83$) shows that ground state influences

$$\Delta\Delta G^{\ddagger}_{elim} = \Delta G^{\ddagger}_{elim}(\mathbf{2}\text{-}R^2) - \Delta G^{\ddagger}_{elim}(\mathbf{2}\text{-}R^1) \sim \beta'\{\Delta G^{\circ}(\mathbf{2}\text{-}R^2) - \Delta G^{\circ}(\mathbf{2}\text{-}R^1)\} \quad (46)$$

on the 1,2-RH-elimination are small ($\beta' = -0.23$) yet clearly indicative of speedier eliminations from **2**-R of higher ground states. This is expected from the parabolic model, since $x(TS_n)$ are not near $x(\mathbf{3})$ and $\partial\Delta G(\mathbf{3})/\partial x(\mathbf{3}) << 0$. Under these circumstances, the 1,2-RH-eliminations are not particularly late, and $\Delta G^{TS_2} - \Delta G^{TS_1}$ will be less than, but approach, the respective ground state differences, resulting in a small $\Delta\Delta G^{\ddagger}_{elim}$ dependence on ground state differences. The remaining groups have too few members to manifest a trend yet are presumably differentiated on the basis of disparate reaction coordinates, with the **2**-CH_2Ar eliminating slower than predicted by an all-encompassing linear free energy relationship and the sp^2-substituents undergoing RH loss faster than expected on that basis. The greater scatter in the data as viewed from the elimination standpoint is consistent with a lesser dependence on ground state in a moderately late reaction coordinate, where subtler influences will be magnified.

As illustrated by the $\Delta G^{\ddagger}_{elim}(\mathbf{2}\text{-}R^n)$ vs extent of reaction plot in Figure 12, the benzylic substituents and sp^2-substituents are shown to be distinct within the somewhat late (i.e., $\{x(TS_n) - x(\mathbf{2}\text{-}R^n)\}/\{x(\mathbf{3}) - x(\mathbf{2}\text{-}R^n)\} > 0.5$)[97] character of the 1,2-RH-elimination transition states. The extent of reaction is near 0.5, indicative of transition states possessing the balanced character implied by the KIE experiments. Again, one can infer from the sp^3-data that $\{x(\mathbf{3}) - x(\mathbf{2}\text{-}R^n)\}$ is fairly constant within the group, higher ground state energies for **2**-R lead to faster eliminations, and the slope ($R^2 = 0.78$) is a consequence of $\{x(TS_n) - x(\mathbf{2}\text{-}R^n)\}$ changes that reflect $\Delta G^{\circ}(\mathbf{2}\text{-}R^n)$ differences. As a corollary, **2**-Bz, **2**-Me, and **2**-Ph have similar extents of reaction values, but the denominators $\{x(\mathbf{3}) - x(\mathbf{2}\text{-}R^n)\}$ for each are different, with $x(\mathbf{2}\text{-Bz}) < (\mathbf{2}\text{-Me}) < (\mathbf{2}\text{-Ph})$ leading to $\Delta G^{\ddagger}_{elim}(\mathbf{2}\text{-Bz}) > \Delta G^{\ddagger}_{elim}(\mathbf{2}\text{-Me}) > \Delta G^{\ddagger}_{elim}(\mathbf{2}\text{-Ph})$ disparities that are greater than predicted on the basis of a linear free energy relationship alone! Again the ∼0.1 Å difference in covalent radii account for the more compressed reaction coordinate for the sp^2-substituents and **2**-^{c}Pr, resulting in generally swifter eliminations. Weak η^3-coordination by aryl groups in **2**-Bz and **2**-Mes should elongate the reaction coordinate, rendering slower 1,2-RH-elimination rates.

4. Other Correlations. Correlations of proton affinity with $\Delta G^{\ddagger}_{elim}(\mathbf{2}\text{-R})$ were previously used to suggest the presence of alkane intermediates,[20,21] and related studies in this system did little but support the contention of sp^2 vs sp^3 substrate classes. Similarly, attempts to correlate 1,2-RH-addition and -elimination processes with gas- and solution-phase pK_a's manifested the three standard groups (i.e., sp^3, sp^2, and **2**-^{c}Pr, **2**-CH_2Ar). Significant scatter was also evident, and no obvious conclusions could be reached, in concert with experimental and calculational[57,60,61] examinations that have failed to elicit evidence of charge build-up on crucial intermediates; these reactions are best considered as concerted four-center processes.

Conclusions

Mechanistic Overview. The mechanism of 1,2-RH-elimination from (silox)$_2$(^{t}Bu$_3$SiNH)TiR (**2**-R) and of 1,2-RH-addition to (silox)$_2$Ti=NSi^{t}Bu$_3$ (**3**) is portrayed in Scheme 1 and Figure 5 and summarized as follows: (1) 1,2-RH-elimination occurs via a four-center transition state in which the amide/imide nitrogen, the transferring hydrogen, and the α-carbon of R are relatively linear, as large KIE's indicate and calculations corroborate; (2) activation parameters, KIE evidence, and thermodynamic estimates accorded $\mathbf{2}\text{-R} \rightleftharpoons \mathbf{3} + RH$ suggest a concerted process, with balanced amounts of N−H and Ti−R bond-breaking and C−H bond-making with little charge build-up; (3) intermediate **3** or solvated **3** is a potent electrophile and uses a d_{z^2}/p_z hybrid orbital to attack the pair of electrons in a substrate C−H bond; (4) 1,2-RH-addition occurs concomitant

Table 4. Pairwise Kinetic Selectivity of (silox)$_2$Ti=NSi^{t}Bu$_3$ (**3**) for R^{1}H vs R^{2}H Expressed as $\Delta\Delta G^{\ddagger}_{addn} = \Delta G^{\ddagger}_{addn}(R^2H) - \Delta G^{\ddagger}_{addn}(R^1H)$ As Calculated via Eq 40 (kcal/mol at 24.8 °C)[a-c]

	R^{1}H													
R^{2}H	^{c}HexH	^{c}PeH	^{n}BuH	^{neo}HexH	EtH	BzH	^{c}BuH	MesH	MeH	PhH	^{c}PrH	VyH	C_2H_4	H_2
^{c}HexH	0.0	0.5	1.4	1.4	1.7	1.8	1.9	2.6	3.4	4.3	5.5	6.1	7.5	8.9
^{c}PeH	−0.5	0.0	0.9	0.9	1.2	1.3	1.4	2.1	2.9	3.8	5.0	5.6	7.0	8.4
^{n}BuH	−1.4	−0.9	0.0	0.0	0.3	0.4	0.5	1.2	2.0	2.9	4.1	4.7	6.1	7.5
^{neo}HexH	−1.4	−0.9	0.0	0.0	0.3	0.4	0.5	1.2	2.0	2.9	4.1	4.7	6.1	7.5
EtH	−1.7	−1.2	−0.3	−0.3	0.0	0.1	0.2	0.9	1.7	2.6	3.8	4.4	5.8	7.2
BzH	−1.8	−1.3	−0.4	−0.4	−0.1	0.0	0.1	0.8	1.6	2.5	3.7	4.3	5.7	7.1
^{c}BuH	−1.9	−1.4	−0.5	−0.5	−0.2	−0.1	0.0	0.7	1.5	2.4	3.6	4.2	5.6	7.0
MesH	−2.6	−2.1	−1.2	−1.2	−0.9	−0.8	−0.7	0.0	0.8	1.7	2.9	3.5	4.9	6.3
MeH	−3.4	−2.9	−2.0	−2.0	−1.7	−1.6	−1.5	−0.8	0.0	0.9	2.1	2.7	4.1	5.5
PhH	−4.3	−3.8	−2.9	−2.9	−2.6	−2.5	−2.4	−1.7	−0.9	0.0	1.2	1.8	3.2	4.6
^{c}PrH	−5.5	−5.0	−4.1	−4.1	−3.8	−3.7	−3.6	−2.9	−2.1	−1.2	0.0	0.6	2.0	3.4
VyH	−6.1	−5.6	−4.7	−4.7	−4.4	−4.3	−4.2	−3.5	−2.7	−1.8	−0.6	0.0	1.4	2.8
C_2H_4	−7.5	−7.0	−6.1	−6.1	−5.8	−5.7	−5.6	−4.9	−4.1	−3.2	−2.0	−1.4	0.0	1.4
H_2	−8.9	−8.4	−7.5	−7.5	−7.2	−7.1	−7.0	−6.3	−5.5	−4.6	−3.4	−2.8	−1.4	0.0

[a] Azametallacyclobutane (silox)$_2$(^{t}Bu$_3$SiN)TiCH$_2$CH$_2$ formation according to eq 22 is included and listed as R^{1}H or R^{2}H = C_2H_4. [b] The selectivity is given on a per molecule basis. [c] For kinetic selectivity on a per hydrogen basis, $\Delta G^{\ddagger}_{addn}$ may be generated by using ΔG°_{corr} (eq 31) in eq 40.

Table 5. Measured and Estimated Relative Rates and $\Delta G^{\ddagger}_{elim}$ for 1,2-RH-Elimination from Group 4 and 5 XY(^{t}Bu$_3$SiNH)MR Complexes

group 4 compound	k_{rel},[a] s^{-1}	$\Delta G^{\ddagger}_{elim}$, kcal/mol	group 5 compound	k_{rel},[a] s^{-1}	$\Delta G^{\ddagger}_{elim}$, kcal/mol
(silox)$_2$(^{t}Bu$_3$SiNH)TiMe	460	24.9	(^{t}Bu$_3$SiNH)$_2$(^{t}Bu$_3$SiN)VMe[b]	12	27.6
(silox)$_2$(^{t}Bu$_3$SiNH)TiPh	5500	23.0	(^{t}Bu$_3$SiNH)$_2$(^{t}Bu$_3$SiN)VPh[b,c]	140	25.8
(^{t}Bu$_3$SiNH)$_3$ZrMe	1	29.4			
(^{t}Bu$_3$SiNH)$_3$ZrPh	22	27.1			
(^{t}Bu$_3$SiNH)$_3$HfMe[b,d]	2.0×10^{-3}	34.0	(^{t}Bu$_3$SiNH)$_2$(^{t}Bu$_3$SiN)TaMe[b]	1.8×10^{-5}	37.4
(^{t}Bu$_3$SiNH)$_3$HfPh[b]	7.9×10^{-2}	31.3	(^{t}Bu$_3$SiNH)$_2$(^{t}Bu$_3$SiN)TaPh[b]	7.7×10^{-4}	34.7

[a] Rate constants were recalculated at 97 °C and corrected for the number of NH units per molecule relative to (^{t}Bu$_3$SiNH)$_3$ZrMe. [b] $\Delta S^{\ddagger}$ assumed to be −10 eu. [c] k_{Ph}/k_{Me} assumed to be similar to that of the titanium case. [d] k_{Ph}/k_{Me} assumed to be similar to that of the tantalum case.

with or subsequent to RH-binding via the four-center transition state; (5) selectivities of C−H bond activation parallel the strengths of the Ti−R bonds formed, with additional perturbations due to a more compressed reaction coordinate for sp^2-substrates and a slightly elongated one for benzylic and presumably allylic activations; (6) the steric "pocket" in **3** must be quite open to accommodate the breadth of substrates observed, including secondary C−H bond activation of cycloalkanes, which had not previously been noted for 1,2-RH-additions aside from those of ^{c}PrH; (7) by inference, similar characteristics apply to related Ti, Zr, V, and Ta systems. 1,2-RH-Elimination studies of the allylic derivatives were not available for study because of substantial ground state stabilizations derived from η^3-coordination. Alkynyl derivatives were also not amenable to investigation, because (silox)$_2$(^{t}Bu$_3$SiNH)TiC≡CR (**2**-C≡CR) derivatives are thermodynamically unstable with respect to corresponding [2+2] addition products, azametallacycles (silox)$_2$(^{t}Bu$_3$SiN)Ti(RC=CH) (**3**-HC$_2$R). Potentially interfering cyclometalation[20,98] reactions were not observed for (silox)$_2$Ti=NSi^{t}Bu$_3$ (**3**), presumably because the geometric requirements for an electrophilic attack on the C−H bonds of silox or ^{t}Bu$_3$SiN were prohibitive.

Selectivities for R^{1}H vs R^{2}H Activation by (silox)$_2$Ti=NSi^{t}Bu$_3$ (3). 1. Ramifications. While the parabolic model is adequate to detail the C−H bond activation process, what are the ramifications of the selectivities on a per molecule basis? As Table 4 indicates, methane activation is preferred by 1.7 kcal/mol over ethane activation, by 2.0 kcal/mol over terminal activation of butane (and presumably propane), and by 2.9 and 3.4 kcal/mol over activation by ^{c}PeH and ^{c}HexH, respectively. These significant selectivities obviate the most critical difficulty encountered by heterogeneous metal oxide catalysts that promote the oxidative coupling of methane. Rideal-type mechanisms operative in $[MO_n]_x$ catalysts are predicated on H atom abstractions that intrinsically favor activation of the saturated products, because their carbon−hydrogen bonds are weaker than those of the methane feedstock.[2,99] Unlike these heterogeneous catalysts, the low-temperature, stoichiometric system herein exhibits greater selectivity for unsaturated hydrocarbons; H−CH=CH$_2$ addition is preferred over H-CH$_3$ addition by 2.7 kcal/mol, while benzene activation is favored over methane activation by 0.9 kcal/mol. Should catalysts be developed that operate via 1,2-RH-addition to either homogeneous or heterogeneous M=X functionalities, or by related concerted additions, it is the latter selectivity that will ultimately present the most difficult problems in methane conversion.[2,100] Selectivity often originates in the steric features of homogeneous[4] and biological[101] systems, yet the trends in C−H activation by (silox)$_2$Ti=NSi^{t}Bu$_3$—virtually opposite those in heterogeneous Rideal-type processes—are inherent to the concerted character of the reaction and its exothermicity, which derives from the strength of the titanium−carbon bonds formed.

2. Comparisons. In a comparison of the selectitivites exhibited by this system, two observations are particularly striking. The general activation trends evident in Table 5 are roughly present in all concerted activations: sp^2-substrates ∼ ^{c}PrH > sp^3-primary alkanes > sp^3-cycloalkanes. Some variation in the position of benzylic and allylic activations with respect to these groups has been noted. Quantitative and qualitative selectivities in oxidative additions of RH to transient [HB(3,5-dimethylpyrazoyl)$_3$]Rh(CNCH$_2$^{t}Bu),[3] Cp*MPMe$_3$ (M = Rh,

(98) (a) Rothwell, I. P. *Acc. Chem. Res.* **1988**, *21*, 153−159. (b) Rothwell, I. P. *Polyhedron* **1985**, *4*, 177−200.

(99) Labinger, J. A.; Ott, K. C. *J. Phys. Chem.* **1987**, *91*, 2682−2684.

(100) For comments on the limitations of MeH activation in Rideal processes, see: Labinger, J. A. *Catal. Lett.* **1988**, *1*, 371−376.

(101) (a) Watanabe, Y.; Groves, J. T. In *The Enzymes*, 3rd ed.; Academic Press: New York, 1992. (b) Stewart, L. C.; Klinman, J. P. *Annu. Rev. Biochem.* **1988**, *57*, 551−592.

Ir),[102] σ-bond metatheses of RH with Cp^*_2ScR,[15] Cp^*_2LuR,[16] and $Cp^*_2ThCH_2CMe_2CH_2$,[17] and transient metal imido systems that also display 1,2-RH-additions all conform to this trend.[103]

Since exoergic C−H bond activation events necessarily involve the formation of strong metal−carbon bonds, similar activation trends in seemingly disparate systems probably stem from the same factors. The strength of the metal−carbon bonds formed is the primary factor that dictates selectivities in all mononuclear systems exhibiting concerted processes, with some moderation by other influences such as the reaction coordinate and steric effects.

Values of $\Delta\Delta G^{\ddagger}(R^1H$ vs $R^2H)$ for 1,2-RH-addition to $(silox)_2Ti{=}NSi^tBu_3$ (**3**) span a greater range than those for oxidative addition events in $[HB(3,5\text{-dimethylpyrazoyl})_3]Rh(CNCH_2{}^tBu)$ (i.e., $\Delta\Delta G^{\ddagger}$ relative to C_6H_6, −15 °C: PhH [0.0 kcal/mol] > H−CH_2-3,5-$Me_2C_6H_3$ [0.15] > MeH [0.4] > ^{n}PeH [0.80] > ^{c}PeH [1.7] > CyH [1.8])[3] and Cp^*MPMe_3 (M = Rh, $\Delta\Delta G^{\ddagger}$(−60 °C, C_6H_6 vs C_6H_{12}) = 1.2 kcal/mol; M = Ir, $\Delta\Delta G^{\ddagger}$(−60 °C) < 0.5 kcal/mol) systems.[102] Relative σ-bond metathesis C−H bond activation events are more difficult to analyze due to the lack of quantitative data and the second-order nature of these reactions, but C_6H_6 activation by Cp^*_2ScMe is about 0.8 kcal/mol easier than that by MeH.[15]

In unsaturated d^8 L_nM fragments such as $[HB(3,5\text{-dimethylpyrazoyl})_3]Rh(CNCH_2{}^tBu)$ or Cp^*MPMe_3 (M = Rh, Ir), R^1H vs R^2H binding is the discriminating event. In contrast, transition states for C−H activation by d^0 $X_nM{=}N-$ complexes exhibit substantial $M-R^1(R^2)$ and N−H bond-making, and $R^1(R^2)$−H bond-breaking in the transition state. Since the C−H bond is broken to a greater degree than it is during a simple binding event, the activations evident in the metal imido systems are intrinsically more selective.

Periodicity and 1,2-RH-Elimination/Addition. Upon completion of this study, examples of 1,2-RH-eliminations are known for all group 4[20,24] and 5[23,25] metals except niobium; specific cases are listed in Table 5. Two assumptions were made in converting measured rates to a common temperature (97 °C) and in estimating missing data: (1) where $\Delta S^{\ddagger}$ was unknown, a value of −10 eu was assigned, and (2) when either the Me or Ph derivative was known but not both, the k_{Ph}/k_{Me} ratio of the nearest system was used.

Progressing down group 4, 1,2-RH-elimination slows by increments of $\Delta\Delta G^{\ddagger}_{elim} \sim 4-5$ kcal/mol, whereas a shift to group 5 within a row constitutes a ∼3 kcal/mol increase in $\Delta G^{\ddagger}_{elim}$. Overall, the table spans a $\sim 10^7$ decrease in 1,2-RH-elimination rates upon traversing from titanium (**2**-R) to corresponding tantalum complexes. Substitution of silox for $^tBu_3SiNH$ has already been shown to induce a modest rate reduction by a factor of 4 in the tantalum system;[23] hence this ligand variation is not considered important.

The trends in Table 5 can be rationalized within the current model. Recall that lower ground states of $(silox)_2(^tBu_3SiN)$-Ti−R (**2**-R, R = sp^3) led to only slightly higher $\Delta G^{\ddagger}_{elim}$ values, because the 1,2-RH-elimination is not particularly "late". In the parabolic model, a greater influence of $\Delta G°$(M−R) on the 1,2-elimination reaction is predicted for later reactions. The data in the table reflect the increasingly "late" character of the elimination event as one proceeds down and to the right on the periodic table. In general terms, 1,2-RH-addition to $X_2M{=}N-$ will become earlier and more exoergic descending group 4, the $\Delta G^{\ddagger}_{addn}$ will decrease accordingly, i.e., Ti > Zr > Hf, and the corresponding 1,2-RH-eliminations will be later descending the group, with $\Delta G^{\ddagger}_{elim}$ increasing as Ti < Zr < Hf.

Weaker metal−carbon bonds in the first-row element—relative to Zr and Hf—permit the transition state, and its partially rendered Ti···R bond, to be more easily achieved. The ∼4−5 kcal/mol difference in 1,2-RH-elimination rates between Zr and Hf is less easily reasoned but is not unusual. Such disparities are usually attributed to slightly stronger Hf−R bonds,[67] augmented by relativistic effects.[104] In addition to ground state influences, the shorter covalent radius of titanium (Ti $r_{cov} \sim$ 1.32 Å) derivatives leads to a compressed reaction coordinate relative to its Zr (Zr $r_{cov} \sim$ 1.45 Å) and Hf (Hf $r_{cov} \sim$ 1.44 Å) congeners and correspondingly swifter rates.

The slower 1,2-RH-elimination rates upon shifting to group 5 appear to derive primarily from the thermodynamics of the event. Consider silox and $^tBu_3SiNH$ to be essentially equivalent $3e^-$ donors and the related imido ligand $^tBu_3SiN$ as a $4e^-$ donor. As a consequence, $(^tBu_3SiNH)_2(^tBu_3SiN{=})MR$ and $(^tBu_3SiNH)$-$(^tBu_3SiN{=})_2M$ (M = V, Ta) can be considered $16e^-$ species, in contrast to their related $14e^-$ group 4 derivatives. Wigley interpreted this disparity in electron count as "π-loading",[105] because the essential difference between groups 4 and 5 is the additional $N(p\pi)\rightarrow M(d\pi)$ bond of the imido ligand common to intermediate and ground states. From the standpoint of a Hammond analysis, it was suggested that "π-loading", or, generally, a more electron rich metal center, should lead to earlier and swifter C−H bond activation events in the case of $(R'NH)(R'N{=})_2M$ (M = V, Ta) + RH vs group 4 derivatives.

In essence, "π-loading" or the greater electron density stabilizes product $(R'NH)_2(R'SiN{=})MR$ states relative to intermediate $(R'NH)(R'N{=})_2M$ + RH states to a greater degree than in group 4. As a corollary, the reverse 1,2-RH-elimination event will be later and slower in group 5 than in group 4. Unfortunately, the lack of ground state data for the V and Ta systems leaves this analysis moot, but calculations by Cundari support this contention, despite commentary to the contrary.[60] Clearly, decreases in 1,2-RH-elimination rates upon shifting from group 4 to 5 need to be assessed by a much more detailed model than is possible from the available kinetic and thermodynamic data and may only be reconciled through careful calculations.[57−62]

Generality of the Parabolic Model. Lacking major steric influences or critical reactant/product surface coupling, concerted reactions should generally follow the parabolic model, responding to thermodynamic and positional effects. While most recognizable in its application to electron transfer reactions, i.e., Marcus theory,[106] the application of parabolas to model free energy surfaces is an old concept in physical organic chemistry with its origins in Hammond analyses,[93] related models,[94] and their predecessors.[107] Given this historical precedent, it is somewhat surprising that the reaction coordinate is often underappreciated when compared to influences of orbital character and π-effects, constructs of modern valence bond and molecular orbital theories. For example, in concerted systems, hydrocarbon selectivities are recognized as crudely paralleling the s-character of the C−H bonds activated. Greater s-character leads to lower activation barriers, perhaps as a consequence of lesser orbital directionality and greater acidity, although slow

(102) Periana, R. A.; Bergman, R. G. *J. Am. Chem. Soc.* **1986**, *108*, 7332−7346.

(103) Cundari, T. R. *J. Am. Chem. Soc.* **1994**, *116*, 340−347.

(104) (a) Kaltsoyannis, N. *J. Chem. Soc., Dalton Trans.* **1997**, 1−11. (b) Pyykkö, P. *Chem. Rev.* **1988**, *88*, 563−594.

(105) (a) Chao, Y. W.; Rodgers, P. M.; Wigley, D. E.; Alexander, S. J.; Rheingold, A. L. *J. Am. Chem. Soc.* **1991**, *113*, 6326−6327. (b) Smith, D. P.; Allen, K. A.; Carducci, M. D.; Wigley, D. E. *Inorg. Chem.* **1992**, *31*, 1319−1320. (c) Bryan, J. C.; Burrell, A. K.; Miller, M. L.; Smith, W. H.; Burns, C. J.; Sattelberger, A. P. *Polyhedron* **1993**, *12*, 1769−1777.

(106) Marcus, R. A. *Angew. Chem., Int. Ed. Engl.* **1993**, *32*, 1111−1121.

(107) Leffler, J. E.; Grunwald, E. *Rates and Equilibria of Organic Reactions*; John Wiley & Sons: New York, 1963.

benzylic and allylic activations in these systems seem to contradict the latter. Since d(R−H) and d(M−R) vary inversely with s-character, the primary effect of hybridization may be to influence the reaction coordinate! Rationalizations of reactivity on the basis of participation or nonparticipation of π-orbitals are often popular and yet are difficult to assess.[96] Again, bond-making and -breaking events that involve sp- and sp^2-carbon centers of unsaturation are likely to reflect the consequences of a compressed reaction coordinate relative to an sp^3-carbon, leading to generally speedier reactions.[108] In summary, thermodynamic influences on reaction rate, usually described via linear or nonlinear free energy relationships, are readily accepted, yet positional dependencies should receive greater attention than less transparent, orbital-based rationalizations (e.g., s-character and π-effects).

Experimental Section

General Considerations. All manipulations were performed using either glovebox or high-vacuum techniques. Hydrocarbon and ethereal solvents were dried over and vacuum transferred from sodium benzophenone ketyl (with 3−4 mL of tetraglyme/L added to hydrocarbons). Benzene-d_6 was sequentially dried over sodium and 4 Å molecular sieves and then stored over and vacuum-transferred from sodium benzophenone ketyl. Cyclohexane-d_{12} was dried over sodium and then stored over and vacuum-transferred from Na/K alloy. All glassware was base-washed and oven-dried. NMR tubes for sealed tube experiments were flame-dried under dynamic vacuum immediately prior to the experiment. $TiCl_4(THF)_2$ was prepared according to the literature procedure,[109] using $TiCl_4$ (Aldrich) as received. $NaOSi^tBu_3$[110,111] and $LiNHSi^tBu_3$[112] were prepared according to the literature procedures. Methane, ethane, propane, butane, ethylene, propene, *cis*-2-butene, *trans*-2-butene, cyclopropane, and isobutylene (Matheson) were passed through a −78 °C trap before use. 2-Butyne (Farach Chemical Co.) was dried over Na and stored over 4 Å molecular sieves in a glass bomb. Neohexane, tetramethylsilane, PMe_3, and NMe_3 (Aldrich) were dried over Na and stored in glass bombs over Na prior to use.

^1H and $^{13}C\{^1H\}$ NMR spectra were obtained using Varian XL-200, XL-400, VXR-400S, and Unity-500 spectrometers. Infrared spectra were recorded on a Perkin-Elmer 299B spectrophotometer. Combustion analyses were performed by Oneida Research Services, Whitesboro, NY, Texas Analytical Labs, Stafford, TX, or Robertson Microlit Laboratories, Madison, NJ. The Center for High Energy Synchrotron Studies (CHESS) at Cornell University was used for the X-ray crystallographic study of $(silox)_2(THF)Ti{=}NSi^tBu_3$ (**3**-THF).

Procedures. 1. $(silox)_2TiCl_2$ (1). To a flask containing $TiCl_4(THF)_2$ (1.69 g, 5.1 mmole) and Na(silox) (2.45 g, 10.2 mmol) was added 60 mL of ether at −78 °C. On warming to 25 °C, the bright yellow solution of $TiCl_4(THF)_2$ bleached to a pale yellow solution. After overnight stirring under argon, the ether was removed and replaced with 40 mL of hexanes. Filtration in hexanes, concentration, and cooling yielded **1** as a white crystalline solid (2.20 g, 78%). IR (Nujol, cm^{-1}): 1018 (w), 1009 (w), 980 (s), 900 (s), 815 (s), 630 (s), 610 (s). Anal. Calcd for $C_{24}H_{54}Si_2O_2Cl_2Ti$: C, 52.44; H, 9.90. Found: C, 52.48; H, 9.78.

2. $(silox)_2(^tBu_3SiNH)TiCl$ (2-Cl). A 100 mL round-bottom flask was charged with $^tBu_3SiNHLi$ (2.876 g, 12.99 mmol) and $(silox)_2TiCl_2$ (7.142 g, 13.18 mmol). Ether (80 mL) was added via vacuum transfer at −78 °C. The mixture was allowed to warm to 25 °C over the course of 20 min, and the solids dissolved. The pale yellow solution was stirred 30 min at 25 °C, and the volatiles were removed to yield an off-white solid, which was triturated with hexanes (3 × 30 mL) and then dissolved in hexanes (40 mL), and the mixture was filtered. The precipitate was washed with hexanes (7 × 40 mL), and the extracts were combined and concentrated (20 mL). Cooling to −78 °C and filtering yielded 7.35 g of microcrystalline **2**-Cl . A second crop gave 1.17 g (8.52 g, 90%). IR (Nujol, cm^{-1}): 1380 (m), 1370 (m), 1360 (m), 1085 (m), 1015 (w), 940 (m), 858 (s), 822 (s), 805 (s), 720 (w), 627 (s). Anal. Calcd for $TiSi_3ClNO_2C_{36}H_{82}$: C, 59.34; H, 11.34; N, 1.92. Found: C, 59.28; H, 11.40; N, 1.86.

3. $(silox)_2(^tBu_3SiNH)TiMe$ (2-Me). Into a solution of **2**-Cl (1.367 g, 1.877 mmol) in 15 mL of ether at 25 °C was syringed 1.25 mL of MeMgBr in ether (3.0 M, 2 equiv). The solution was stirred for 1 h, and the volatiles were removed. The solid was triturated with hexanes (3 × 15 mL) and then dissolved in hexanes (10 mL), and the mixture was filtered. The precipitate was washed with hexanes (5 × 15 mL), and the extracts were combined and concentrated to 5 mL. Cooling to −78 °C and filtering gave 0.852 g (64%) of microcrystalline **2**-Me. A second crop afforded 0.157 g (1.009 g total, 76%). IR (Nujol, cm^{-1}): 3248 (w), 1390 (m), 1380 (w), 1368 (m), 1089 (m), 1016 (w), 1009 (w), 950 (s), 940 (s), 875 (s), 828 (s), 775 (w), 725 (w), 625 (s). Anal. Calcd for $TiSi_3NO_2C_{37}H_{85}$: C, 62.75; H, 12.10; N, 1.98. Found: C, 62.23; H, 12.11; N, 1.63.

4. $(silox)_2(^tBu_3SiNH)TiCH_2CH_3$ (2-Et). To a slurry of **2**-Cl (462 mg, 0.634 mmol) in ether was added 0.35 mL of EtMgCl (2.0 M in ether) at 25 °C. The mixture was stirred for 4 h, and the volatiles were removed. The solid was triturated with hexanes (3 × 5 mL) and then dissolved in hexanes, and the mixture was filtered. The residue was washed with hexanes (7 × 3 mL), and the extracts were combined and concentrated to 2 mL. Cooling to −78 °C and filtering afforded microcrystalline **2**-Et (187 mg, 41%). A second crop yielded 45 mg (232 mg, 51%). IR (Nujol, cm^{-1}): 3228 (w), 1382 (s), 1372 (m), 1360 (s), 1085 (s), 1009 (m), 1001 (m), 945 (s), 941 (s), 914 (s), 865 (s), 815 (s), 720 (w), 620 (s). Anal. Calcd for $TiSi_3NO_2C_{38}H_{87}$: C, 63.19; H, 12.14; N, 1.94. Found: C, 63.08; H, 12.21; N, 1.90.

5. $(silox)_2(^tBu_3SiNH)TiCH_2Ph$ (2-Bz). To a solution of **2**-Cl (620 mg, 0.790 mmol) in 15 mL of ether was added 0.64 mL of $PhCH_2$-MgCl (2.0 M in ether) at 25 °C. The mixture was stirred for 3 h, and the solution turned yellow-orange. The volatiles were removed, the residue was triturated with hexanes (3 × 5 mL) and then dissolved in hexanes (5 mL), and the mixture was filtered. The precipitate was washed with hexanes (5 × 5 mL), and the extracts were combined and concentrated to 3 mL. Cooling to −78 °C and filtering gave microcrystalline **2**-Bz (480 mg, 72%). IR (Nujol, cm^{-1}): 3222 (w), 1604 (w), 1390 (m), 1379 (w), 1368 (m), 1216 (w), 1105 (s), 1032 (w), 1025 (w), 1015 (w), 1000 (w), 933 (s), 895 (m), 870 (s), 820 (s), 744 (m), 696 (m), 625 (s). Anal. Calcd for $TiSi_3NO_2C_{43}H_{89}$: C, 65.85; H, 11.44; N, 1.79. Found: C, 65.58; H, 11.57; N, 1.73.

6. $(silox)_2(^tBu_3SiNH)TiCH{=}CH_2$ (2-Vy). A 25 mL round-bottom flask was charged with **2**-Cl (333 mg, 0.457 mmol) and vinyllithium (prepared from ^{n}BuLi and tetravinyltin, 37 mg, 1.09 mmol).[113] Ether was added via vacuum transfer at −78 °C, and the mixture was stirred for 1 h. Volatiles were removed under vacuum at 0 °C. ^1H NMR spectroscopy showed the mixture to be ∼90% **2**-Vy, ∼ 5% **2**-Cl, and the remainder **3**-C_2H_4 and **3**-OEt_2. The solid was triturated with hexanes (2 × 5 mL) and then dissolved in hexanes, and the mixture was filtered. The filtrate was concentrated (0.5 mL) to yield an off-white powder, which was collected by filtration (98 mg, 30%). IR (Nujol, cm^{-1}): 3225 (w), 1554 (w), 1394 (w), 1382 (s), 1371 (w), 1360 (m), 1080 (m), 1009 (m), 1000 (m), 990 (m), 952 (m), 930 (s), 900 (s), 865 (s), 810 (s), 711 (w), 615 (s).

7. $(silox)_2(^tBu_3SiNH)TiPh$ (2-Ph). A solution of **2**-Me (145 mg, 0.205 mmol) in benzene (5 mL) was heated (60 °C) for 4 h in a 30 mL glass bomb. The bomb was immersed in liquid nitrogen, and volatiles (methane) were removed under vacuum. The vessel was then heated for 4 h at 60 °C and cooled to 25 °C. The volatiles were removed to yield a yellow powder (109 mg, 69%). A portion was set aside for characterization while the rest was immediately taken up in C_6D_6 for use in kinetics studies. Attempts to concentrate the solution and recrystallize this material from benzene led to the precipitation of a yellow insoluble material, probably **2**-C_6H_4-**2** (see text). IR (Nujol, cm^{-1}) 3215 (w), 1578 (w), 1386 (m), 1373 (w), 1363 (m), 1090 (m),

(108) For example, note that the reductive elimination rates of $(Ph_3P)_2$-Pt(H)R (R = Ph > Et > Me > allyl) conform to the parabolic model. See: Abis, L.; Sen, A.; Halpern, J. *J. Am. Chem. Soc.* **1978**, *100*, 2915−2916.

(109) Manzer, L. *Inorg. Synth.* **1982**, *21*, 135−140.

(110) Covert, K. J.; Wolczanski, P. T.; Hill, S. A.; Krusic, P. J. *Inorg. Chem.* **1992**, *31*, 66−78.

(111) Weidenbruch, M.; Pierrard, C.; Pesel, H. Z. *Z. Naturforsch., B: Anorg. Chem. Org. Chem.* **1978**, *33B*, 1468−1471.

(112) Nowakowski, P. M.; Sommer, L. H. *J. Organomet. Chem.* **1979**, *178*, 95−103.

(113) Seyferth, D.; Weiner, M. A. *J. Org. Chem.* **1961**, *26*, 3583−3586.

1010 (m), 925 (s), 880 (s), 815 (s), 803 (s), 775 (m), 720 (w), 620 (s). Anal. Calcd for $TiSi_3NO_2C_{42}H_{87}$: C, 65.47; H, 11.38; N, 1.82. Found: C, 65.38; H, 11.47; N, 1.84.

8. (silox)$_2$(^{t}Bu$_3$SiNH)TiH (2-H). To a 30 mL glass bomb containing **2**-Me (1.756 g, 2.479 mmol) at −196 °C was added 12 mL of cyclohexane. Hydrogen (500 Torr) was admitted at −196 °C; then the vessel was warmed to 25 °C, heated at 90 °C for 2 h, and cooled to 25 °C. The volatiles were removed, the solid was dissolved in hexanes (10 mL), and the mixture filtered. The residue was washed with hexanes (5 × 5 mL), and the extracts were concentrated to 3 mL. Cooling to −78 °C and filtration gave a thick slurry of microcrystalline **2**-H (885 mg). A second crop yielded 279 mg (1.164 g, 67%). IR (Nujol, cm^{-1}): 3225 (w), 1645 (m, TiH), 1348 (m), 1370 (w), 1360 (m), 1080 (m), 1010 (w), 950 (m), 930 (w), 875 (s), 830 (s), 815 (s), 765 (m), 715 (w), 620 (s). Anal. Calcd for $TiSi_3NO_2C_{36}H_{83}$: C, 62.29; H, 12.05; N, 2.02. Found: C, 62.01; H, 11.98; N, 1.44.

9. (silox)$_2$(^{t}Bu$_3$SiNH)Ti(CH$_2$)$_3$CH$_3$ (2-^{n}Bu). To a slurry of **2**-Cl (395 mg, 0.542 mmol) in 10 mL of ether was added 0.35 mL of ^{n}BuLi (1.6 M in hexanes, 1.03 equiv) at 0 °C. Upon addition of the alkyllithium, the solution turned yellow and a fine white precipitate began to appear. After 5 min, the volatiles were removed to give a yellow foam, which was triturated with hexanes (3 × 5 mL). The product would not crystallize from cold hexanes, so the crude solid (>90% **2**-^{n}Bu by ^{1}H NMR, principal impurity **2**-Cl) was removed (225 mg, 55%) and used for kinetics studies. IR (Nujol, cm^{-1}): 3225 (w), 1390 (s), 1380 (s), 1370 (s), 1190 (w), 1100 (m), 1015 (m), 930 (s), 880(3), 820 (s), 610 (m).

10. (silox)$_2$(^{t}Bu$_3$SiNH)Ti-c-C$_3$H$_5$ (2-^{c}Pr). A small bomb was charged with **2**-Me (460 mg, 0.649 mmol) and hexanes (10 mL). Cyclopropane (10 equiv) was admitted via a calibrated volume gas bulb. The bomb was heated at 60 °C for 14 h and then cooled to 25 °C, whereupon colorless crystals precipitated from the pale yellow solution. The crystals were collected by decantation and washed with cold hexanes (3 mL) to afford 156 mg of **2**-^{c}Pr (33%). IR (Nujol, cm^{-1}): 3235 (w), 1390 (m), 1379 (m), 1367 (m), 1088 (m), 1015 (w), 945 (m), 875 (s), 840 (s), 820 (s), 725 (w), 627 (s). Anal. Calcd for $TiSi_3NO_2C_{39}H_{87}$: C, 63.79; H, 11.94; N, 1.91. Found: C, 63.61; H, 12.03; N, 1.86.

11. (silox)$_2$(^{t}Bu$_3$SiNH)Ti-c-C$_5$H$_9$ (2-^{c}Pe). A small bomb was charged with **2**-Me (484 mg, 0.683 mmol) and cyclopentane (4 mL). The solution was thrice subjected to heating (50 °C) followed by a freeze−pump−thaw degas cycle to remove methane, thereby driving the reaction to completeness. Product **2**-c-C_5H_9 was was precipitated from a 1:1 mixture of cyclopentane/$Me_3SiOSiMe_3$ at 0 °C and collected via filtration (223 mg, 42%). IR (Nujol, cm^{-1}): 3210 (w), 1395 (m), 1383 (s), 1372 (m), 1360 (m), 1296 (w), 1093 (s), 1009 (w), 1004 (w), 930 (s), 860 (s), 815 (s), 730 (w), 620 (s). Anal. Calcd for $TiSi_3NO_2C_{41}H_{91}$: C, 64.60; H, 12.03; N, 1.84. Found: C, 64.41; H, 12.14; N, 1.80.

12. a. (silox)$_2$(^{t}Bu$_3$SiNH)Ti-c-C$_6$H$_{11}$ (2-^{c}Hex) and [(silox)$_2$-Ti=NSi^{t}Bu$_3$]$_2$ (3$_2$). A glass bomb was charged with **2**-Me (566 mg, 0.799 mmol) and 15 mL cyclohexane. The solution was stirred for 7 days at 55 °C, concentrated (10 mL), and allowed to cool slowly to 25 °C, affording yellow microcrystalline material (122 mg). ^{1}H NMR analysis indicated a mixture of sparingly soluble **2**-Cy and **3**$_2$. IR (Nujol, cm^{-1}): 1395 (w), 1384 (m), 1360 (w), 1280 (m), 1200 (s), 1035 (m), 962 (s), 898 (s), 865 (s), 812 (m), 720 (m), 618 (m).

b. 2-^{c}Hex for Kinetic Study. A small glass bomb was charged with **2**-Me (577 mg, 815 mmol) and 10 mL of cyclohexane. The bomb was sealed and heated at 65 °C for 3 h. The solution was thrice subjected to 77 K freeze−pump−thaw degas cycles to remove methane. Removal of the volatiles afforded a yellow solid, which was extracted with 2.2 mL of C_6D_6. This solution was filtered to remove residual solids and used immediately for kinetics studies.

13. (silox)$_2$(^{t}Bu$_3$SiNH)TiCH$_2$CH$_2$^{t}Bu (2-^{neo}Hex). A glass bomb was charged with **2**-Me (373 mg, 0.527 mmol) and 7 mL of $CH_3CH_2C(CH_3)_3$. The solution was heated for 6 h at 50 °C, cooled to 25 °C, and concentrated to 2 mL, which induced crystallization. Colorless **2**-^{neo}Hex was obtained via filtration (82 mg, 20%). IR (Nujol, cm^{-1}): 3238 (w), 1390 (m), 1380 (w), 1365 (m), 1238 (w), 1092 (m), 1061 (w), 1014 (m), 1005 (m), 940 (s), 870 (s), 820 (s), 735 (w), 625 (s). Anal. Calcd for $TiSi_3NO_2C_{42}H_{95}$: C, 64.81; H, 12.30; N, 1.80. Found: C, 64.73; H, 12.38; N, 1.75.

14. (silox)$_2$(^{t}Bu$_3$SiNH)TiCH$_2$C$_6$H$_3$(Me)$_2$ (2-Mes). In a small glass bomb, **2**-Me (445 mg, 0.628 mmol) was dissolved in 10 mL of mesitylene. The solution was heated at 55 °C for 14 h. The resulting orange solution was cooled to 25 °C, the volatiles were removed to yield an orange solid, which was taken up in hexanes (6 mL), and the mixture was filtered. Yellow crystalline **2**-Mes was collected by recrystallization from 2 mL of hexanes at 0 °C (207 mg, 41%). IR (Nujol, cm^{-1}): 3585 (w), 3222 (w), 1600 (w), 1385 (m), 1380 (m), 1370 (m), 1160 (w), 1090 (m), 1020 (w), 930 (s), 850 (s), 820 (s), 810 (s), 670 (w), 650 (w), 620 (s). Anal. Calcd for $TiSi_3NO_2C_{45}H_{93}$: C, 66.54; H, 11.54; N, 1.72. Found: C, 66.43; H, 11.81; N, 1.66.

15. (silox)$_2$(^{t}Bu$_3$SiNH)Ti-c-C$_4$H$_7$ (2-^{c}Bu). To a solid mixture of **2**-Cl (517 mg, 0.710 mmol) and ^{c}BuLi (46 mg, 0.742 mmol) was added 15 mL of ether at −78 °C. The resulting slurry was warmed to −30 °C, and the solids were dissolved to generate a brown solution. After 5 min, the volatiles were removed while the reaction mixture was kept at −30 °C. The solids were triturated with hexanes (3 × 10 mL) at 0 °C and then dissolved in hexanes, and the mixture was filtered. The residual was washed with hexanes (2 × 10 mL), and the extracts were combined and concentrated to 3 mL. Cooling to −78 °C and filtration gave microcrystalline **2**-^{c}Bu (186 mg, 35%). IR (Nujol, cm^{-1}): 3233 (w), 1385 (s), 1380 (m), 1240 (w), 1195 (w), 1090 (s), 1035 (w), 1020 (m), 940 (s), 870 (s), 820 (s), 665 (w), 620 (s). **2**-^{c}Bu was not of sufficient purity (>90% by ^{1}H NMR) for combustion analysis.

16. (silox)$_2$(^{t}Bu$_3$SiN)TiCH$_2$CH$_2$ (3-C$_2$H$_4$). A glass bomb was charged with **2**-Et (317 mg, 0.439 mmol) and 12 mL of cyclohexane. The bomb was immersed in liquid nitrogen and 2 equiv of C_2H_4 (125.2 mL at 130 Torr) was added. The mixture was warmed to 25 °C and stirred for 20 h and then warmed to 45 °C and stirred for 4 h. The solution was cooled to 25 °C, concentrated to 4 mL, and filtered to remove the polyethylene that had formed. The residue was washed with cyclohexane (2 × 3 mL), and the extracts were combined. The solvent was removed and replaced with pentane (1 mL). Concentrating to 0.6 mL, cooling to −78 °C, and filtration afforded yellow microcrystalline **3**-C_2H_4 (131 mg, 42%). IR (Nujol, cm^{-1}): 1390 (m), 1380 (m), 1365 (m), 1190 (w), 1005 (w), 945 (m), 910 (s), 880 (s), 820 (s), 720 (w), 625 (s). Because of the thermal instability of **3**-C_2H_4, combustion analysis was not attempted.

17. (silox)$_2$(THF)Ti=NSi^{t}Bu$_3$ (3-THF). A solution of **2**-Me (503 mg, 0.710 mmol) in THF (8 mL) was stirred in a bomb reactor for 3.5 d. The volatiles were removed, the resulting yellow solid was triturated with hexanes (3 × 10 mL) and then dissolved in hexanes, and the mixture was filtered. Concentrating to 1.5 mL, cooling to −78 °C, and filtration yielded microcrystalline **3**-THF (220 mg, 40%). IR (Nujol, cm^{-1}): 1395 (w), 1385 (s), 1365 (m), 1180 (w), 1074 (s), 1040 (w), 1013 (m), 930 (s), 890 (s), 821 (s), 755 (w), 615 (s). Anal. Calcd for $TiSi_3NO_3C_{40}H_{89}$: C, 62.86; H, 11.74; N, 1.83. Found: C, 62.78; H, 11.86; N, 1.80.

18. (silox)$_2$(py)Ti=NSi^{t}Bu$_3$ (3-py). To a solution of **2**-Me (480 mg, 0.678 mmol) dissolved in hexanes (25 mL) was added 4 mL of pyridine. The resulting solution was sealed in a glass bomb and stirred at 65 °C for 7 h. The volatiles were removed to give a yellow powder, which was subsequently triturated with hexanes (3 × 10 mL) and then dissolved in hexanes (5 mL). Yellow crystalline **3**-py was filtered (350 mg, 66%) from the hexanes (3 mL) at −78 °C. IR (Nujol, cm^{-1}) 1615 (m), 1380 (s), 1365 (m), 1220 (w), 1135 (w), 1080 (s), 1075 (s), 1045 (w), 1020 (m), 920 (s), 890 (s), 735 (m), 700 (m), 625 (w), 610 (s). Anal. Calcd for $TiSi_3N_2O_2C_{41}H_{86}$: C, 63.85; H, 11.24; N, 3.63. Found: C, 64.08; H, 11.50; N, 3.51.

19. (silox)$_2$(OEt$_2$)Ti=NSi^{t}Bu$_3$ (3-OEt$_2$). A solution of **2**-Me (1.196 g, 1.69 mmol) in Et_2O (25 mL) was stirred for 4 d at 25 °C. Upon removal of the volatiles, the solid was triturated with hexanes (3 × 15 mL) and then dissolved in hexanes (15 mL) and filtered. Faint yellow crystalline **3**-OEt_2 was filtered (895 mg, 69%) from the hexanes (3 mL) at 0 °C. IR (Nujol, cm^{-1}): 3680 (w), 1391 (m), 1380 (m), 1369 (m), 1189 (w), 1150 (w), 1092 (m), 1063 (m), 1036 (w), 1015 (w), 1008 (w), 999 (m), 920 (s), 890 (s), 822 (s), 770 (m), 721 (w), 625 (s). Anal. Calcd for $TiSi_3NO_2C_{40}H_{91}$: C, 62.69; H, 11.97; N, 1.84. Found: C, 62.55; H, 12.80; N, 1.46.

20. (silox)$_2$(PMe$_3$)Ti=NSi^{t}Bu$_3$ (3-PMe$_3$). To a 10 mL round-bottom flask charged with **2**-Me (221 mg, 0.312 mmol) and 5 mL of hexanes at −78 °C was added 2.3 equiv of PMe$_3$ via a gas bulb. The reaction mixture was stirred for 5 d at 25 °C, and the volatiles were removed to afford a yellow powder (115 mg, 48%). IR (Nujol, cm^{-1}): 1380 (m), 1363 (m), 1308 (w), 1288 (w), 1064 (s), 1010 (w), 960 (m), 945 (w), 930 (w), 910 (s), 883 (s), 842 (w), 818 (s), 730 (w), 618 (m). Anal. Calcd for $TiSi_3NO_2PC_{39}H_{90}$: C, 60.97; H, 11.81; N, 1.82. Found: C, 60.76; H, 12.05; N, 1.84.

21. (silox)$_2$(^{t}Bu$_3$SiN)TiC(Me)=CMe (3-MeCCMe). Into a solution of **2**-H (463 mg, 0.667 mmol) in cyclohexane (5 mL) was condensed 1.1 equiv of 2-butyne (287.8 mL at 47 Torr). The solution was stirred for 1 h at 25 °C, whereupon it turned orange-brown. The volatiles were removed, the residue was taken up in hexanes (3 mL), and the mixture was filtered. The residual was washed with hexanes (3 × 5 mL), and the extracts were collected and concentrated to 1 mL. Cooling to −78 °C, stirring for 1 h, and filtration afforded dark orange microcrystalline **3**-MeCCMe (227 mg). A second crop yielded 45 mg (272 mg total, 55%). IR (Nujol, cm^{-1}): 1382 (m), 1372 (w), 1360 (w), 1232 (w), 1147 (s), 1040 (w), 1000 (w), 908 (s), 867 (s), 814 (s), 713 (m), 619 (m). Anal. Calcd for $TiSi_3NO_2C_{40}H_{87}$: C, 64.38; H, 11.75; N, 1.88. Found: C, 64.19; H, 11.70; N, 1.71.

NMR Tube Reactions. a. (silox)$_2$(^{t}Bu$_3$SiN)TiC(Et)=CEt (3-EtCCEt). An NMR tube attached to a ground glass joint was charged with 16 mg (0.023 mmol) of **2**-Me and attached to a calibrated gas bulb. The apparatus was attached to a vacuum line, evacuated, and cooled to −78 °C. Cyclohexane-d_{12} (0.4 mL) was admitted via vacuum transfer. The tube was cooled to 77 K and reevacuated to admit 3-hexyne (1 equiv) via the gas bulb. The tube was sealed with a torch and allowed to stand at 25 °C for 4 d. **3**-EtCCEt formed in >95% yield as judged by ^{1}H NMR spectroscopy.

b. (silox)$_2$(^{t}Bu$_3$SiN)TiC(H)=CH (3-HCCH). An NMR tube attached to a ground glass joint was charged with 30 mg (0.042 mmol) of **2**-Me and attached to a calibrated gas bulb. The apparatus was attached to a vacuum line, evacuated, and cooled to −78 °C. Cyclohexane-d_{12} (0.4 mL) was admitted via vacuum transfer. The tube was cooled to 77 K and reevacuated to admit acetylene (1.2 equiv) via the gas bulb. The tube was sealed with a torch and allowed to stand at 25 °C for 4 d. **3**-HCCH formed in >70% yield as judged by ^{1}H NMR spectroscopy. A black flocculant solid, assumed to be polyacetylene, also formed.

c. (silox)$_2$(R$_3$N)Ti=NSi^{t}Bu$_3$ (3-NR$_3$, R = Me, Et). An NMR tube attached to a ground glass joint was charged with 30 mg (0.042 mmol) of **2**-Me and attached to a calibrated gas bulb. The apparatus was attached to a vacuum line, evacuated, and cooled to −78 °C. Cyclohexane-d_{12} (0.4 mL) was admitted via vacuum transfer. The tube was cooled to 77 K and reevacuated to admit NR$_3$ (1.2 equiv) via the gas bulb. The tube was sealed with a torch and allowed to stand at 25 °C for 4 d. **3**-NR$_3$ formed in >90% yield as judged by ^{1}H NMR.

General Kinetics Procedures. Solutions of **2**-R were prepared in C_6D_6 in 2 mL volumetric flasks. In the cases of R = ^{n}Bu, ^{c}Bu, and ^{c}Hex, the solutions were filtered to remove insoluble material. Either $Me_3SiSiMe_3$ or $Me_3SiOSiMe_3$ (~1 μL) was added as an internal standard. Three samples of 0.6 mL each were transferred to flame-dried 5 mm NMR tubes joined to 14/20 joints and attached to needle valves. The tubes were subjected to three freeze−pump−thaw degas cycles and flame-sealed under vacuum. Temperatures above 25 °C were regulated in a polyethylene glycol bath with a Tamson immersion circulator. The temperature of 24.8 °C was obtained by placing the tubes in an Hewlett Packard model 5890A gas chromatograph oven kept in a room at 20−22 °C with the nominal temperature set to 25 °C. In both cases, the temperature was stable to ±0.3 °C. Rates of disappearance of amido NH peaks were monitored in most cases. For some **2**-R derivatives a better signal intensity was obtained by monitoring proton resonances from the R group (R = Et, Bz, ^{c}Pr, ^{c}Bu, ^{c}Pe, ^{c}Hex, ^{neo}Hex). All runs were monitored for 5−6 half-lives. Single transient spectra were used to obtain the most reproducible integrals. Rates and uncertainties were obtained from nonlinear, nonweighted least-squares fitting to the exponential form of the rate expression. Occasionally only two of the three tubes would survive the entire kinetic run, but in all cases at least two tubes survived.

General Equilibria Procedures. 1. Sample Preparation. A flame-dried 5 mm NMR tube joined to a 14/20 joint and attached to a needle valve was charged with ca. 20 mg of an organotitanium species. The apparatus was attached to the vacuum line and evacuated. Cyclohexane-d_{12} (0.4−0.7 mL) was admitted to the tube via vacuum transfer followed by a known amount of a volatile reagent admitted through a calibrated gas bulb. In some cases, a second reactant was added (H_2 for example). The mixture was cooled to 77 K, and the tube was sealed with a torch.

2. Measurement of Equilibria. Equilibrium concentrations of reactants and products were determined by 400 MHz (or 500 MHz in certain cases of difficult signal overlap) ^{1}H NMR spectroscopy. All tubes were measured at least twice after it was certain the reactions had come to equilibrium. Because of the need to accurately measure very low concentrations of species in many cases, the following protocol for data collection was observed: (1) a delay time (D_1) of 120 s was used between acquisitions, (2) the filter bandwidth was set to ensure no attenuation of signal within the spectral window, and (3) the acquisition time was set to the largest value allowed by the computer software (ca. 8−12 s; sweep width dependent). These precautions ensured complete relaxation of nuclei under investigation, accuracy of integrals of peaks near the edge of the spectrum, and elimination of ringing in intense peaks. Depending on the intensity of the weakest resonance to be measured, spectra were acquired with 4−32 transients. In a few cases, deconvolution of overlapping peaks was required.

Single-Crystal X-ray Diffraction Studies. 1. (^{t}Bu$_3$SiO)$_2$(^{t}Bu$_3$SiNH)-TiCH$_2$CH$_2$^{t}Bu (2-^{neo}Hex). Large block-shaped crystals (approximately 0.5 × 0.5 × 0.5) formed upon concentration of a solution of **2**-^{neo}Hex at room temperature. These crystals were mounted in thin walled glass capillaries which were subsequently flame-sealed. Preliminary rotation photographs indicated orthorhombic Laue symmetry. Precise lattice constants (Table 2) were determined from a least-squares fit of 15 diffractometer-measured 2θ values at 25 °C. The structure was solved by direct methods and refined by least-squares methods (SHELXL-93). Severe disorder (silox cannot be distinguished from ^{t}Bu$_3$SiNH) in the periphery of the molecule limited interpretation of the structural model to a description of the overall geometry and the alkyl fragment.

2. (silox)$_2$(THF)Ti=NSi^{t}Bu$_3$ (3-THF). A supersaturated solution of **3**-THF in hexanes was prepared in a 10 mL flask by heating 800 mg of **3**-THF in 3 mL of hexanes. The hot flask was wrapped with glass wool and aluminum foil and allowed to stand undisturbed for 14 h. Upon standing, many small crystals of **3**-THF formed along with a few large (ca. 3 mm on an edge), well-formed, crystalline blocks. Preliminary unit cell determination using a fragment (ca. 0.8 × 0.8 × 0.8 mm) of a larger crystal revealed orthorhombic symmetry but even this large crystal exhibited a sharp drop in observed reflections with increasing 2θ on a sealed-tube instrument.

A similar fragment (0.8 × 0.8 × 0.4 mm) was coated in Paratone-N oil and cooled in a nitrogen cold stream at the CHESS A-1 station. X-ray data were collected using 13.65 keV (0.908 Å) X-rays generated by the A-line 1.3 T, 24-pole wiggler magnet. A total of 1.66 mrad of the available 4.22 mrad synchrotron radiation was doubly focused into the A-1 hutch by a horizontally focusing Si(111), cylindrically bent, triangular monochromator followed by a vertically focusing, cylindrically bent, rhodium-coated silicon mirror with final collimation and beam shaping by a 0.5 mm double-pinhole collimator. The uncollimated beam is 0.15 × 2.6 mm (fwhm) in dimension at the focus with a flux of 1.3 × 10^{13} photons/s and an energy resolution of 52 eV at 13 keV. A flux of 4 × 10^{11} photons/s with an energy resolution of 15 eV has been measured through a 0.3 mm collimator in this configuration. A Molecular Structure Corp. cryostat operating around −165 °C was used to flash cool the crystal in Paratone-N oil and maintain it at cryogenic temperatures throughout the data collection (Table 2). Diffraction patterns were recorded with a 2K × 2K CCD operating in binned mode (effective 1K × 1K). The data were merged and processed using DENZO and SCALEPACK. The reflections were corrected for background effects, integrated using DENZO, and scaled together using SCALEPACK, and the structure was solved by direct methods and refined by least-squares methods (SHELXL-93). For the

11 536 unique integrated observations of ca. 18 500 observed reflections an $R_{sym} = 3.1\%$ was obtained to 0.8 Å resolution.

Acknowledgment. Support from the National Science Foundation (Grant CHE-9218270 (past), Grant CHE-9528914 (current)) is gratefully acknowledged. We thank Barry K. Carpenter, Thomas R. Cundari, and Thomas P. Vaid for helpful discussions, Steve Ealick, Dan Thiel, Marian Szebenyi, Rick Walter, Emil Lobkovsky, Jorge Rios Steiner, Dave Fuller, and Aidan Harrison for assistance in X-ray crystallography and NMR measurements, and Lee M. Slaughter for experimental aid. Funding for the Cornell NMR Facility from the NIH and NSF Instrumentation Programs is acknowledged.

Appendix: Parabolas 2-R^n, 3, and ΔG^{TS_n} at $x(TS_n)$ in Figure 7

The parabolas corresponding to **2**-R^n and **3** in Figure 7 are indicated in eqs A1 and A2, where $\Delta G°$(**2**-R^n), $\Delta G°$(**3**), and

$$\Delta G(\mathbf{3}) = \Delta G°(\mathbf{3}) + K(x - x(\mathbf{3}))^2 \quad \text{(A1)}$$

$$\Delta G(\mathbf{2}\text{-R}^n) = \Delta G°(\mathbf{2}\text{-R}^n) + K(x - x(\mathbf{2}\text{-R}^n))^2 \quad \text{(A2)}$$

their free energies are in kcal/mol relative to $\Delta G°$(**3**-py) = 0 kcal/mol. x(**2**-R^n) and x(**3**) are the positions of the corresponding states along the reaction coordinate, x. The steepness of parabolas **2**-R^n and **3** is set arbitrarily ($K = 1$). The following are defined or known: $x(\mathbf{3}) = 0$, $\Delta G°(\mathbf{3}) = 24$ kcal/mol, $\Delta G°$(**2**-R^n), and $\Delta G^{‡}_{elim}$(**2**-R^n). Values of $x(TS_n)$ and x(**2**-R^n) are sought. The **2**-R and **3** parabolas intersect at $x(TS_n)$ and ΔG^{TS_n}, and

$$\Delta G^{TS_n} = \Delta G°(\mathbf{2}\text{-R}^n) + \Delta G^{‡}_{elim}(\mathbf{2}\text{-R}^n) \quad \text{(A3)}$$

At the intersection (i.e., $\Delta G(\mathbf{2}\text{-R}^n) = \Delta G^{TS_n}$), eq A1 is rewritten as

$$\Delta G°(\mathbf{2}\text{-R}^n) + \Delta G^{‡}_{elim}(\mathbf{2}\text{-R}^n) = \Delta G°(\mathbf{3}) + (x(TS_n))^2 \quad \text{(A4)}$$

Solving for $x(TS_n)$, which is <0, since x(**3**) was defined as 0, we have

$$x(TS_n) = -(\Delta G°(\mathbf{2}\text{-R}^n) + \Delta G^{‡}_{elim}(\mathbf{2}\text{-R}^n) - \Delta G°(\mathbf{3}))^{1/2} \quad \text{(A5)}$$

At the intersection, we rewrite eq A2 using eq A3 and rearrange to a polynomial in x(**2**-R) using A5:

$$\Delta G°(\mathbf{2}\text{-R}^n) + \Delta G^{‡}_{elim}(\mathbf{2}\text{-R}^n) = \Delta G°(\mathbf{2}\text{-R}^n) + (x(TS_n) - x(\mathbf{2}\text{-R}^n))^2 \quad \text{(A6)}$$

$$(x(\mathbf{2}\text{-R}^n))^2 - 2(x(TS_n))(x(\mathbf{2}\text{-R}^n)) + (\Delta G°(\mathbf{2}\text{-R}^n) - \Delta G°(\mathbf{3})) = 0 \quad \text{(A7)}$$

Solving for x(**2**-R), we obtain eqs A8 and A9.

$$x(\mathbf{2}\text{-R}^n) = x(TS_n) - (\Delta G^{‡}_{elim}(\mathbf{2}\text{-R}^n))^{1/2} \quad \text{(A8)}$$

$$x(\mathbf{2}\text{-R}^n) = -(\Delta G°(\mathbf{2}\text{-R}^n) + \Delta G^{‡}_{elim}(\mathbf{2}\text{-R}^n) - \Delta G°(\mathbf{3}))^{1/2} - (\Delta G^{‡}_{elim}(\mathbf{2}\text{-R}^n))^{1/2} \quad \text{(A9)}$$

Supporting Information Available: A table listing individual equilibrium measurements, a discussion of NH IR stretching frequencies for **2**-R, comments on azametallacyclobutene vs alkylidene−imine structures, a perspective on cyclometalation, and X-ray structural information pertaining to (^{t}Bu$_3$SiO)$_2$(^{t}Bu$_3$SiNH)TiCH$_2$CH$_2$^{t}Bu (**2**-^{neo}Hex) and (silox)$_2$(THF)Ti═NSi^{t}Bu$_3$ (**3**-THF), including tables of crystal data encompassing data collection and solution/refinement, atomic coordinates, isotropic and anisotropic temperature factors, hydrogen atom coordinates, and bond lengths, and bond angles (28 pages). See any current masthead page for ordering and Internet access instructions.

JA9707419